Universität Potsdam

Institut für Erd- und Umweltwissenschaften

und

Helmholtz-Zentrum Potsdam-Deutsches GeoForschungsZentrum GFZ

Sektion 5.2-Klimadynamik und Landschaftsentwicklung

Mid- to Late Holocene flood reconstruction from two varved sediment profiles of pre-alpine Lake Ammersee (southern Germany)

Dissertation
zur Erlangung des akademischen Grades
„doctor rerum naturalium"
(Dr. rer. nat.)
in der Wissenschaftsdisziplin Geologie

eingereicht in Form einer kumulativen Arbeit an der
Mathematisch-Naturwissenschaftlichen Fakultät
der Universität Potsdam

von
Markus Czymzik

Potsdam, August 2012

Published online at the
Institutional Repository of the University of Potsdam:
URL http://opus.kobv.de/ubp/volltexte/2013/6509/
URN urn:nbn:de:kobv:517-opus-65098
http://nbn-resolving.de/urn:nbn:de:kobv:517-opus-65098

Supervisor:

Prof. Dr. Achim Brauer

Universität Potsdam
Helmholtz-Zentrum Potsdam, Deutsches GeoForschungsZentrum GFZ

Table of contents

List of figures

List of tables

Abstract

Climate is the principal driving force of hydrological extremes like floods and attributing generating mechanisms is an essential prerequisite for understanding past, present, and future flood variability. Successively enhanced radiative forcing under global warming enhances atmospheric water-holding capacity and is expected to increase the likelihood of strong floods. In addition, natural climate variability affects the frequency and magnitude of these events on annual to millennial time-scales. Particularly in the mid-latitudes of the Northern Hemisphere, correlations between meteorological variables and hydrological indices suggest significant effects of changing climate boundary conditions on floods. To date, however, understanding of flood responses to changing climate boundary conditions is limited due to the scarcity of hydrological data in space and time. Exploring paleoclimate archives like annually laminated (varved) lake sediments allows to fill this gap in knowledge offering precise dated time-series of flood variability for millennia. During river floods, detrital catchment material is eroded and transported in suspension by fluid turbulence into downstream lakes. In the water body the transport capacity of the inflowing turbidity current successively diminishes leading to the deposition of detrital layers on the lake floor. Intercalated into annual laminations these detrital layers can be dated down to seasonal resolution.

Microfacies analyses and X-ray fluorescence scanning (μ-XRF) at 200 μm resolution were conducted on the varved Mid- to Late Holocene interval of two sediment profiles from pre-alpine Lake Ammersee (southern Germany) located in a proximal ($AS10_{prox}$) and distal ($AS10_{dist}$) position towards the main tributary River Ammer. To shed light on sediment distribution within the lake, particular emphasis was (1) the detection of intercalated detrital layers and their micro-sedimentological features, and (2) intra-basin correlation of these deposits. Detrital layers were dated down to the season by microscopic varve counting and determination of the microstratigraphic position within a varve. The resulting chronology is verified by accelerator mass spectrometry (AMS) ^{14}C dating of 14 terrestrial plant macrofossils.

Since ~5500 varve years before present (vyr BP), in total 1573 detrital layers were detected in either one or both of the investigated sediment profiles. Based on their microfacies, geochemistry, and proximal-distal deposition pattern, detrital layers were interpreted as River Ammer flood deposits. Calibration of the flood layer record using instrumental daily River

Ammer runoff data from AD 1926 to 1999 proves the flood layer succession to represent a significant time-series of major River Ammer floods in spring and summer, the flood season in the Ammersee region.

Flood layer frequency trends are in agreement with decadal variations of the East Atlantic-Western Russia (EA-WR) atmospheric pattern back to 200 yr BP (end of the used atmospheric data) and solar activity back to 5500 vyr BP. Enhanced flood frequency corresponds to the negative EA-WR phase and reduced solar activity. These common links point to a central role of varying large-scale atmospheric circulation over Europe for flood frequency in the Ammersee region and suggest that these atmospheric variations, in turn, are likely modified by solar variability during the past 5500 years.

Furthermore, the flood layer record indicates three shifts in mean layer thickness and frequency of different manifestation in both sediment profiles at ~5500, ~2800, and ~500 vyr BP. Combining information from both sediment profiles enabled to interpret these shifts in terms of stepwise increases in mean flood intensity. Likely triggers of these shifts are gradual reduction of Northern Hemisphere orbital summer forcing and long-term solar activity minima. Hypothesized atmospheric response to this forcing is hemispheric cooling that enhances equator-to-pole temperature gradients and potential energy in the troposphere. This energy is transferred into stronger westerly cyclones, more extreme precipitation, and intensified floods at Lake Ammersee.

Interpretation of flood layer frequency and thickness data in combination with reanalysis models and time-series analysis allowed to reconstruct the flood history and to decipher flood triggering climate mechanisms in the Ammersee region throughout the past 5500 years. Flood frequency and intensity are not stationary, but influenced by multi-causal climate forcing of large-scale atmospheric modes on time-scales from years to millennia. These results challenge future projections that propose an increase in floods when Earth warms based only on the assumption of an enhanced hydrological cycle.

Zusammenfassung

Globale Klimamodelle prognostizieren eine Zunahme von Starkhochwassern aufgrund eines intensivierten hydrologischen Kreislaufs infolge der Klimaerwärmung. Weiterhin werden natürliche Klimafaktoren wie solare Aktivität, explosiver Vulkanismus, Meereis, atmosphärische und ozeanische Zirkulation, die Intensität und Häufigkeit solcher Ereignisse auf Zeitskalen von Jahren bis Jahrtausenden beeinflussen. Für ein umfassendes Verständnis hochwassergenerierender Klimamechanismen müssen daher lange Zeiträume und regionale Muster in Betracht gezogen werden. Aufgrund der Limitierung der meisten instrumentellen Abflusszeitreihen auf die letzten 100 Jahre, bieten diese allerdings nur einen sehr begrenzten Einblick in das Spektrum möglicher Klima-Hochwasser Zusammenhänge.

Die Nutzung natürlicher Hochwasserarchive, wie jährlich laminierter (warvierter) Seesedimente, erlaubt die Untersuchung von Hochwasseraktivität auf Zeitskalen von Jahrtausenden und damit in unterschiedlichen Klimaszenarien, wie der Kleinen Eiszeit und der Mittelalterlichen Wärmeperiode auf Basis präziser Chronologien. Durch Hochwasser in einen See eingetragenes detritisches Material aus dem Einzugsgebiet bildet, eingeschaltet in den jährlichen Sedimentationszyklus, eine charakteristische Abfolge von Hochwasserlagen auf dem Seeboden. Das Zählen jährlicher Laminierungen und die Position innerhalb eines jährlichen Sedimentationszyklus ermöglichen die Datierung einzelner Hochwasserlagen mit bis zu saisonaler Genauigkeit.

Der Ammersee im Alpenvorland bildet ein ideales Archiv zur Rekonstruktion von Hochwassern. Detritisches Material wird durch nur einen Hauptzufluss, die Ammer, in das rinnenförmige Becken transportiert. Die warvierten Sedimente erlauben eine zuverlässige Detektion und Datierung selbst mikroskopischer Hochwasserlagen. Instrumentelle Hochwasserdaten der Ammer und Wetterzeitreihen des Meteorologischen Observatoriums Hohenpeißenberg ermöglichen eine Kalibration der Sedimentdaten.

An zwei warvierten Sedimentprofilen des Ammersees ($AS10_{prox}$ und $AS10_{dist}$), die entlang eines proximal-distalen Transekts zur Ammermündung entnommen wurden, sind hochauflösende Mikrofazies und Röntgenfluoreszenz (µ-XRF) Analysen durchgeführt worden. Zum besseren Verständnis der Sedimentverteilung im See lag der Fokus der Untersuchungen auf der Detektion detritischer Lagen anhand ihrer sedimentologischen und geochemischen Eigenschaften und der Korrelation dieser Lagen zwischen beiden

Sedimentprofilen. Die Datierung der detritschen Lagen erfolgte durch Warvenzählung und wurde durch 14 AMS Radiokarbondatierungen an terrestrischen Pflanzenresten bestätigt.

In den Sedimenten der letzten 5500 Jahre wurden 1573 detritische Lagen in einem oder beiden der untersuchten Ammerseeprofile gefunden. Aufgrund ihrer Eigenschaften lassen sich diese Lagen als Ammerhochwasserlagen interpretieren: (1) Die Mikrofazies deutet auf eine Ablagerung nach Starkabflussereignissen hin. (2) Die geochemische Zusammensetzung beweist die terrestrische Herkunft des Materials. (3) Das proximal-distale Ablagerungsmuster deutet auf die Ammer als Eintragsquelle des Materials hin. Eine Kalibrierung mit instrumentellen Hochwasserdaten der Ammer im Zeitraum von AD 1926 bis 1999 bestätigt die Sukzession der detritischen Lagen als eine Zeitreihe starker Ammerhochwasser im Frühling und Sommer, der Hochwassersaison am Ammersee.

Die Häufigkeit der Hochwasserlagen in den letzten 5500 Jahren weist eine deutliche dekadische Variabilität auf. Trends in der Häufigkeit von Hochwasserlagen korrelieren negativ mit dem Index der East Atlantic-Western Russia Oszillation (EA-WR) während der letzten 250 Jahre (Zeitraum der durch die genutzten atmosphärischen Daten abgedeckt ist) und der solaren Aktivität während des kompletten Zeitraums. Diese Übereinstimmungen deuten möglicherweise auf einen solaren Einfluss auf die atmosphärische Zirkulation über Europa und damit auf die Häufigkeit von Hochwassern am Ammersee hin.

Weiterhin weist die Zeitreihe der Hochwasserlagen drei Veränderungen der durchschnittlichen Lagenhäufigkeit und -mächtigkeit vor etwa 5500, 2800 und 500 Jahren auf. Die Kombination der Daten beider Sedimentprofile ermöglicht es, diese Veränderungen als schrittweise Anstiege der Hochwasserintensität zu interpretieren. Vermutliche Auslöser sind graduelle Reduktion der solaren Insolation in der Nordhemisphäre und langfristige Minima der solaren Aktivität. Die wahrscheinliche atmosphärische Reaktion auf dieses Klimaforcing ist ein verstärkter Temperaturgradient zwischen den niederen und hohen Breiten, der zu einer Erhöhung der potenziellen Energie in der Atmosphäre und verstärkter Baroklinität führt. Diese Energie wird transferiert in eine Verstärkung der zyklonalen Westwindzirkulation, extremere Niederschläge und eine Intensivierung der Hochwasser am Ammersee.

Die Interpretation der Häufigkeit und Mächtigkeit von Hochwasserlagen in den Sedimenten des Ammersees ermöglicht in Kombination mit Reanalysemodellen und Zeitreihenanalysen eine Rekonstruktion der Hochwassergeschichte und die Identifizierung

hochwasserauslösender Klimafaktoren in der Ammerseeregion während der letzten 5500 Jahre. Hochwasserhäufigkeit und -intensität sind nicht stationär, sondern durch komplexe Veränderungen im Klimasystem auf Zeitskalen von Jahren bis Jahrtausenden geprägt. In diesem Zusammenhang erscheinen die Resultate globaler Klimamodelle, die einen Anstieg des Hochwasserrisikos allein auf Basis eines thermodynamisch intensivierten hydrologischen Kreislaufs infolge der Klimaerwärmung prognostizieren, als stark simplifiziert.

Acknowledgements

This research was financed by a PhD grant of the Helmholtz-Centre Potsdam-GFZ German Research Centre for Geosciences.

First of all, I would like to thank my PhD supervisor Achim Brauer, head of Section 5.2 'Climate Dynamics and Landscape Evolution' at the GFZ. I am grateful for his continuous support, his inspiration, and for letting me benefit from his comprehensive expertise.

I want to quote Peter Dulski, Rudolf Naumann, Gerrit Lohmann, Birgit Plessen, Norel Rimbu, and Raphael Scheffler who substantially contributed to the results of this thesis. Brian Brademann, Achim Brauer, Michael Köhler, Richard Niederreiter, Florian Ott, Oliver Rach, and Uli von Grafenstein are acknowledged for taking part in the coring campaigns at Lake Ammersee. I thank Gaby Arnold, Dieter Berger, and Michael Köhler for preparation of thin sections and am indebted to Petra Meier for C/N measurements and Helga Kemnitz for introducing me into the REM facility at the GFZ. Christine Gerschke managed the administrative work, Andreas Hendrich helped with the layout of the figures, and Marcus Günzel kept the computer running throughout the years. Thanks.

Special thank goes out to my roommates Helge Arz, Beatrice Ghilardi, Lucas Kämpf, Takeshi Nakagawa, Michael O'Connell, Florian Ott, for the right mixture of concentration, discussion, and a lots of fun. Thanks to my further PhD fellows Anoop Ambili, Ina Neugebauer, Stefan Lauterbauch, Gordon Schlolaut, Tina Swierczynski, as well as everyone at Section 5.2 of the GFZ for their astonishing engagement, continuous support, and patience.

Finally, I want to express my gratitude to all my friends and family for their love, support and inspiration.

(1) Introduction

1.1. Scientific context

Climate is the principle driving force of hydrological extremes like floods, and thermodynamic increase in atmospheric water vapor is expected to increase the likelihood of such events when Earth warms (IPCC, 2007). Furthermore, natural climate variability affects the frequency and magnitude of floods on annual to millennial time-scales (IPCC, 2012). Particularly in the mid-latitudes of the Northern Hemisphere, correlations between meteorological variables and hydrological indices suggest significant effects of changing climate boundary conditions on floods (Knox, 2000; Mudelsee et al., 2003). To date, however, understanding of changes in frequency and magnitude of floods in response to varying climate forcing is limited due to the scarcity of hydrological data in space and time (IPCC, 2012). For adequately evaluating and anticipating the response of floods to changing climate boundary conditions it is, therefore, crucial to study the receptiveness of floods to natural climate forcing mechanisms on both short and long time-scales and on a regional basis (Knox, 1993; Mudelsee et al., 2003).

Geological records potentially provide long-term information on floods (Kochel and Baker, 1982). The classical approach in 'paleoflood hydrology' is to explore the potential of geomorphological features along the river like erosional marks, silt lines, and overbank deposits for flood reconstruction (Gilli et al., 2013). For the latter, in the backwaters of floods fine sediments deposit when the flow velocity of the transporting stream is reduced. Using multiple of these overbank deposits at different elevations in the floodplain allows to assess the magnitude of a flood. The resulting succession of flood deposits can be chronologically constrained by means of ^{14}C and OSL dating (Baker, 2008). Overbank records, however, suffer from incompleteness due to erosion of earlier deposited sediments by the river and varying lateral limits of flood triggered sedimentation (Gilli et al., 2013).

Lake sediments provide more continuous records of flood activity (e.g. Noren et al., 2002; Gilli et al., 2013). During floods, detrital catchment material is transported in suspension into downstream lakes (Fig. 1.1) and deposited as a distinct detrital layer, when the transport capacity of the inflowing turbidity current successively diminishes in the water body

(Lambert et al., 1976; Sturm and Matter, 1978). Even though already recognized in the late 1970's the potential of flood triggered detrital layers in lakes for long flood calendars was not explored until more than a decade later, when Siegenthaler and Sturm (1991) established a 700-year record of extreme floods from sediments of Lake Uri. Since than, a growing number of flood reconstructions particularly from Europe and North America has been established using various geochemical, geophysical, and biological proxies on non-varved lake sediments (e.g. Thorndycraft et al., 1998; Nesje et al., 2001; Noren et al., 2002; Chapron et al., 2002; Gilli et al., 2003; Arnaud et al., 2005; Osleger et al., 2009; Støren et al., 2010; Debret et al., 2010; Stewart et al., 2011; Gilli et al., 2012; Wilhelm et al., 2012). These flood records provide valuable data on multi-decadal changes in flood frequency and magnitude in response to varying natural baseline climate, but lack the time-resolution necessary for identifying short-term flood variability and seasonality.

Figure 1.1. Suspended sediments in Lake Ammersee supplied by Ammer river floods.

Intra-annual climate variability, however, strongly affects regional flood characteristics with respect to triggering atmospheric circulation patterns (Mudelsee et al., 2003; Sivapalan et al., 2005). Varved lake sediments allow to isolate these effects. Individual flood layers can be dated to the season by varve counting and determination of the microstratigraphic position within an annual sedimentation cycle (Fig. 1.2) (Mangili et al., 2005; Czymzik et al., 2010; Swierczynski et al., 2012a). In addition, the seasonal resolution narrows the usually decadal to multi-decadal gap between geological and instrumental data and enables a more direct calibration of flood layer time-series with measured runoff records (Czymzik et al., 2010).

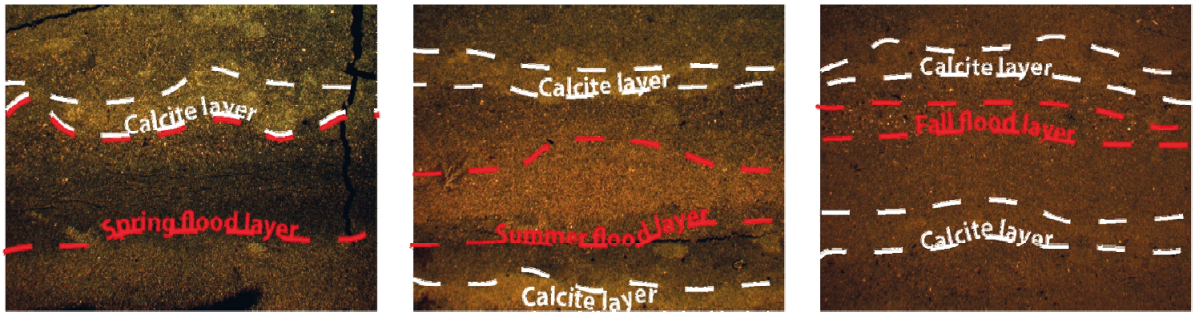

Figure 1.2. Determination of flood layer seasonality in Lake Ammersee sediments by the microstratigraphic position within a varve.

1.2. Site and sediments

Lake Ammersee is located in the pre-alpine region of southern Germany ~20 km southwest of Munich (48°00'N, 11°07'E), at an elevation of 533 m asl. (Fig. 1.3) The basin was eroded into Cenozoic sediments by the Ammersee lobe of the Isar-Loisach glacier. The present day lake has a surface area of 47 km² and a maximum water depth of 81 m (Alefs, 1997).

Previous studies on oxygen isotopes from ostracods have proven the sediment record as a reliable paleoclimate archive enabling high-resolution temperature reconstruction (von Grafenstein et al., 1996; 1999). Annual layering of the sediments enables precise detection and dating of flood triggered fluxes of catchment material into the lake (Alefs, 1997). Flysch, molasse, and late moraine formations in the meso-scale catchment provide abundant fine-grained detrital material for downstream transport into the gully shaped lake by only one main tributary, River Ammer (Fig. 1.3). High water tables in the northern part of the catchment and low water holding capacities of the alpine soils favor the translation of extreme rainfall into floods through saturation excess overland flow (Ludwig et al., 2003). Available instrumental River Ammer runoff data back to AD 1926 (provided by the Wasserwirtschaftsamt Weilheim) allow calibrating the sedimentary record.

Today, hydrology in the Ammersee region is controlled by competing influences of maritime cyclonic weather regimes transporting moisture from the North Atlantic into central Europe and continental atmospheric blocking by high-pressure cells (Petrow and Merz, 2009). Mean annual precipitation is 1200 mm. The strongest River Ammer floods occur after rainfall maxima from late spring to summer (Czymzik et al., 2010).

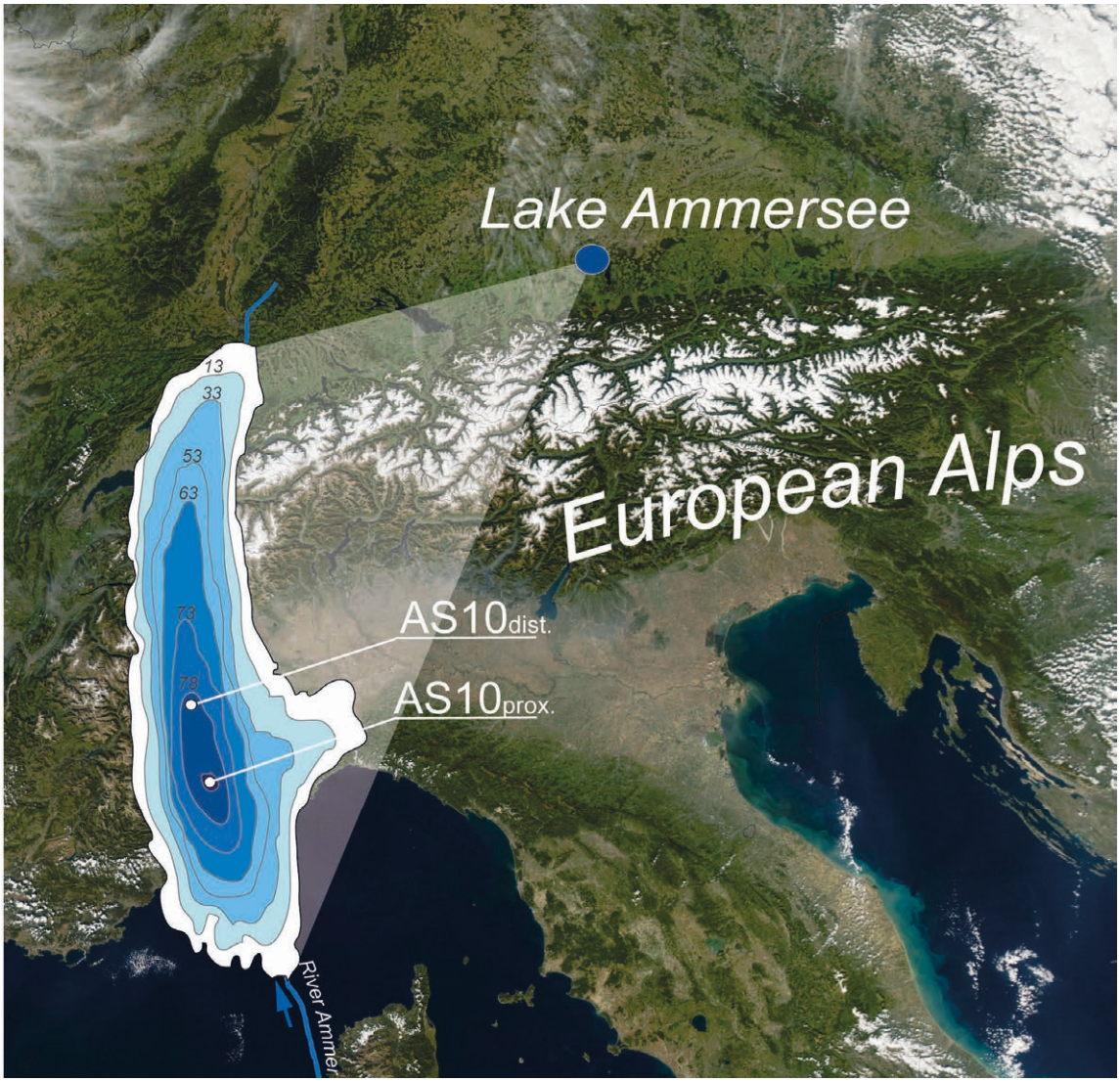

Figure 1.3. Geographical position and bathymetric map of Lake Ammersee showing the Ammer river inflow and coring locations of sediment profiles $AS10_{prox}$ and $AS10_{dist}$.

Continuous sediment profiles $AS10_{prox}$ and $AS10_{dist}$. In summer 2010, at two locations in the profundal of Lake Ammersee, overlapping sediment cores consisting of 2 m segments were retrieved at a distance of a few meters using a modified UWITEC piston corer installed on a stationary float (Fig. 1.4). Sediment profile $AS10_{prox}$ (overlapping cores C and D) is located in a more proximal (4.4 km) and sediment profile $AS10_{dist}$ (overlapping cores A and B) in a more distal (6.2 km) position towards the Ammer river inlet. Retrieving parallel sediment cores with overlapping segments enables to establish continuous composite profiles. Short sediment cores AS07-P1 and AS07-P2 (Manuscript 1) were retrieved from the same locations as sediment profiles $AS10_{dist}$ and $AS10_{prox}$ (Manuscripts 2 and 3) and, thus, represent parallel sequences.

Figure 1.4. Sediment coring on Lake Ammersee in summer 2010 using a modified UWITEC piston corer installed on a stationary float.

1.3. Scientific objectives

(***1***) Primary scientific objective of this thesis is *to explore and better understand the potential of varved lake sediments as long-term seasonally resolved flood archives*. Flood layer deposition is influenced by both climatic impacts and environmental effects like e.g. anthropogenic land-use change and seasonally varying soil moisture and erosion conditions. A systematic survey of the results from both Lake Ammersee sediment profiles will shed light on the physical processes behind detrital layer deposition and allow to better distinguish both effects.

(***2***) The varved nature of Lake Ammersee sediments reduces the usually decadal-scale resolution of non-varved lake sediment records to the season allowing to better calibrate the sediment data using instrumental time-series. *Comparison to instrumental River Ammer runoff and meteorological data from the Meteorological Observatory Hohenpeißenberg* will help to assess the 'completeness' of the geological flood record and enables a process-orientated evaluation of detrital deposition, based on a broad database for each single event.

(***3***) Further scientific objective is *to attribute flood generating climate forcing mechanisms* by comparison with well-dated paleoclimate and climate forcing time-series and using reanalysis

models. The selected time interval covering the last 5500 years is suitable to adequately detect flood-triggering climate mechanisms on both short and long time-scales.

1.4. Scientific tasks/Methods

Establishment of a seasonal flood layer record from two varved sediment profiles includes three main methodological steps:

(***1***) *Microscopic microfacies analyses on overlapping petrographic thin sections and X-ray fluorescence scanning at 200 µm step size* on Lake Ammersee sediment profiles $AS10_{prox}$ and $AS10_{dist}$ to detect the sedimentological and geochemical features of even fractions of a mm thick detrital layers (Fig. 1.5).

(***2***) *Microscopic varve counting*, verified by accelerator mass spectrometry (AMS) ^{14}C dating of terrestrial plant macrofossils, for down to seasonally resolved flood layer stratigraphies.

(***3***) *Intra-basin correlation of flood layers in $AS10_{prox}$ and $AS10_{dist}$* by means of varve chronology and stratigraphy in order to better understand sediment transport and deposition processes within the lake basin.

To investigate Lake Ammersee sediments in more detail, the continuous high-resolution record is complemented by multi-proxy analyses of discrete varve and detrital layer samples. The methodological approach includes X-ray diffractometry, scanning electron microscopy, grain-size analyses with a laser particle sizer, stable oxygen and carbon isotope ratios, as well as total carbon and nitrogen contents.

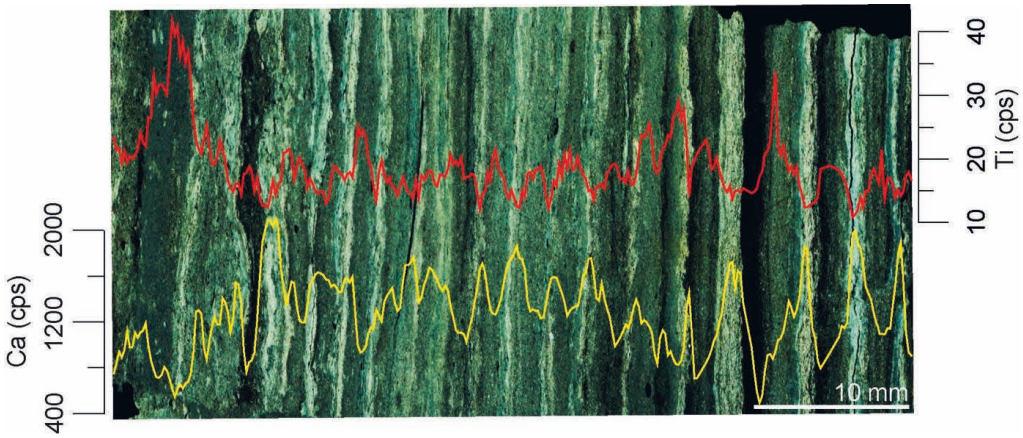

Figure 1.5. Thin section scan showing Lake Ammersee varves and detrital layers overlain by corresponding µ-XRF data of the elements Titan (Ti) and Calcium (Ca).

1.5. Organization of the thesis

The thesis is conceptualized as a 'cumulative thesis' subdivided into seven chapters and a data appendix. Following this introduction giving essential background information (Chapter 1), chapters 2 to 4 present the scientific work subdivided into three manuscripts (Table 1.1). The essentials of the three manuscripts build up on each other. The first manuscript titled 'A 450-year record of spring-summer flood layers in annually laminated sediments from Lake Ammersee (southern Germany)' (Chapter 2) informs about the establishment of a 450-year flood layer time-series from two varved short sediment cores of Lake Ammersee. In order to verify the detrital layer succession as a flood record through time and to better understand flood triggering atmospheric circulation at Lake Ammersee, the time-series is calibrated with instrumental runoff, local precipitation, and weather regime data. The second manuscript 'Shifts of Mid- to Late Holocene flood intensity in detrital layers from varved sediments of pre-alpine Lake Ammersee (southern Germany)' (Chapter 3) informs about the reconstruction of a 5500-year flood layer time-series from two varved Lake Ammersee sediment profiles and gives detailed insight into sedimentology and geochemistry of the cores, chronological issues, and correlation of both sediment profiles. The interpretation section of the manuscript elaborates on potential biases in flood layer time-series, as well as multi-millennial effects on flood intensity at Lake Ammersee. The third manuscript 'Atmospheric control of flood frequency in central Europe throughout the past 5500 years' (Chapter 4) focuses on paleoclimatological issues. Decadal to millennial-scale correlations of flood frequency at Lake Ammersee with climate variables are presented and potential flood triggering atmospheric mechanisms are analyzed by means of reanalysis models. Summary and conclusions of the thesis are given in chapter 5. The references are listed in chapter 6. Flood layer data from $AS10_{prox}$ and $AS10_{dist}$ are presented in the data appendix (Chapter 7) and are/will be available at the PANGAEA data library after publication of the single manuscripts.

Chapter	Publication	Status
Chapter 2 (Manuscript 1)	*Markus Czymzik, Peter Dulski, Birgit Plessen, Ulrich von Grafenstein, Rudolf Naumann, Achim Brauer*. A 450-year record of spring-summer flood layers in annually laminated sediments from Lake Ammersee (southern Germany).	*Water Resources Research* **46,** W11528 (2010). Data at: doi:10.1594/PANGAEA.746240
Chapter3 (Manuscript 2)	*Markus Czymzik, Achim Brauer, Peter Dulski, Birgit Plessen, Rudolf Naumann, Ulrich von Grafenstein, Raphael Scheffler.* Shifts of Mid- to Late Holocene flood intensity in detrital layers from varved sediments of pre-alpine Lake Ammersee (southern Germany).	*Quaternary Science Reviews* **submitted** (2012).
Chapter 4 (Manuscript 3)	*Markus Czymzik, Achim Brauer, Gerrit Lohmann, Norel Rimbu, Peter Dulski.* Atmospheric control of flood frequency in central Europe throughout the past 5500 years.	**in prep**. (2012).

Table 1.1. Manuscripts presented within this thesis.

1.6. Author's contribution

Manuscript 1 (Chapter 2). I performed microfacies analyses and varve counting on two short sediment cores, measured μ-XRF data in cooperation with Peter Dulski, oxygen and carbon isotope ratios, as well as total carbon and nitrogen contents in cooperation with Birgit Plessen, XRD data in cooperation with Rudolf Naumann, and took scanning electron microscopy photos in cooperation with Helga Kemnitz. I analyzed the data, reviewed the relevant literature, and wrote the manuscript. I developed the idea of a flood record and calibrated the detrital layer stratigraphy with instrumental River Ammer runoff and weather regime data. The co-authors, the reviewers, and particularly Achim Brauer substantially helped to improve the final manuscript.

Manuscript 2 (Chapter 3). I organized and lead the coring campaign at Lake Ammersee. I constructed the composite profiles, performed microfacies analyses, varve counting, and intra-basin correlation. I performed μ-XRF measurements in collaboration with Peter Dulski, total carbon and nitrogen measurements in collaboration with Birgit Plessen, XRD measurements in collaboration with Rudolf Naumann, and laser particle sizer grain-size measurements. I analyzed all data, reviewed the relevant literature, and wrote the manuscript. I induced the concept of combined orbital and solar forcing on flood intensity at Lake Ammersee. Achim

Brauer critically reviewed and substantially improved the draft manuscript. The co-authors reviewed the paper.

Manuscript 3 (Chapter 4). I analyzed microfacies and μ-XRF data, developed the idea of a solar influence on atmospheric circulation and flood frequency at Lake Ammersee, and wrote the draft manuscript. Gerrit Lohmann and Norel Rimbu established reanalysis models and performed single spectrum analyses. All co-authors critically reviewed and helped to improve the manuscript.

(2) A 450-year record of spring-summer flood layers in annually laminated sediments from Lake Ammersee (southern Germany)

Markus Czymzik,[1] Peter Dulski,[1] Birgit Plessen,[1] Ulrich von Grafenstein,[2] Rudolf Naumann,[3] Achim Brauer[1]

[1] GFZ German Research Centre for Geosciences, Section 5.2 Climate Dynamics and Landscape Evolution, Telegrafenberg, 14473 Potsdam, Germany

[2] Laboratoire des Sciences du Climat et de l'Environnement, UMR CEA-CNRS, Orme des Mersiers, 91191 Gif-sur-Yvette, France

[3] GFZ German Research Centre for Geosciences, Section 4.2 Inorganic and Isotope Geochemistry, Telegrafenberg, 14473 Potsdam, Germany

published in *Water Resources Research*, 46, W11528 (2010)

Abstract. A 450-year spring-summer flood layer time-series at seasonal resolution has been established from the varved sediment record of Lake Ammersee (southern Germany) applying a novel methodological approach. The main results are (1) a precise chronology obtained by microscopic varve counting, (2) the identification of detrital layers representing flood-triggered fluxes of catchment material into the lake, and (3) the recognition of the seasonality of these flood layers from their micro-stratigraphic position within a varve. Tracing flood layers in a proximal and a distal core and correlating them applying the precise chronology provided information on the depositional processes. Comparing the seasonal flood layer record with daily runoff data of the inflowing River Ammer for the period from 1926 to 1999 allowed defining an approximate threshold in flood magnitude above which the formation of flood layers becomes very likely. Moreover, it was for the first time possible to estimate the 'completeness' of the flood layer time-series and to recognize that mainly floods in spring and summer representing the main flood seasons in this region are well preserved in the sediment archive. Their frequency distribution over the entire 450-year time-series is not stationary, but reveals maxima for colder periods of the Little Ice Age when solar activity was reduced. The observed spring-summer flood layer frequency further shows similar trends as the occurrence of flood-prone weather regimes since AD 1881, probably suggesting a causal link between solar variability and changes in mid-latitude atmospheric circulation patterns.

2.1. Introduction

Assumptions about an increase in extreme flood events due to an intensified hydrological cycle caused by global warming still are in discussion and have to be better verified. Statistical flood analyses indicate that simple mechanistic explanations are not straightforward and that complex seasonal (Mudelsee et al., 2003) and regional (Petrow and Merz, 2009) effects have to be considered. Some historical flood records even indicate that flood frequencies were higher during colder periods (Knox, 1993; Glaser and Stangl, 2004) questioning the hypothesis of a correlation between the frequency of extreme floods and warmer climate. However, the length of presently available flood time-series is not sufficient for a profound understanding of possible relations between flood frequencies and climatic boundary conditions. This is largely due to the lack of long-term instrumental flood data that rarely exceeds a century (Baker, 2006) and thus only covers the period of strongest human interferences in most river catchments.

In addition to the extension of flood time-series into the recent past by exploiting historical archives, natural archives are available that record climate changes and the occurrence of extreme events even much further back in times without any human activity. Particularly, river and lake sediments have been proven as suitable long flood records (e.g. Dearing, 1991; Thorndycraft et al., 1998; Dearing et al., 2001; Thorndycraft and Benito, 2006). These geological archives provide crucial information for a better evaluation of flood occurrences under different climate boundary conditions, which are often not considered for flood frequency calculations assuming a stationary climate (Knox and Kundzewicz, 1997). However, it must be considered that investigating geological archives focusing on extreme event occurrences is still at its beginning. One key question is the degree of 'completeness' to which geological archives record flood events. Filling this gap in knowledge requires calibrating the paleoflood record with instrumental and/or historical flood data. However, merging geological and instrumental time-series is not straightforward because of their very different temporal resolution. A novel approach to bridge these gaps in time resolution is to reduce the commonly not better than decadal-scale resolution of geo-archives by utilizing annually laminated lake sediments. Fine, millimeter to sub-millimeter laminations in lake sediments formed by seasonally varying deposition processes are defined as varves and provide both, precise time control by varve counting and climatic and environmental information at seasonal resolution (Brauer and Casanova, 2001; Brauer, 2004).

In varved lake sediments, flood-triggered fluxes of eroded fine catchment material result in the deposition of characteristic detrital layers which can be determined with seasonal precision by their micro-stratigraphical position within the annual sedimentation cycle (Mangili et al., 2005; Brauer et al., 2008). However, reconstructing flood time-series from lake sediments necessitates a comprehensive understanding of the entire cascade of processes from sediment erosion and transport in the catchment, to distribution and deposition in the lake basin in order to rule out other causes for event layer deposition such as slope failure or debris flow (Mangili et al., 2005; Swierczynski et al., 2009).

Lake Ammersee is an ideal location to build up a long flood record because previous work has proven this sediment profile a sensitive proxy archive for high-resolution paleotemperature reconstruction (e.g., von Grafenstein et al., 1996, 1999). Preservation of annual laminations enables accurate detection and precise dating of flood triggered detrital material in the sediment with seasonal precision. In addition, a wealth of meteorological and hydrological data is available from local authorities in order to compare the geological and instrumental time-series. Therefore, two new short sediment cores have been studied applying a novel methodological approach which combines microfacies analyses, high-resolution element scanning (µ-XRF), stable isotope data from bulk carbonate samples ($\delta^{13}C_{carb}$, $\delta^{18}O_{carb}$), and X-ray diffraction (XRD) analyses (Brauer et al., 2009). Integrating these analytical techniques enables a better and more precise identification and interpretation of flood layers at microscopic scales which previously have not been detected.

2.2. Study Site

Lake Ammersee (533 m asl.) is a hardwater lake located in South Germany (48°00'N, 11°07'E) with a surface area of 47 km^2 and a maximum depth of 81.1 m (Fig. 2.1). The 16.2 km long and 2.8 km wide basin is shaped into Cenozoic sediments by the Ammersee lobe of the Isar-Loisach glacier (Alefs, 1997). The catchment of the main tributary River Ammer has a size of 709 km^2 and reaches a maximum elevation of 2185 m asl. (Ludwig et al, 2003). The Ammer arises in the Bavarian Calcareous Alps and flows northwards through smoothly shaped pre-alpine flysch, molasse, and late moraine formations (Mangelsdorf and Zelinka, 1973) before entering the lake at its southern end (Fig. 2.1). Detrital sediment is supplied to the lake nearly exclusively by the Ammer River (Alefs, 1997). Secondary inflows like the River Rott and the Fischbach have negligible effects on the detrital sediment supply into the

lake basin (LfW, 2005). The Ammer river mouth was artificially displaced for approx. 1 km to the southeastern part of the lake during channelization of the river bed between AD 1920 and 1924 (Alefs, 1997) (hereafter all dates are given in the AD notation). Before that time the River Ammer inlet was located at the present-day inlet of the River Rott, a former Ammer tributary (Fig. 2.1).

The Ammer catchment is located in the hydrologic transition zone between maritime North-Atlantic and continental climate influenced by both, weather regimes related to frequent cyclonic westerly airflow and atmospheric blocking through high-pressure fields (Petrow and Merz, 2009). The pluvio-nival runoff regime indicates maximum flow rates during the transition from snow melt periods in spring to precipitation maxima in summer. Limited storage capacities of the alpine soils and high water tables in the northern valleys of the catchment favor frequent floods dominated by saturation excess overland flow. The steep (relief difference of 1652 m) and rather small catchment favors short but high runoff peaks (Ludwig et al, 2003).

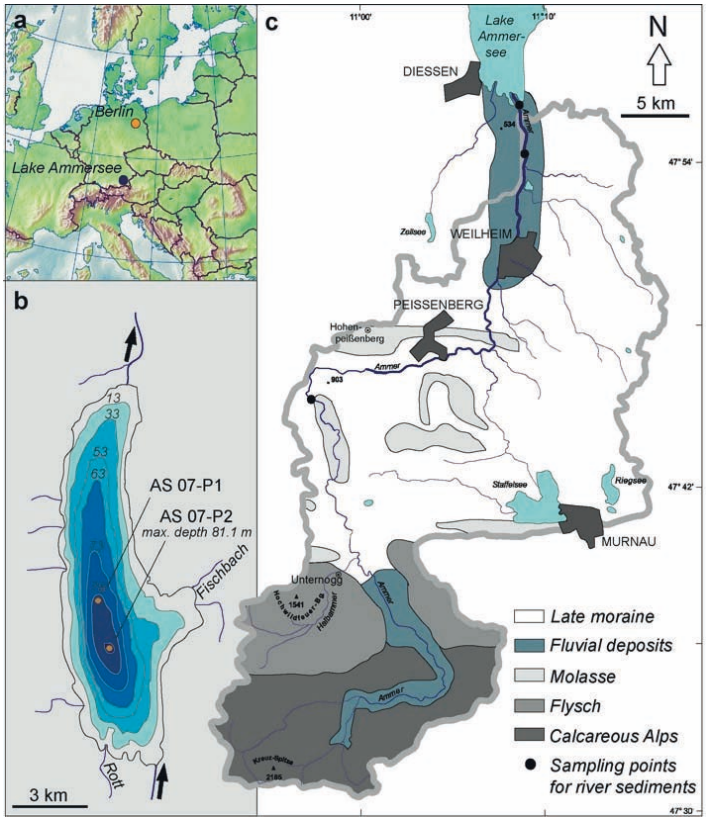

Figure 2.1. (**a**) Geographical overview and (**b**) bathymetric map of Lake Ammersee including positions of cores AS07-P1 (distal) and AS07-P2 (proximal). (**c**) Hydrogeological sketch of the Ammer catchment.

2.3. Methods

2.3.1. Sediment coring

Two short sediment cores (AS07-P1= 133 cm and AS07-P2 = 134 cm) were retrieved from the deepest part of the lake basin in June 2007 with a modified UWITEC short-core system. Core AS07-P1 is located in a distal (6.2 km) and core AS07-P2 in a more proximal (4.4 km) position towards the Ammer river mouth (Fig. 2.1).

2.3.2. Microfacies analyses

For microfacies analyses and measurements of seasonal sub-layer properties, two overlapping series of 16 thin sections from core AS07-P1 and 9 thin sections from core AS07-P2 were investigated using a petrographic microscope (Carl Zeiss-Axiophot, Jena). Preparation of undisturbed thin sections from wet and soft sediments is a crucial methodological prerequisite to adequately perform micro-stratigraphical investigations and includes careful freeze-drying and epoxy resin impregnation (Brauer and Casanova, 2001). The bottom part of core AS07-P2 was disturbed during core-splitting thus preventing from further thin section preparation. Consequently, the investigated interval of this core is shorter. Various magnifications, optical and light conditions were used for microfacies analyses. Thickness measurements of detrital layers were performed at 25x magnification. Microfacies analyses were not always applicable for very thin detrital layers (< 1 mm). A precise chronology was constructed by calcite varve counting. Short intervals of poor varve preservation were interpolated using annual sedimentation rates as calculated from varve thickness measurements in well-preserved adjacent varve sections.

Owing to the disturbances in the bottom part of core AS07-P2 and higher sedimentation rates at this more proximal location, this core covers a shorter time interval than the distal core AS07-P1. Therefore, precise varve-to-varve correlation including comparison of microfacies is available only for the upper 60 cm of the distal core AS07-P1 covering the last 200 years (Fig. 2.2). The older interval of the entire 450-year flood layer record has been established from the bottom part of core AS07-P1 alone without the parallel sediment sequence from the proximal site.

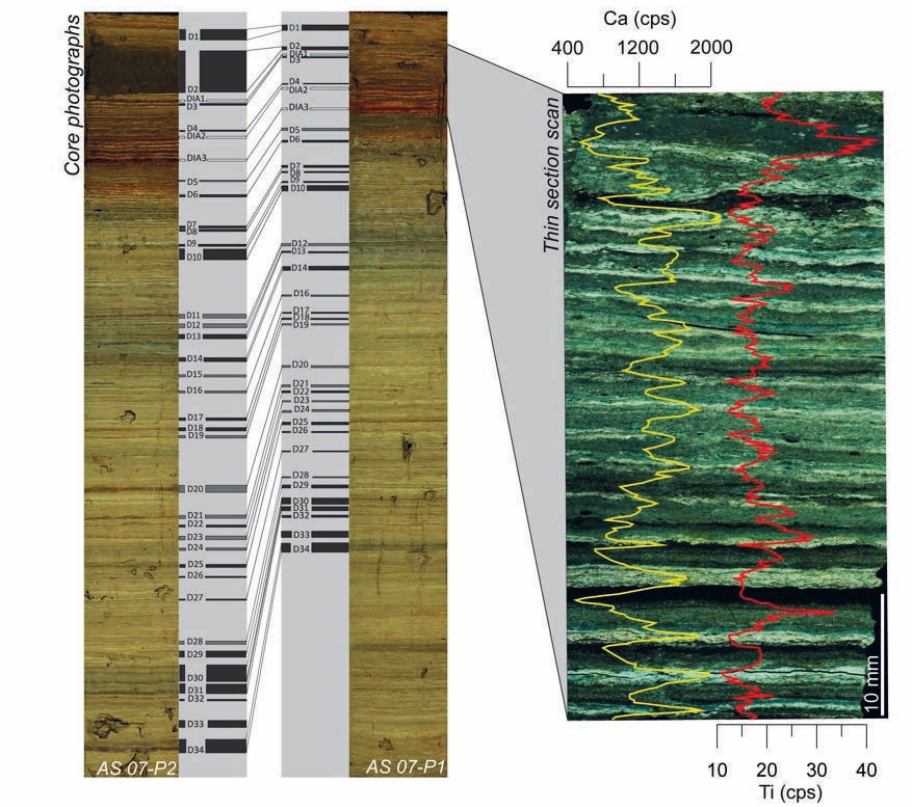

Figure 2.2. (left) Varve-to-varve correlation of detrital layers D1 to D34 and monospecific diatom layers DIA1 to DIA3 (white bars; not mentioned in the text) between core AS07-P1 and AS07-P2. Dark gray bars mark microscopically correlated detrital layers showing both, the same micro-stratigraphic position and microfacies. Correlating detrital layers indicated with light gray bars exhibit different microfacies in each core. (right) Thin section scan with polarizing filter but without microscopic magnification showing calcite varves with intercalated detrital and diatom layers (AS07-P1, 3-8 cm core depth). Distinct positive µ-XRF excursions of the element Ti (cps) indicate detrital layers. Calcite layers are represented by positive Ca (cps) and darker layers by small positive Ti (cps) excursions.

2.3.3. Micro X-ray fluorescence scanning, stable isotope ratios from bulk carbonates, and X-ray diffraction

Microscopic data have been combined with high-resolution element scanning (µ-XRF), stable isotope ratios from bulk carbonate samples ($\delta^{18}O_{carb}$, $\delta^{13}C_{carb}$), and X-ray diffraction (XRD). Micro-XRF scanning of major elements (Mg, Al, Si, P, S, Cl, K, Ca, Ti, Mn, Fe, Sr) at 200 µm resolution has been carried out on the fresh sediment surface of both cores with an EAGLE III BKA µ-XRF spectrometer (Röntgenanalytik Messtechnik GmbH, Taunusstein). The resulting time resolution is about 10 data points for each varve (*i.e.* year). The scanner data can be precisely matched to microfacies data because both datasets were measured from the same section plane of the splitted cores (Brauer et al., 2009). For single line measurements

the tube voltage was set at 40 kV, with a tube current of 450 µA. Dwell time for each measurement was 30 seconds. Each data point reflects the mean element intensity of one measured spot, expressed in counts per second (cps).

Stable oxygen and carbon isotope ratios of bulk carbonate samples were measured with a GasBench II (Thermo Electron, Bremen) connected to a DELTAplusXL Isotope Ratio Mass Spectrometer (ThermoFisher Scientific, Waltham) working in continuous flow mode. Samples were extracted from freeze dried and powdered 5 mm sediment slices of both cores representing a two-year resolution. Depending on the carbonate content, 0.25 to 0.5 mg of sample material was loaded into 10 ml vials. After automatically flushing the vials with He, the samples were treated with 100 % phosphoric acid at 75°C for 60 min in the GasBench preparation system following the analytical procedure described in Spötl and Vennemann (2003). Isotopic compositions of the samples are given relative to the VPDB standard in the δ notation. $\delta_A=(R_{SA}/R_{ST}-1)x10^3$ (‰), where R_{SA} is the isotopic ratio ($^{13}C/^{12}C$; $^{18}O/^{16}O$) of the sample and R_{ST} that of the standard. Calibration was performed against three international reference standards (NBS 19, CO1, CO8). The 1-sigma precision of replicate measurements of NSB 19 is 0.06‰ for $\delta^{13}C$ and 0.08‰ for $\delta^{18}O$.

XRD analyses of 11 representative samples selected by microscopic observations were carried out using a Siemens Diffraktometer 5000 (Siemens, Karlsruhe). Seven measurements were performed on 1 cm sediment samples reflecting the different types of detrital microfacies. Four measurements were carried out on 1 cm bulk samples of regularly varved sediment, thus representing 4-5 varve years.

2.4. Results

2.4.1. Varve microfacies and chronology

The sediments consist of calcite varves with intercalated detrital layers (Alefs, 1997; Alefs and Müller, 1999). 97 % of the sediment profile exhibits well known structures of calcite varves consisting of couplets of discrete light calcite layers and darker organic layers (e.g. Lotter and Lemcke, 1999; Brauer et al., 2008). Since endogenic calcite precipitation is mainly induced through (1) biogenic assimilation of CO_2 by photosynthesizing phytoplankton and (2) temperature increase (Kelts and Hsü, 1978; Stabel, 1986; Bluszcz et al., 2008) calcite layers form in the spring-summer season. Darker layers consist of detrital and amorphous organic

material, and littoral calcite, all internally re-deposited through wave activity during fall and winter seasons. A clear change in varve microfacies is observed for the interval from 1960 to 1980. During this period, two sub-layers of a coarser (5-7 µm) basal and a finer (2-4 µm) upper calcite layer were deposited, each preceded by a diatom layer. This double calcite layer pattern is related to higher productivity during the lake's main eutrophication phase and has been also observed at Lake Zurich (Kelts and Hsü, 1978).

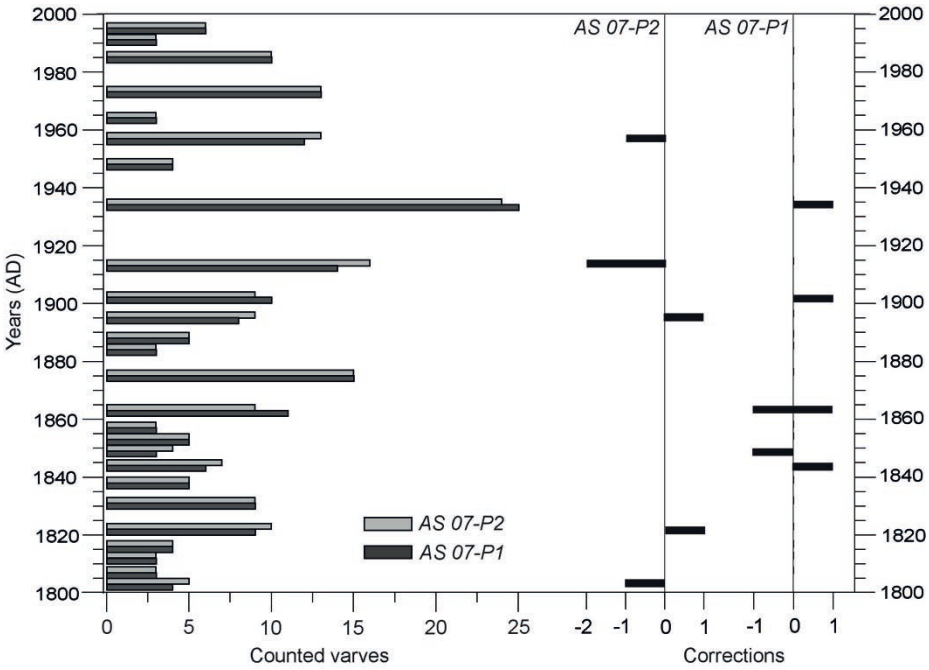

Figure 2.3. Comparison of varve chronologies for AS07-P1 and AS07-P2. Varves counted between two marker layers and corrections made for the composite chronology.

In the first step, two independent varve chronologies were established for each core by microscopic calcite varve counting from 1999 back to 1545 (AS07-P1) and 1800 (AS07-P2). The disturbed sediment-water interface due to the coring process prevented from counting the uppermost seven varves. Therefore, the resulting chronology was floating and had to be anchored to the absolute time scale using an exceptional detrital layer of known age (D2, Fig. 2.2). Sediment trap studies close to the coring site of AS07-P2 have proven the deposition of this layer in July 1993 (Alefs et al., 1996) after a break-up of an armor layer in the Ammer tributary Halbammer (see section 2.5.1). The deposition time of this layer is confirmed by a sediment core obtained from Lake Ammersee on October 06th 1993 (AS T_{max}93) by U. von Grafenstein showing layer D2 on the top of the core. Some short intervals of poor varve

preservation comprising between two and six years appear in 14.9 % of AS07-P1 and in 22.5 % of AS07-P2. These intervals were interpolated using the mean varve thickness of well-preserved adjacent sediment intervals (2.2 mm for AS07-P1 and 2.6 mm for AS07-P2).

In the second step, a composite chronology was established back to 1800 through combining counts of the best preserved parts of each chronology ('best-of' composite). This has been achieved through comparison of varve counts separately for 26 intervals of about the same length precisely defined through distinct marker layers (Fig. 2.3). Such detailed comparison allowed identification of even single missing varves in either of the cores and to bridge poorly preserved varve intervals in one core by using the varve count from the parallel core (Brauer et al., 2008).

In the final step, the resulting composite chronology was compared with historical Ammer flood observations from the city chronicle of Weilheim/Ammer (Alefs, 1997) indicating an over-estimation of two varves in the interval from 1884 to 1912. The entire varve chronology back to 1545 has then been corrected for this bias. The resulting composite chronology differs less than 2% from a previous varve chronology for Lake Ammersee sediments reaching back to 1786 (Alefs, 1997).

2.4.2. Detrital layer microfacies

Three main classes of detrital microfacies have been distinguished in the studied sediment interval: (1) graded layers, (2) silt/clay layers, and (3) matrix-supported layers (Fig. 2.4). Thirty-four detrital layers in the parallel parts of both cores were studied and compared in detail for microfacies and layer thickness:

1. Graded layers. This layer type is characterized by a normal grading from fine sand and coarse silt (average grain size of 30 µm) to clay (< 2 µm). A sharp lower boundary clearly segregates the basal part of the layer from the underlying sediment. Multiple grading and flame structures in the basal part appear within few layers of this type. Thirteen of 34 correlating detrital layers exhibit this microfacies in both cores. The thickest graded layer is 10.8 mm (Figs. 2.4 and 2.5).

2. Silt/clay layers. No particular textural organization, except for a hardly visible faint grading in few cases, defines this layer type. The fine silt/clay detritus lacks the coarser material included in graded layers but shows the same elemental, isotopic, and mineralogical

composition as the other detrital microfacies (see section 2.4.3). Four of 34 correlating detrital layers exhibit this layer type in both cores (Figs. 2.4 and 2.5). The thickest layer of this type is 9.6 mm.

3. Matrix-supported layers. These layers consist of predominantly fine sand to coarse silt detrital grains in a matrix of clots of endogenic calcite. Horizontally oriented plant remains and littoral diatoms appear solely in this layer type. The textural organization shows in a few cases weak grading. Six of 34 correlating detrital layers are matrix-supported layers in both cores (Figs. 2.4 and 2.5). The thickest matrix-supported layer is 47.1 mm (D2).

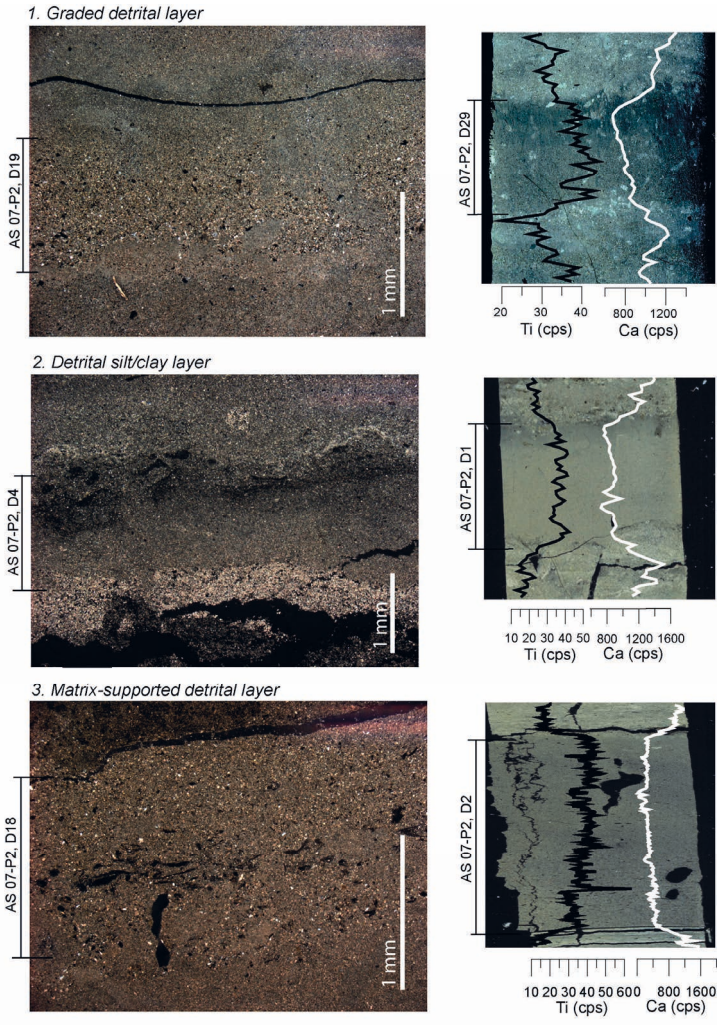

Figure 2.4. Polarized microscope photos (25x) and thin section scans of detrital microfacies: (**1**) graded layers, (**2**) silt/clay layers, and (**3**) matrix-supported layers. Detrital microfacies are confirmed by positive Ti and negative Ca µ-XRF excursions. Note that microscope and thin section images are from different layers.

Varve-to-varve correlation between both cores allowed identifying differences in microfacies for the same event of detrital matter flux into the lake basin and provides information on sediment transport processes within the lake. Four out of 34 layers exhibit different microfacies in each core. These are graded layers in the proximal core AS07-P2 which correlate to matrix-supported layers in the distal core AS07-P1 (D12, D16, D19, D21). For one graded (D11) and one matrix-supported layer (D15) in the proximal core, no correlating layer has been found in the distal core (Fig. 2.5). In one case (D 11) this might be due to slight sediment distortions probably caused during sample preparation, while the amount of detrital matter forming layer D15 at the proximal site was too low (very thin layer) to reach the distal core position. Microfacies types for four layers could not be unambiguously classified in one of the cores (Fig. 2.5): two of these are matrix-supported layers in the proximal core (D20, D23), one is a graded layer in the proximal core (D28), and one a graded layer in the distal core (D5). One layer was not classifiable in both cores (D24). A likely explanation for these problems in microfacies classification are minor artifacts caused during sample preparation.

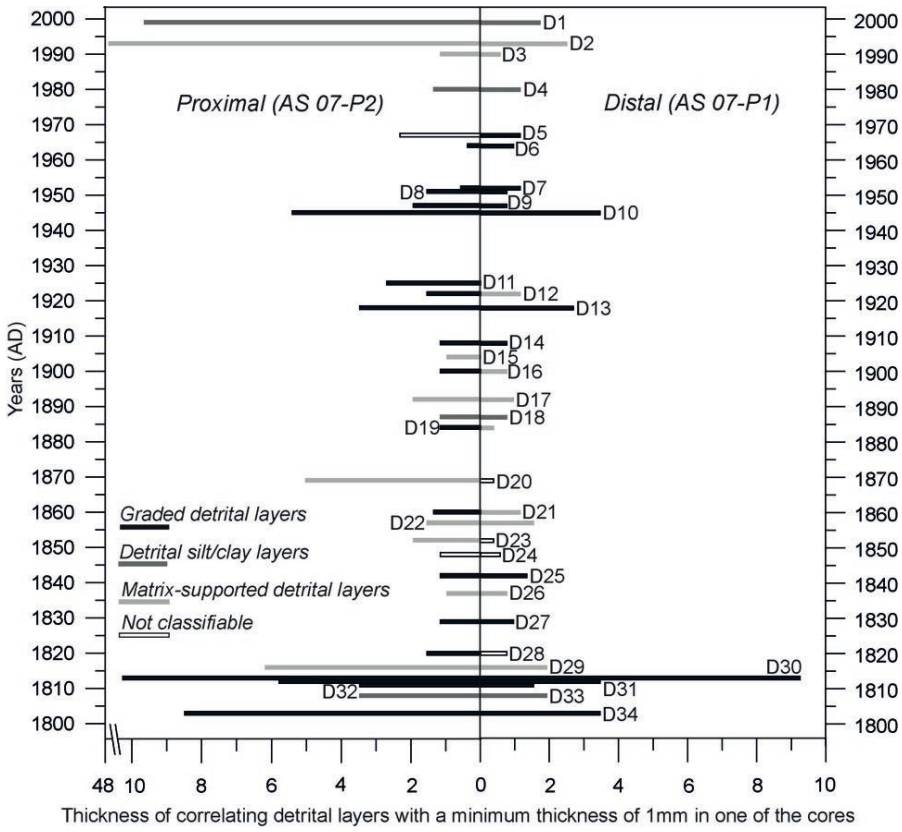

Figure 2.5. Thickness and microfacies for detrital layers thicker than 1 mm in one of the cores (AS07-P1 and AS07-P2) between 1800 and 1999 (time span covered by both cores).

Detrital layer thickness of all three detrital microfacies exhibits a distinct proximal-distal pattern (Figs. 2.2 and 2.5). Consequently, the accumulated detrital layer thickness is by a factor of 2.6 higher in the proximal core. Thirty of 34 detrital layers are as expected thicker in the proximal core AS07-P2. The four exceptions either are equally thick (D22) or slightly thicker (D6, D7, D25) in the distal core (Fig. 2.5). However, these differences in thickness measurements are not significant and likely biased by sediment disturbances during sample preparation.

2.4.3. Composition of detrital layers

µ-XRF scanning provides high-resolution data of major element variations. Ti was selected as indicator for detrital input since it is redox-insensitive and clearly of terrigenous origin (Binder, 1999; Haug et al., 2001). Positive correlations in cores AS07-P1 and AS07-P2 between Ti and Fe (r = 0.87/0.90), K (r = 0.88/0.89), Si (r = 0.74/0.77), and Al (r = 0.55/0.60) indicate this element cluster as of detrital origin. Ca in contrast, is strongly anticorrelated to Ti and exhibits a stronger anticorrelation in the proximal core AS07-P2 (r = -0.53/-0.70). Confirming microfacies analyses, µ-XRF profiles exhibit distinct positive Ti and negative Ca excursions for detrital layers (Figs. 2.2, 2.4, and 2.6). Mg count rates are very low and thus do not exhibit variations for a reliable interpretation. XRD analyses reveal quartz, calcite, albite, and clinochlore as mineral phases in all detrital microfacies. A very weak signal of dolomite is in agreement with the low µ-XRF Mg count rates. This result differs from reports by Müller and Sigl (1977) who describe dolomite as a main mineral phase in the surface sediments near the Ammer river mouth.

$\delta^{18}O_{carb}$ isotope values from core AS07-P1 range between -9.62‰ and -5.71‰ with an average of -7.67‰, while $\delta^{18}O_{carb}$ isotope values from core AS07-P2 range between -9.30‰ and -3.96‰ with an average of -7.03‰. $\delta^{13}C_{carb}$ isotope values from core AS07-P1 range between -5.69‰ and -1.70‰ with an average of -4.15‰, while $\delta^{13}C_{carb}$ isotope values from core AS07-P2 range between -5.31‰ and 0.22‰ with an average of -3.44‰ (Fig. 2.6). For both cores, a strong covariance between $\delta^{18}O_{carb}$ and $\delta^{13}C_{carb}$ is revealed (AS07-P1, r = 0.91; AS07-P2, r = 0.98). Covariance of $\delta^{18}O$ and $\delta^{13}C$ commonly indicates either a hydrologically closed lake system (Leng and Marshall, 2004) or detrital contamination (Mangili et al., 2010).

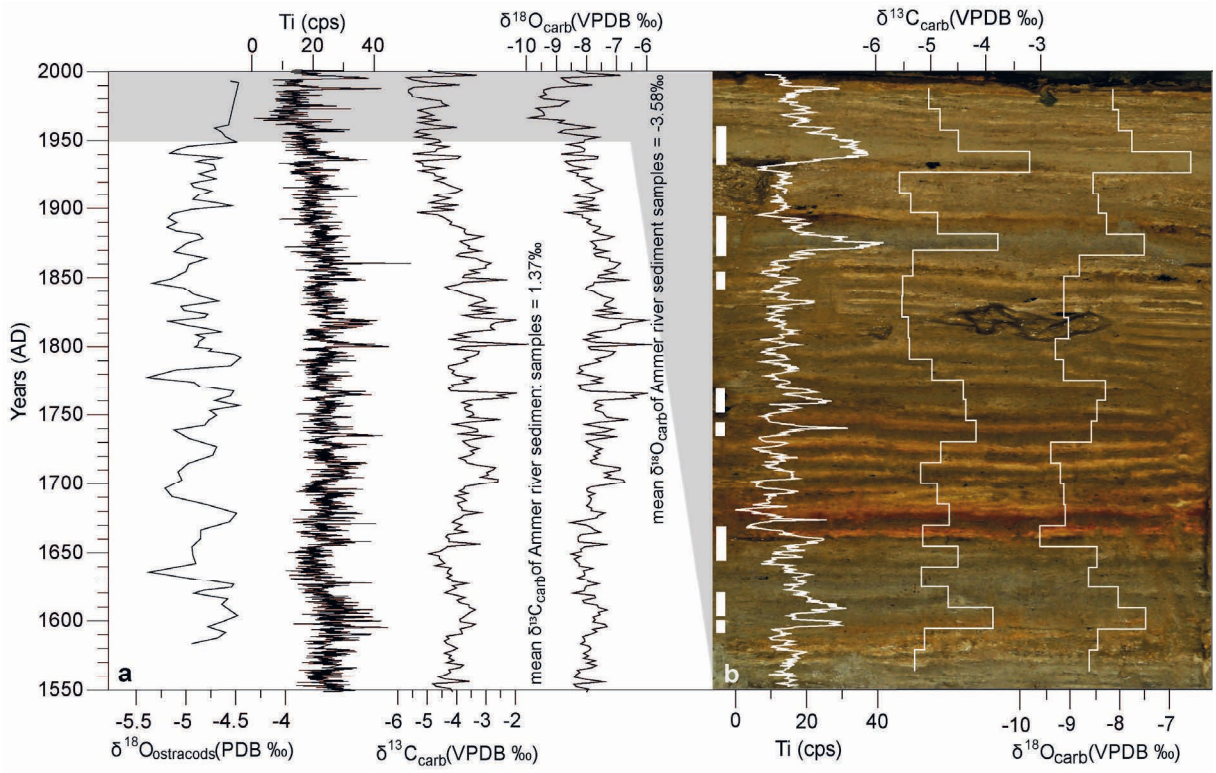

Figure 2.6. (**a**) $\delta^{18}O_{ostracods}$ (von Grafenstein et al., 1992), Ti count rates (cps), $\delta^{13}C_{carb}$ and $\delta^{18}O_{carb}$ (‰) data from core AS07-P1. (**b**) The highlighted varve interval underlain by a core photo exhibits detrital layers (white bars) with coinciding positive Ti (cps) excursions, heavier $\delta^{13}C_{carb}$ and $\delta^{18}O_{carb}$ values. Note the different resolution of µ-XRF (200 µm) and stable isotope data (0.5 cm).

Since Lake Ammersee is a hydrologically open lake system (Alefs, 1997) and clearly heavier isotope peaks coincide with detrital microfacies, it is obvious that $\delta^{18}O_{carb}$ and $\delta^{13}C_{carb}$ data are mainly controlled by detrital (carbonate) contamination and do not reflect climatic fluctuations as $\delta^{18}O$ from benthic ostracods in Lake Ammersee (von Grafenstein et al., 1992, 1996, 1999) (Fig. 2.6). This result is confirmed by isotope measurements of six samples of fine grained detrital Ammer riverbed material from three locations (Fig. 2.1) indicating heavy isotope values between -4.54‰ and -3.29‰ with a mean of -3.58‰ for $\delta^{18}O_{carb}$, and 1.04‰ and 1.70‰ with a mean of 1.37‰ for $\delta^{13}C_{carb}$ (Fig. 2.6). A wider isotope value range, heavier average and maximum isotope values suggest a higher detrital contamination in the proximal core AS07-P2. Source of the detrital carbonates are probably outcrops of Cretaceous and Triassic carbonates, late moraine, flysch, and molasse formations in the Ammer catchment, all containing considerable amounts of calcite. The period of strongest eutrophication between 1960 and 1980 (Alefs, 1997; Alefs and Müller, 1999) is reflected by more negative $\delta^{18}O_{carb}$ values in the Lake Ammersee sediments (Fig. 2.6).

Table 2.1. Runoff and precipitation data for the 17 highest River Ammer floods (daily runoff ≥ 125 m³/s), date of deposition, and thickness of detrital layers from 1926 to 1999 and for floods below 125 m³/s causing detrital layer deposition[a].

Date of Flood	Max. Daily Runoff During Flood (m³/s)	Peak Runoff During Flood (m³/s)	Days with ≥ 100 m³/s Daily Runoff During Flood	Max. Precipitation During Flood (mm/d)	Precipitation Total During Flood	Category	Year and Season of Detrital Layer Deposition	Detrital Layer Thickness (mm)
			Highest River Ammer Floods					
21/22/23.5.1999	534.64	649.4	3	138.5	186.4	3	Summer 1999	1.74
19/20.7.1981	174	238.9	2	69.7	156.6	3	Summer 1981	1.16
17/18/19.6.1979	257	291	3	39.1	116	3	Spring 1979	0.39
2.6.1976	161	216.3	1	81.6	120	3	Summer 1976	0.39
10.8.1970	261.941	338	1	91.2	137.5	3		
23.7.1966	130.991	258	2	46.2	70.7	2		
11.6.1965	224.953	273	2	72.2	119	3	Summer 1965	0.96
14.6.1959	136.971	155	1	47.9	81.6	2	Spring 1959*	0.58*
8/9/10.7.1954	169.993	208	4	51.6	155.7	3	Summer 1954	1.16
22/23.5.1949	203.973	222	3	74	164.2	3	Summer 1949	0.77
7/8/9.7.1946	261.261	461	3	69.2	188.8	3	Summer1946	3.47
24.11.1944	158.972	197	1	19.5	35.2	3		
30/31.5.1940	389.906	400	3	97.7	209.5	3	Disturbed sediments	Disturbed sediments
24.8.1937	139.371	163	1	49.1	84	2	Summer 1937*	0.58*
10.7.1932	129.976	216	1	47.1	78.5	2	Summer 1932	0.58
15.5.1930	149.974	216	1	63.8	92.5	2	Summer 1930	0.58
20.8.1929	146.974	167	1	74.2	105.5	2	Disturbed sediments	Disturbed sediments
			Floods below 125 m³/s					
11.7.1993	103.096		1	63.9	81.4	1	Summer 1993	2.51
15.2.1990	105.507	153.7	1	54.4	72.8	1	Spring 1990	0.58
21.3.1978	70.5	130.4	0	29.6	39.4	0	Spring 1978*	0.77*
22.11.1972	39.8	58.5	0	40.1	53.9	0	Fall 1972	0.58
2.10.1968	89.185	139	0	48.9	63.6	0	Fall 1968	1.16
2.12.1952	45.596	52.6	0	13.2	24	0	Winter 1952	0.77
2.9.1950	55.5	134	0	28.9	40.5	0	Fall 1950*	0.77*
24.11.1947	44.596	104	0	11.2	14.4	0	Fall 1947	0.39
1.9.1938	70.999		0	35.8	45.6	0	Fall 1938	0.39
5.2.1935	49.5	57	0	11.3	30.2	0	Spring 1935*	0.58*

[a]Categories for flood events are: ≥ 150 m³/s=3, ≥ 125 m³/s=2, ≥ 100 m³/s=1, and < 100 m³/s=0. Detrital layer thickness is from core AS07-P1 except when marked with * (than AS07-P2). Precipitation sums for flood events are calculated by adding the daily precipitation during and two days before ≥ 100 m³/s daily runoff.

2.4.4. Seasonal detrital layers versus instrumental data (1926-1999)

A comparison of the detrital layer record from of the composite profile with instrumental daily runoff data from 1926 to 1999 proves that all detrital layers deposited during this time interval have been triggered by floods (Table 2.1) and confirms the micro-stratigraphically determined seasonality of flood layers. For 15 of 22 detrital layers the ascertained season has been exactly determined. Three detrital layers designated as ‘summer’ layers correspond to May floods, two designated ‘spring’ layers correspond to February floods, while two other designated ‘spring’ layers reflect a June flood (Table 2.1). These uncertainties are due to the criteria used for determining the season of a detrital layer. A ‘summer’ layer is defined as a

layer deposited after initial calcite formation in the lake. Since calcite formation in warm years may start as early as March or April, a detrital layer triggered by a May flood may appear as 'summer' layer in the micro-stratigraphic record. Flood layers deposited directly before the onset of calcite precipitation are considered as 'spring' layers, so that a February flood layer may appear as 'spring' layer. Interpretation of June floods as 'spring' layers can be explained by micro-erosion that could have displaced the thin layer of precipitated calcite on the lake floor. Taken these information into consideration makes us confident to have obtained a reasonably precise seasonal flood layer record.

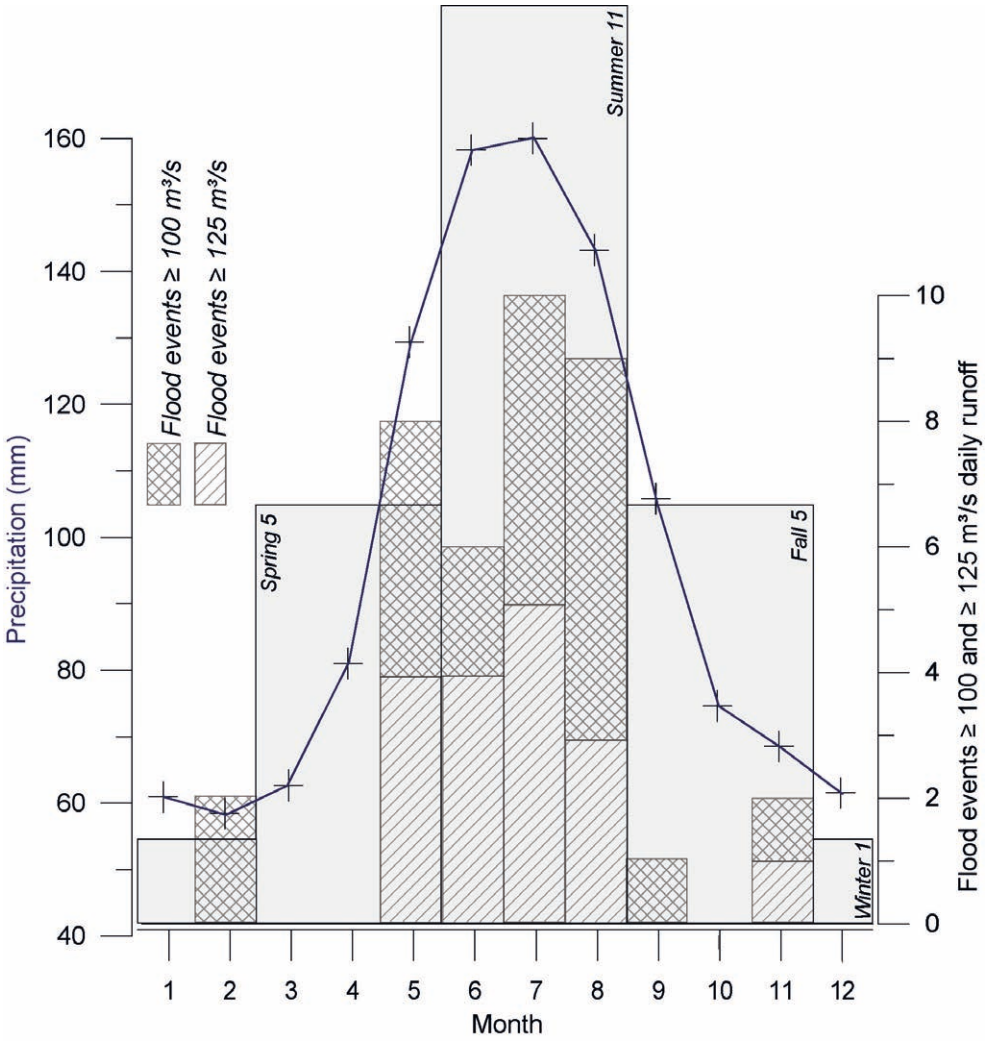

Figure 2.7. Seasonal distribution of detrital layers in the composite profile, monthly distribution of River Ammer flood events with daily runoff ≥ 100 (n=38) and ≥ 125 m³/s (n=17), and monthly precipitation distribution measured at the Meteorological Observatory Hohenpeißenberg approx. 20 km southwest of Lake Ammersee (blue line) within 1926 and 1999.

For evaluating the relation between flood layers and high-magnitude floods the 38 strongest floods during the instrumental period were sub-divided into three classes with mean daily runoff (3) ≥ 150 m³/s (n=11), (2) ≥ 125 m³/s (n=17), and (1) ≥ 100 m³/s (n=38) (hereafter all daily runoff information refer to mean daily runoff). Recurrence time of floods in class 3 is 6.8 years, while it is 4.4 and 2.0 years for classes 2 and 1, respectively. Except the November 1944 flood, all floods with a daily runoff ≥ 125 m³/s occurred between May and August indicating spring and summer as major flood seasons (Fig. 2.7). This pattern does not change much when all floods ≥ 100 m³/s (LfU, 2007) are considered (Fig. 2.7). As confirmed by previously published data, floods of this magnitude (Ludwig et al., 2003), monthly precipitation (Meteorological Observatory Hohenpeißenberg), and seasonality of detrital layers, all show a distinct maximum for spring and summer. For eight of the 11 floods (73%) with a daily runoff ≥ 150 m³/s and 12 of the 17 floods (71 %) with a daily runoff ≥ 125 m³/s corresponding spring-summer detrital layers have been found in the sediment record, respectively (Table 2.1; Fig. 2.8). Below 125 m³/s daily runoff the number of floods leading to detrital layer deposition clearly decreases. Only two out of 21 floods with a daily runoff between 100 and 125 m³/s are reflected in the sediment record (Table 2.1). This suggests that a daily runoff of approx. 125 m³/s represents a threshold below which the deposition of a flood layer becomes less likely. The apparent lack of a relationship between flood magnitude and flood layer thickness (Fig. 2.8) suggests complex nonlinearities in the erosion-transport-deposition process cascade (e.g. Lamb and Mohrig, 2009) which require further investigations.

Such problems might also explain the lack of detrital layers corresponding to the July 1966 and August 1970 floods with ≥ 125m³/s daily runoff. Probably, lake internal currents led to an inhomogeneous distribution of detrital material on the lake floor resulting in a lack of deposition at the coring sites. This can only be verified by a denser net of surface cores in order to obtain an improved spatial view on the distribution of detrital layers on the lake floor. Two other spring-summer floods (August 1929; May 1940) that are not recorded in the sediment are likely missed because of sediment disturbances in the relevant core sections. The November 1944 flood likely is not recorded because after three weeks of daily surface temperatures below 0°C (Meteorological Observatory Hohenpeißenberg) the soil surface was frozen during the time of the flood triggering rainfall on November 22nd/ 23rd impeding soil erosion in the catchment and detrital matter flux into the lake.

Besides the possibility of lacking detrital layers for some floods ≥ 125 m³/s, also ten floods below 125 m³/s led to the deposition of a detrital layer. However, six of these layers are related to fall-winter floods which are not considered in our spring-summer flood time-series. The production of fall flood layers during lower magnitude floods might be explained by possible sediment re-distribution processes in the lake triggered by enhanced wave activity in fall. Additionally, two spring-summer layers are triggered by floods with 103 (thick layer D2) and 106 m³/s daily runoff which is close to the defined threshold value of 125 m³/s daily runoff. That leaves two spring layers triggered by floods clearly below 125 m³/s daily runoff, which are only present in the proximal core (Table 2.1).

In conclusion, the detrital layer record in Lake Ammersee represents a time-series of spring-summer floods ≥ 125 m³/s daily runoff. Four spring-summer floods of this magnitude are not detected in the sediment record (two due to sediment disturbances), while four flood layers are related to spring-summer floods below this threshold (two rather close to 125 m³/s daily runoff) (Table 2.1).

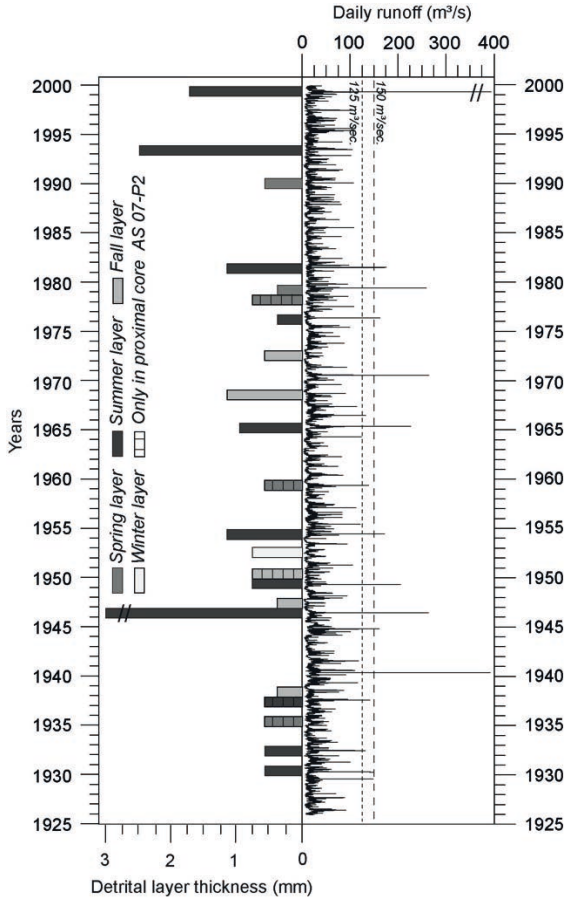

Figure 2.8. Daily River Ammer runoff (m³/s) and seasonal detrital layer thickness (mm) from 1926 to 1999. Detrital layer thickness is from core AS07-P1 except when layers occur only in the proximal core AS07-P2.

2.4.5 Detrital layer frequency and seasonal distribution (1545-1999)

To establish a long flood time-series back to 1545 only detrital layers occurring in core AS07-P1 have been considered, because core AS07-P2 reaches not further back in time than 1800. A total of 24 spring and 51 summer flood layers have been identified during this period. Average layer thickness is higher in summer (1.24 mm), than in spring (0.79 mm). Frequency distributions of spring-summer flood layers exhibit distinct maxima of summer and minor maxima of spring layers between 1545 and 1590, 1650 and 1730, and 1800 and 1840 (see Fig. 2.12). The 12 fall (0.70 mm), 5 winter (0.62 mm), and 5 not seasonally definable layers in AS07-P1 do not exhibit a clear distribution pattern.

Detailed micro-stratigraphic comparison of both sediment cores for the calibration period has shown that four detrital spring-summer layers (1978, 1959, 1937, 1935) found in the proximal core are not detected in the distal core located 6.2 km away from the Ammer river mouth and 1.8 km away for core AS07-P2 (Table 2.1). Consequently we have to expect a further underestimation of floods in this core which might affect the frequency distribution in case that the not recorded floods are clustered in periods of low flood layer frequency. Since the identified missing spring-summer layers in AS07-P1 during the calibration period are randomly distributed (Table 2.1), we are, however, confident that additional missing layers in the distal core do not significantly affect general trends in flood layer distribution.

2.4.6. Detrital layers versus weather regime data

To evaluate large-scale atmospheric circulation effects on River Ammer runoff, the 17 strongest River Ammer flood events (daily runoff ≥ 125 m^3/s) measured at gauge Weilheim (LfU, 2007) were compared with the occurrence of weather regimes over Europe from 1926 to 1999 (time covered by River Ammer runoff and weather regime data) using the weather regime (Großwetterlagen) catalogue by Gerstengarbe and Werner (2005). This catalogue deciphers the daily occurrence of 30 characteristic weather regimes over Europe starting 1881. The temporal offset between weather regime and river runoff was corrected using precipitation data from the Meteorological Observatory Hohenpeißenberg 20 km southwest of Lake Ammersee. Five weather regimes can be attributed to more than one of the highest 17 flood events. Three floods were caused each by Cyclonic Westerly (WZ) and High over the British Isles (HB) weather regimes. Two floods occurred during Cyclonic North-Westerly

(NWZ), Zonal Ridge across Central Europe (BM), and Cyclonic North-Easterly (NEZ) weather regimes (Figs. 2.9 and 2.10). The remaining five floods ≥ 125 m³/s are related to Anticyclonic Westerly (WA), Trough over Central Europe (TRM), High Scandinavia-Iceland/Trough Central Europe (HNFZ), Anticyclonic South-Easterly (SEA), and Cyclonic South-Easterly (SEZ) weather regimes (Fig. 2.9).

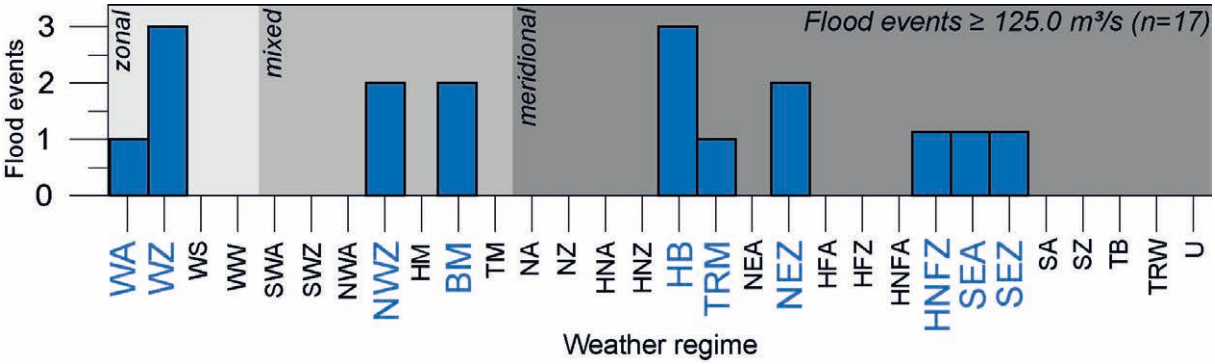

Figure 2.9. Weather regimes triggering the 17 highest River Ammer flood events (daily runoff ≥ 125 m³/s) between 1926 and 1999. BM, Zonal Ridge Across Central Europe; HB, High Over the British Isles; HNFZ, High Scandinavia-Iceland/Trough Central Europe; NEZ, Cyclonic Northeasterly; NWZ, Cyclonic Northwesterly; SEA, Anticyclonic Southeasterly; SEZ, Cyclonic Southeasterly; TRM, Trough Over Central Europe; WA, Anticyclonic Westerly; WZ, Cyclonic Westerly.

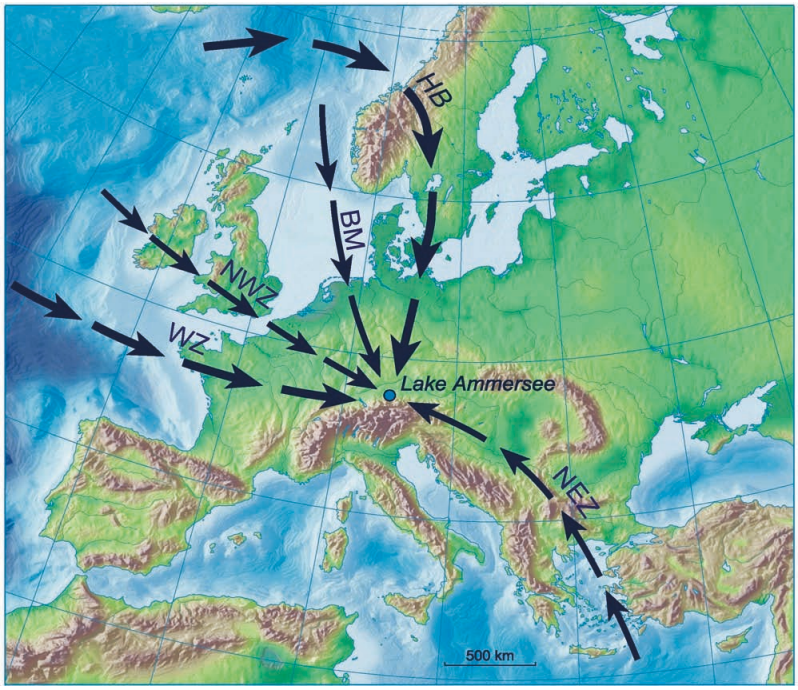

Figure 2.10. Expected pathway of cyclones during the main flood-prone weather regimes at Lake Ammersee: BM, HB, NEZ, NWZ, and WZ.

The summer and annual occurrences of these flood-prone weather regimes were compared with the detrital layer distribution in the longer core AS07-P1 between 1881 and 1999 (time span covered by varve and weather regime data). Particularly, annual frequencies of flood-prone weather regimes indicate similar trends as the detrital layer distribution (Fig. 2.11). The weaker agreement between summer flood-prone weather regimes and detrital layers might be due to difficulties regarding the seasonal segmentation of detrital layers (section 2.4.4). The link between flood prone-weather regimes and detrital layers seems weakened between 1920 and 1924, when additional detrital sediments enter the lake during construction work in the Ammer catchment for river channelization (Fig. 2.11).

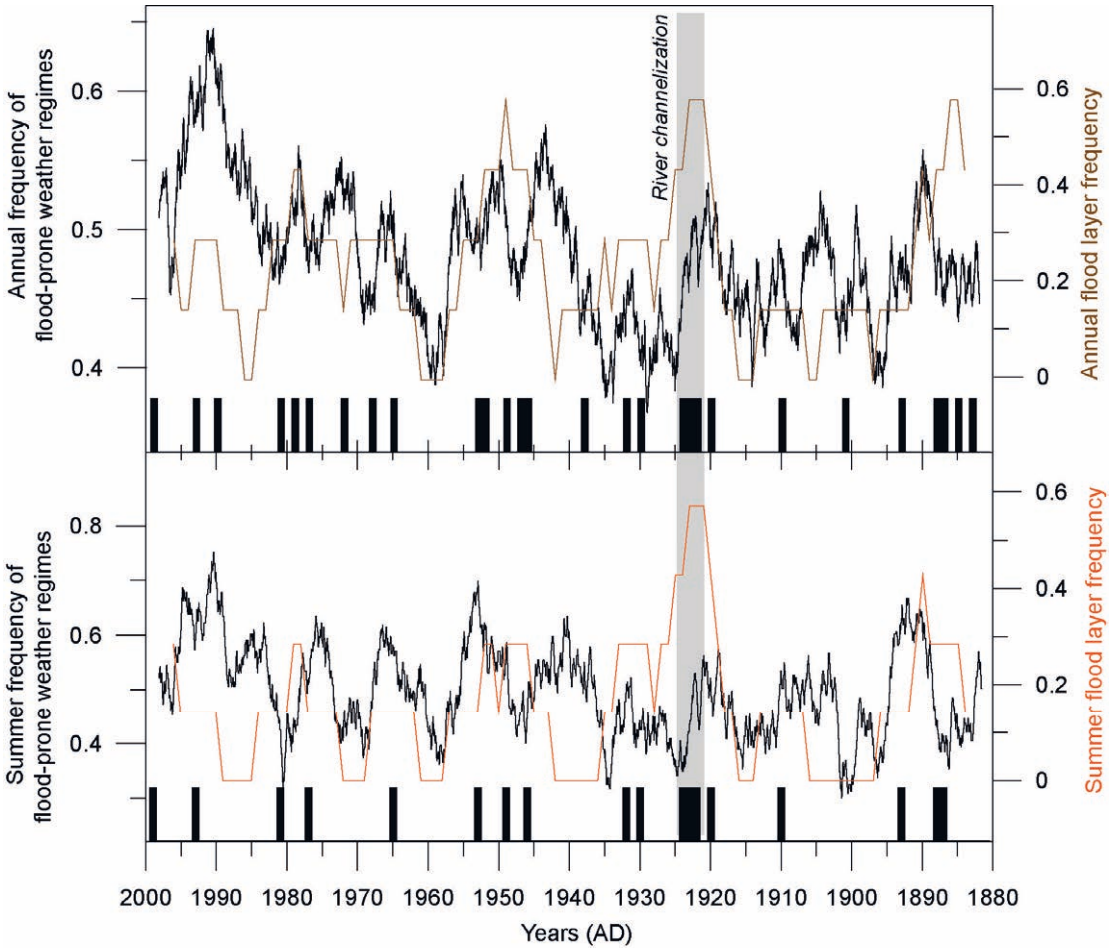

Figure 2.11. Summer and annual flood layer frequency in core AS07-P1 between 1881 and 1999 on a 7-year running mean and frequency of flood-prone weather regimes (WA, WZ, NWZ, BM, HB, TRM, NEZ, HNFZ, SEA, SEZ) on a 249 and 999 point running mean, respectively. Detrital layers are marked by black bars. The different smoothing of the individual datasets was chosen to obtain a similar running mean with respect to the resolution of the records. The period of River Ammer channelization is shaded.

2.5. Discussion

2.5.1. Depositional processes of detrital layers

All three observed detrital microfacies types can be interpreted in terms of various depositional processes.

1. Graded layers. Grading, as well as abrasion and flame structures in the basal part of some layers, point to deposition of hyperpycnal underflows (Mangili et al., 2005). Because of the amount of suspended matter and water temperature, the inflowing water/sediment suspension is of higher density than the surrounding water body and moves as a density current along the lake floor (Sturm and Matter, 1978). During the spread within the lake basin the density difference between the water body and turbidity current diminishes, leading to a reduced transport capacity and consequently successively finer grain sizes (Siegenthaler and Sturm, 1991). This is reflected by grading and the proximal-distal pattern of detrital layer thickness in Lake Ammersee (Figs. 2.4 and 2.5).

2. Silt/clay layers. This layer type may form when fine silt and clay detrital material is transported into the lake by low-density currents. After entering the lake, the detrital grains are distributed in the water column as over- or interflow owing to the density of the inflowing current and that of the surrounding water body (Sturm and Matter, 1978; Mangili et al., 2005). As reflected in the hardly visible faint grading in some of these layers, the fine-grained material falls out of the water column and deposits within a few days on the lake bottom (Siegenthaler and Sturm, 1991). Alternatively, this layer type might reflect distal deposits of high density currents from which the coarser fraction already deposited (Mangili et al., 2005).

3. Matrix-supported layers. Various detrital and reworked sediment components as littoral calcite and diatom frustules and plant remains well-mixed within the sediment matrix form matrix-supported layers which are commonly thought to reflect major slope failures or debris flows. Correlation of the two studied cores, however, exhibits four matrix-supported layers in core AS07-P1 as distal deposits of graded layers. This confirms deposition after runoff events induced by underflows that have eroded material in the littoral zone of the lake. A special case is the thick matrix-supported layer D2. The processes triggering the deposition of this layer in summer 1993 are well documented by (1) observations made by the Weilheim water authorities in the lake catchment, (2) sediment trap data obtained near the location of our core AS07-P2 (Alefs, 1997), and (3) a sediment core obtained in October 1993. On July 17th 1993

a short (1.5 h) but intense local precipitation event (100 mm) caused a flood in the Ammer tributary Halbammer. This caused a break-up of the armor layer near the village Unternogg in close vicinity to the confluence of both rivers (Fig. 2.1) causing an incision of the riverbed of some meters and the collapse of a Halbammer bridge (Wasserwirtschaftsamt-Weilheim, personal communication, 2008).

In conclusion, microfacies analyses combined with instrumental runoff data from 1926 to 1999 (Table 2.1) prove that detrital layers in the Lake Ammersee sediments represent flood deposits (Sturm and Matter, 1978; Siegenthaler and Sturm, 1991) of the River Ammer. Alternative triggering mechanisms which are not directly related to floods (Mangili et al., 2005) are unlikely. No indications for debris flow deposits as observed in Lake Mondsee (Swierczynski et al. 2009) have been found in the studied sediment interval. The only observed trigger for detrital sediment flux into the lake basin not directly related to a flood is the construction work for channelizing the Ammer river from 1920 to 1924 (Alefs, 1997). Increased erosion led to a generally higher detrital input facilitating detrital layer deposition even during low-magnitude floods.

2.5.2. Paleoclimatic implications

Much of the current climate debate focuses on global temperature fluctuations. Less well constrained are the responses of the hydrological cycle and, particularly, extreme flood events to changes in climate boundary conditions. In addition to high-resolution temperature reconstructions (von Grafenstein et al., 1996, 1999), the Lake Ammersee sediment profile has a large potential for establishing long flood time-series at seasonal precision. Despite the still remaining lack of knowledge in understanding the entire cascade of processes from a flood to the deposition of a flood layer at a certain point in the lake basin, methodological improvements allowed to establish a reliable spring-summer flood layer time-series including an assessment of the uncertainties. We are confident that these data are sufficient to identify a distinct and apparently not stationary temporal pattern in the distribution of flood layers. Higher frequencies particularly of summer floods are observed for colder periods during the Little Ice Age. Similar observations have been made in historical flood time-series of River Main located approx. 200 km north of Ammersee (Glaser and Stangl, 2004), pointing to a wider regional significance of this finding.

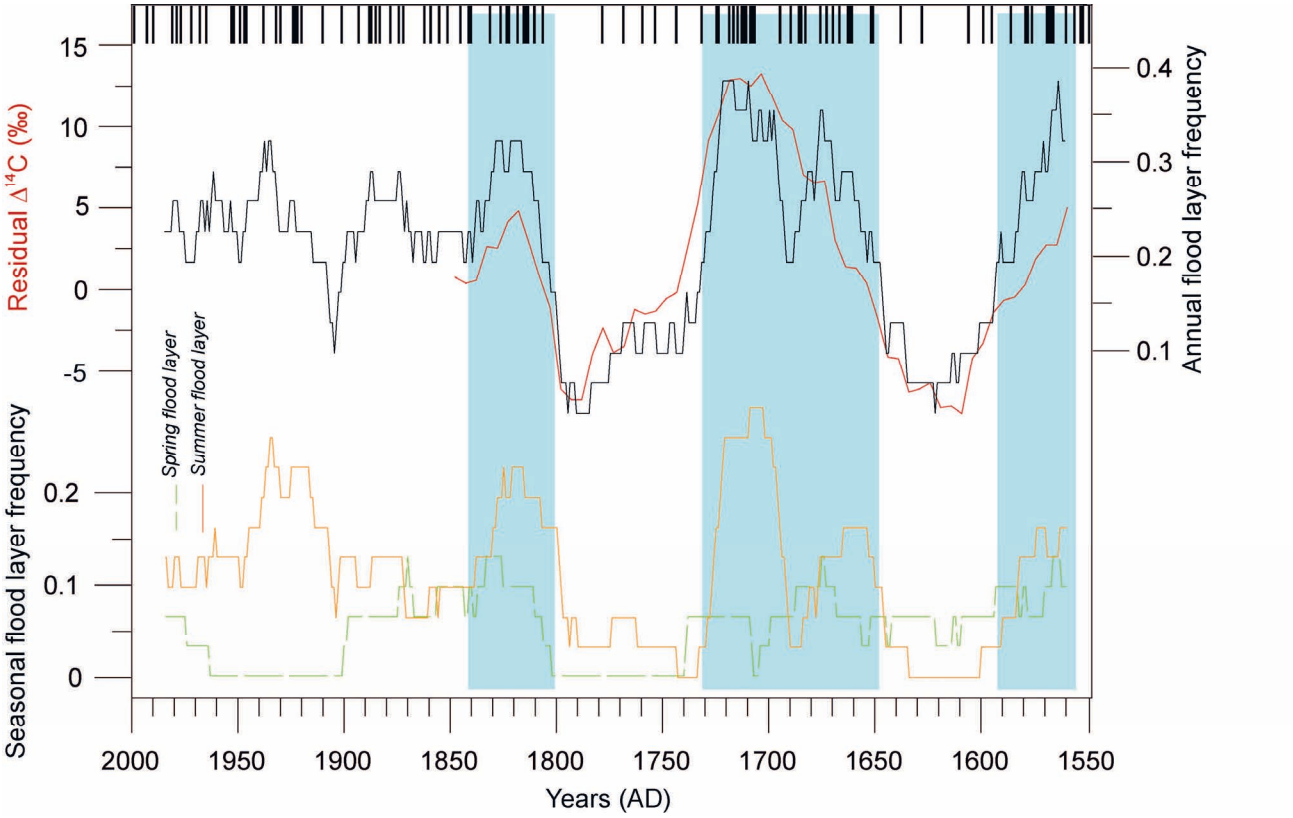

Figure 2.12. (top) Flood layers (black bars) and annual flood layer frequency in core AS07-P1 on a 31-year running mean (black line). Residual $\Delta^{14}C$ on a 1000-year running mean (red line) (Reimer et al., 2004). (bottom) Spring and summer flood layer frequencies on a 31-year running mean. Phases of lower solar activity during the Little Ice Age are highlighted by blue rectangles.

The flood layer frequency pattern coincides well for the period from 1545 to 1845 with reconstructed variations of residual $\Delta^{14}C$, commonly regarded as proxy for solar activity (Usoskin et al., 2003; Solanki et al., 2004). Particularly striking is the good agreement of maxima in summer and spring flood layers with residual $\Delta^{14}C$ maxima during the Little Ice Age between 1545 and 1590, 1650 and 1730, and 1800 and 1840 (Fig. 2.12). The production of ^{14}C in the upper stratosphere is higher during times of lower solar activity because more cosmic radiation can reach the Earth's atmosphere where it transforms ^{14}N to ^{14}C. Past atmospheric ^{14}C concentrations ($\Delta^{14}C$) have been reconstructed from tree rings and are expressed relative to the NBS oxalic acid standard activity in the Δ notation (Stuiver and Polach, 1977). The residual $\Delta^{14}C$ has been calculated from the IntCal04 $\Delta^{14}C$ dataset by removing a 1000-year running average from the record to reduce long-term geomagnetic field and reservoir effects. The residual $\Delta^{14}C$ data does not extend in times younger than 1845 in order to exclude a bias through contamination by fossil-fuel burning (Reimer et al., 2004).

The coincidence between decadal-scale solar activity minima and cooling (Waple et al., 2002) particularly in Europe during the Little Ice Age in the 15th to 19th centuries (Mann, 2002), suggests large-scale climatic responses to solar forcing. However, since the physical processes behind the solar/climate link are not yet fully understood this remains a controversial discussion. Two hypotheses for possible amplifying mechanisms of the rather small variations in solar activity have been suggested (van Geel et al., 1999). (1) Variations in UV irradiance alter the stratospheric ozone production leading to changes in total radiative forcing and atmospheric circulation (Haigh, 1994, 1996). (2) Effects of solar magnetic variability on Earth's cosmic ray shielding alter the production of cloud condensation nuclei and consequently cloud cover and precipitation (Svensmark and Friis-Christensen, 1997; Svensmark, 2000). Although it is not straight forward to elaborate these feedback mechanisms in the climate system based on the Lake Ammersee flood record, the apparent link between high-magnitude floods and the occurrence of certain weather regimes in the Ammer catchment from 1881 to 1999 (Fig. 2.11) gives cause for further deliberations. Accepting that extreme floods are triggered by typical flood-prone weather regimes suggests that atmospheric circulation plays a major role in extreme flood initiation. Most of the high-magnitude River Ammer flood events in the observation period back to 1926 occurred in summer (Fig. 2.7) during particular weather regimes (Fig. 2.9). The increase in summer flood frequency during intervals of solar minima (Fig. 2.12), therefore, points to a more frequent occurrence of these flood-prone weather regimes and, thus, to changes in large-scale atmospheric circulation patterns. The increase in spring floods during times of lower solar activity (Fig. 2.12) might be additionally affected by stronger snow melt due to an increase in winter snowfall (Beniston and Jungo, 2002; McEwen, 2006). The coincidences between changes in flood frequency and both, solar activity and the occurrence of flood-prone weather regimes might be a further argument in support of the hypothesis of solar variability effects on atmospheric circulation patterns. However, this hypothesis has to be further tested by extending the flood layer record from Lake Ammersee further back in time to cover also older intervals of reduced solar activity in the Holocene. Moreover, comparable flood records from other regions are required to obtain a better regional view of flood frequency patterns.

2.6. Conclusions

All detrital layers in the Lake Ammersee sediment record have been proven as flood deposits. Microscopic analyses on petrographic thin sections identified spring and summer as the main seasons of flood layer deposition. Based on a precise varve chronology a 450-year flood layer time-series has been contributing to a better understanding of the effects of changing climatic boundary conditions on flood frequency. This underlines the potential of varved lake sediments as promising archives for establishing even longer flood records.

However, evaluating sediment archives necessitates considering the inherent data characteristics. On the one hand, sediment data cannot provide the same precision as instrumental or historical hydrological data in terms of time control, time resolution, and process quantification. On the other hand, only sediment archives reach far enough back in time to provide long-term information that cover even up to several climatic cycles including periods without any human interference on landscape evolution. These differences between instrumental and geological data obviously require different analytical approaches. It is a challenging task to link both approaches by bridging the different time concepts. A first step in this respect is to improve the time resolution of geological records by using annually laminated sediments.

In addition to the time scale issue, the complex processes involved in the deposition and preservation of a sediment archive must be better understood. Linking the Lake Ammersee flood layer record with instrumental Ammer flood data allowed, for the first time, defining an approximate threshold in spring-summer flood magnitude making the deposition of a flood layer likely. Moreover, we were able to assess the degree of ‘completeness’ of the flood layer record, *i.e.* to identify floods for which no corresponding flood layer has been found. The resulting number of flood layers was sufficient to determine changes in frequency trends of spring and summer floods representing the main flood seasons in the region. These frequency patterns were compared with proxy data of solar activity revealing an intriguing coincidence between periods of reduced solar irradiance and increased flood frequency. The additional observation that strong spring-summer floods correspond to the frequency of particular flood-prone weather regimes arises speculations about possible effects of solar variability on mid-latitude atmospheric dynamics.

This study is a first step in developing varved lake sediments as flood records at, for geological archives, unprecedented seasonal resolution. It particularly highlights the great

potential of this approach, but at the same time clearly points out the remaining problems in interpretation that have to be solved. Future work has to aim at a better understanding of the processes controlling flood triggered detrital matter erosion, transport, and deposition.

Acknowledgements

This study is a contribution to the Helmholtz TERENO research project and the Helmholtz climate initiative REKLIM. The Wasserwirtschaftsamt Weilheim (WWA-WM) and the Bayerisches Landesamt für Umwelt (LfU) are acknowledged for providing River Ammer runoff data. Precipitation and temperature data from the Meteorological Observatory Hohenpeißenberg was supplied by the Deutscher Wetterdienst (DWD). We would like to thank D. Berger and G. Arnold (GFZ-Potsdam) for preparing high-quality thin sections, J. Zimmermann for his help with stable isotope measurements, and R. Niederreiter (UWITEC) for his support during sediment coring. A. Hendrich helped with the layout of Figures. Flood layer data files are available at http://doi.pangaea.de/10.1594/PANGAEA.746240.

(3) Shifts of Mid- to Late Holocene flood intensity in detrital layers from varved sediments of pre-alpine Lake Ammersee (southern Germany)

Markus Czymzik[a], Achim Brauer[a], Peter Dulski[a], Birgit Plessen[a], Rudolf Naumann[b], Ulrich von Grafenstein[c], Raphael Scheffler[a]

[a] GFZ German Research Centre for Geosciences, Section 5.2 Climate Dynamics and Landscape Evolution, Telegrafenberg, 14473 Potsdam, Germany

[b] GFZ German Research Centre for Geosciences, Section 4.2 Inorganic and Isotope Geochemistry, Telegrafenberg, 14473 Potsdam, Germany

[c] Laboratoire des Sciences du Climat et de l'Environnement, UMR CEA-CNRS, Orme des Mersiers, 91191 Gif-sur-Yvette, France

submitted to *Quaternary Science Reviews* (2012)

Highlights

- We present a 5500 year record of 1573 flood layers in varved lake sediments.

- Integrating microfacies data from two sediment profiles shed light on depositional processes.

- These would have remained undetected using one sediment profile and without layer based analyses.

- Three shifts towards higher flood intensities occur at ~5500, ~2800, and ~500 varve years BP.

- Likely forcing mechanisms are gradual reduction in summer insolation and centennial-scale solar minima.

Abstract. Microfacies analyses and X-ray fluorescence scanning (µ-XRF) at sub-mm resolution were conducted on the varved Mid- to Late Holocene interval of two sediment profiles ($AS10_{prox}$ and $AS10_{dist}$) from pre-alpine Lake Ammersee (southern Germany) located in a proximal and distal position towards the tributary river Ammer. To shed light on sediment distribution within the lake, particular emphasis was (1) the detection of intercalated detrital layers and their micro-sedimentological features, and (2) intra-basin correlation of these event deposits. Detrital layers were dated by microscopic varve counting, verified by accelerator mass spectrometry ^{14}C dating of terrestrial plant macrofossils.

Since ~5500 varve years BP, in total 1573 detrital layers were detected in either one or both of the investigated sediment profiles. Based on their microfacies, geochemistry, and proximal-distal deposition pattern, detrital layers were interpreted as River Ammer flood deposits. Earlier studies on flood layer seasonality have proven that flood layer deposition occurs predominantly during spring and summer, the flood seasons at Lake Ammersee. The flood layer record indicates three shifts in mean layer frequency and thickness at ~5500, ~2800, and ~500 varve years BP. Combining information from both sediment profiles allowed to interpret these shifts in terms of stepwise increases in mean flood intensity. Likely trigger of these shifts are gradual reduction in Northern Hemisphere orbital summer forcing and superimposed centennial-scale solar activity minima. Proposed response to this forcing is hemispheric cooling causing strengthened equator-to-pole temperature gradients and higher potential energy in the troposphere. This energy is translated into more intense cyclones, extremer rainfall events, and higher floods at Lake Ammersee.

3.1. Introduction

During river floods, detrital catchment material is eroded and transported in suspension by fluid turbulence into downstream lakes. In the water body the transport capacity of the inflowing turbidity current successively diminishes leading to the deposition of characteristic detrital layers on the lake floor (Sturm and Matter, 1978; Schiefer et al., 2011). Intercalated into annually laminated (varved) sediments the sequence of these flood layers provides an archive of flood activity that extends instrumental time-series for millennia even down to seasonal resolution (Czymzik et al., 2010; Swierczynski et al., 2012a). However, interpreting the succession of flood layers on the lake floor in terms of extreme environmental events requires a mechanistic understanding of the depositional processes. In addition to (1)

calibrating the detrital layer stratigraphy using instrumental data (Czymzik et al., 2010; Kämpf et al., 2012a), (2) monitoring individual turbidity currents in lakes and streams using current meters and turbidity sensors (Lambert et al., 1976; Gilbert and Crookshanks, 2009), and (3) inferring turbidity flow characteristics from model experiments (Lamb and Mohrig, 2009), the dynamics behind detrital layer deposition can be deduced from the micro-sedimentological features (microfacies) of the deposited layers themselves (Middleton, 1993; Lauterbach et al., 2012; Swierczynski et al., 2012b). Intra-basin correlation of complementary flood layers in two sediment profiles located in a proximal and distal position towards the tributary river of a lake enables interpretation of detrital layer microfacies with respect to sediment source and transport processes in the basin (Mangili et al., 2005; Wirth et al., 2011; Kämpf et al., 2012b).

Lake Ammersee in the pre-alpine region of southern Germany is an ideal location to build up a long time-series of flood-triggered sedimentation. Previous studies on oxygen isotopes from ostracods have proven the sediment record as a reliable paleoclimate archive enabling high-resolution temperature reconstruction (von Grafenstein et al., 1996, 1999). Extensive flysch, molasse, and late moraine formations in the meso-scale catchment provide abundant fine-grained detrital material for downstream transport into the gully shaped lake by only one main tributary, River Ammer (Fig. 3.1). Annual layering of the sediments enables both accurate detection and precise dating of detrital microfacies down to seasonal resolution (Czymzik et al., 2010). Calibration studies on two short sediment cores from Lake Ammersee using instrumental River Ammer runoff data verified the succession of detrital layers as an archive of major flood events (Czymzik et al., 2010). Due to this potential, two new long sediment profiles have been retrieved from Lake Ammersee located in a proximal and distal position towards the Ammer river mouth in order to establish a detailed Mid- to Late Holocene flood layer record and to examine changes in flood triggered detrital sedimentation in response to climate forcing.

3.2. Study Site

Lake Ammersee is a hardwater lake in the pre-alpine region of South Germany (48°00'N, 11°07'E) located 20 km southwest of Munich, at an elevation of 533 m (Fig. 3.1). The present day lake has a maximum water depth of 81.1 m and a surface of 47 km². The north-south

orientated basin was eroded into Cenozoic sediments by the Ammersee lobe of the Isar-Loisach glacier during the last glaciation (Alefs, 1997).

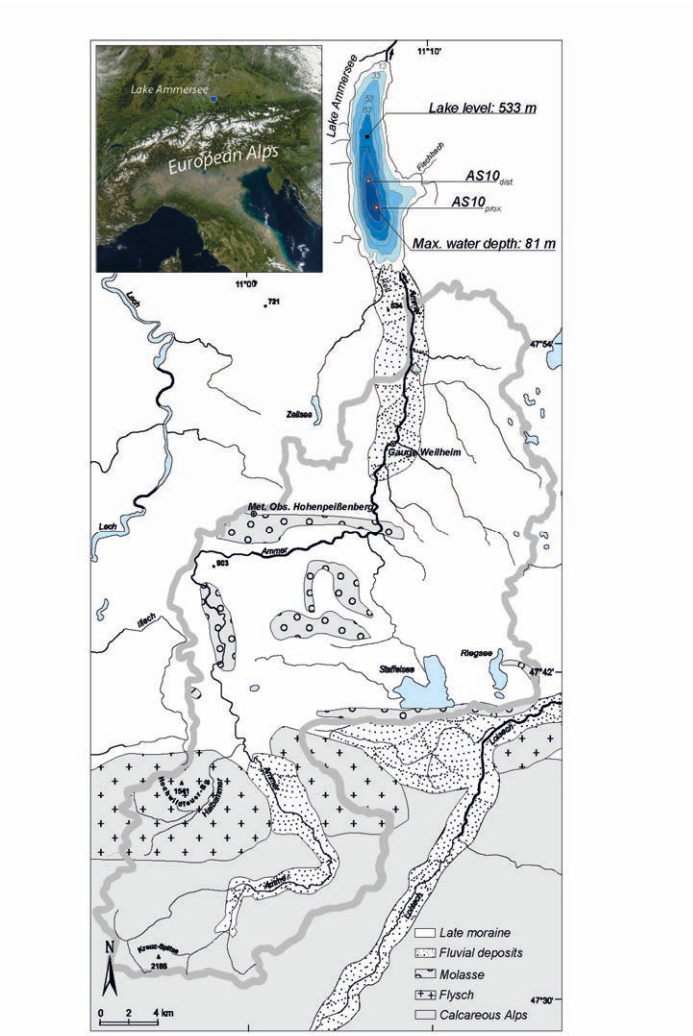

Figure 3.1. Geographical position and geological sketch of the Ammer catchment including bathymetric map of Lake Ammersee with positions of sediment profiles $AS10_{prox}$ and $AS10_{dist}$.

The main tributary of Lake Ammersee springs in the southwestern Ammergau Alps. Due to the region's karstic geology, the stream drains into a subterranean channel system to reach the surface again some hundred meters downstream – from there on named River Ammer. After leaving the Calcareous Alps in a northward direction the 84 km long river with a catchment of 709 km^2 flows through gently shaped flysch, molasse, and late moraine formations (Mangelsdorf and Zelinka, 1973) (Fig. 3.1). The river inflow into the lake was displaced by about 1 km to the southeast during construction works for River Ammer channelization between AD 1920 and 1924 (Czymzik et al., 2010).

Today, hydroclimate in the Ammer catchment is influenced by both maritime North Atlantic weather characterized by frequent westerly cyclonic disturbances and atmospheric blocking by continental high-pressure regimes (Petrow and Merz, 2009). Mean annual precipitation is approx. 1200 mm/year and shows a clear maximum during summer (Fig. 3.2). Due to the high relief difference of 1652 m between the highest point of the catchment in the northern Calcareous Alps (Kreuzspitze, 2185 m) and Lake Ammersee, precipitation shows a decreasing gradient from south to north. High water tables in the northern catchment and limited storage capacities of the alpine soils favor frequent floods through saturation excess overland flow (Ludwig et al., 2003) during precipitation maxima from late spring to summer (Fig. 3.2).

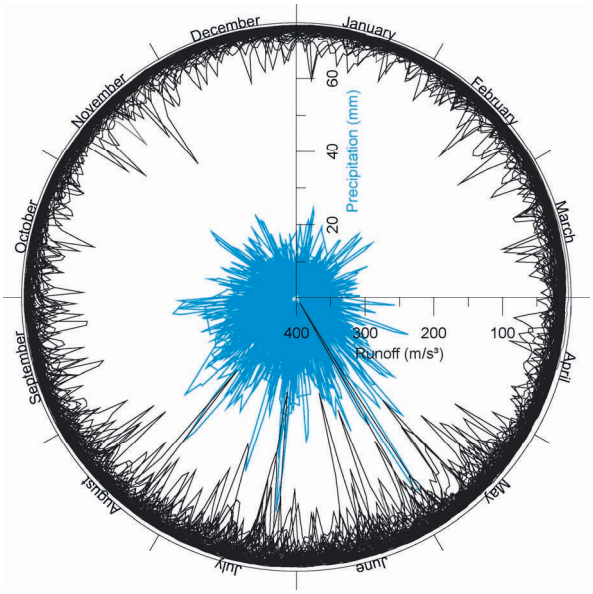

Figure 3.2. Daily River Ammer runoff from gauge Weilheim and precipitation from the Meteorological Observatory Hohenpeißenberg located approx. 20 km south of Lake Ammersee from AD 1926 to 1999. Since strong floods at Lake Ammersee occur after consecutive days of strong rainfall, precipitation data are shown on a 3-day running mean.

3.3. Methods

3.3.1. Sediment coring and continuous varve profiles

At two locations in the deepest part of Lake Ammersee (Fig. 3.1), overlapping sediment cores consisting of 2 m segments were retrieved in July 2010 in a distance of a few meters using a modified UWITEC piston corer (Fig. 3.3). Sediment profile $AS10_{prox}$ (overlapping cores C and D) is located at a more proximal (4.4 km) and sediment profile $AS10_{dist}$ (overlapping

cores A and B) at a more distal position (6.2 km) towards the Ammer river mouth. Maximum sediment depth is 9.8 m for the proximal and 12.5 m for the distal coring location (Fig. 3.3). Retrieving overlapping sediment profiles at one coring location ensures continuity by bridging two consecutive core segments from one profile with a segment from the parallel profile (Fig. 3.3).

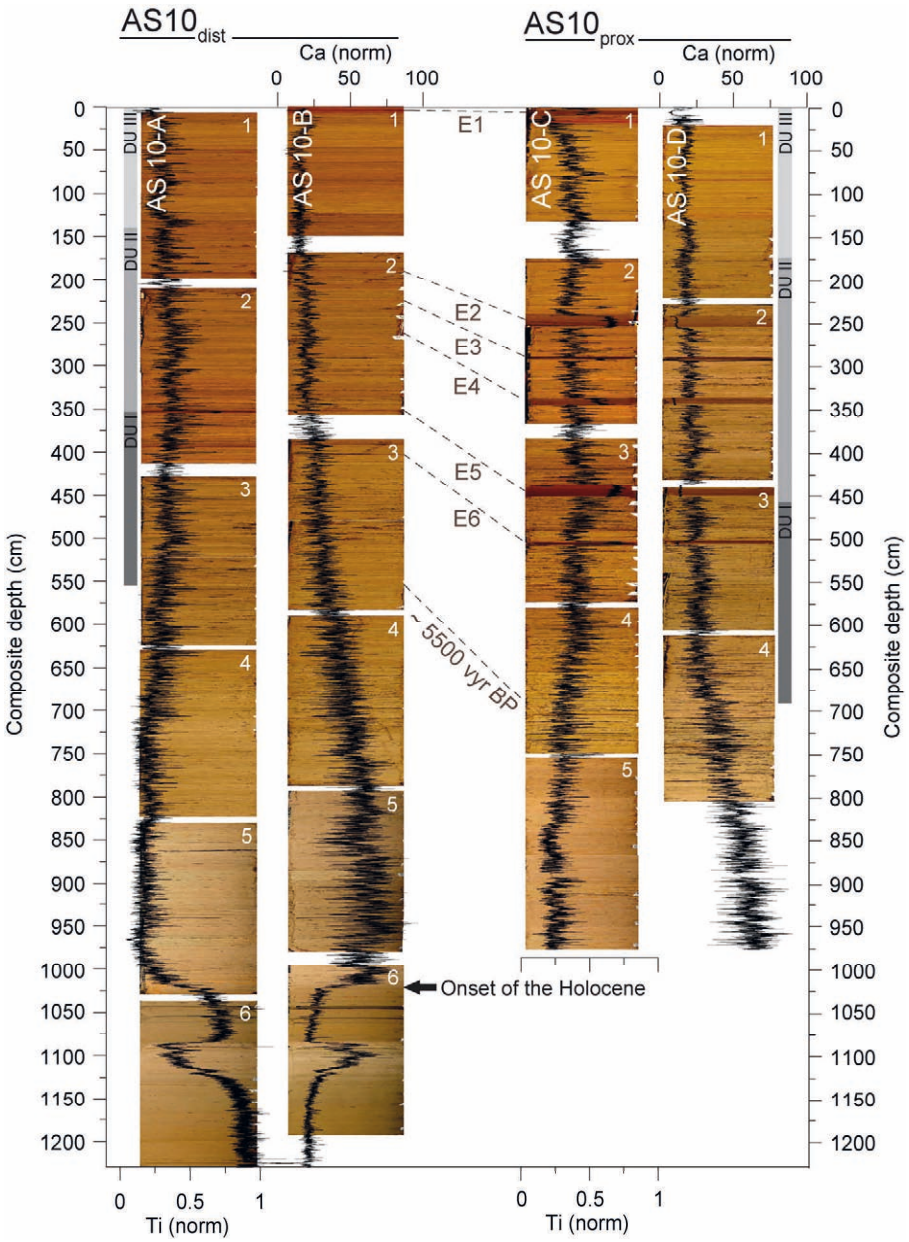

Figure 3.3. Composite profiles $AS10_{prox}$ and $AS10_{dist}$ exhibiting the correlation between individual core segments, the position of exceptional thick detrital layers E1 to E6, and the end of the investigated interval at ~5500 vyr BP. The lithostratigraphy is overlain by corresponding µ-XRF data of the elements Ti (norm) and Ca (norm). Depositional units (DU) I to III and the onset of the Holocene are marked. Note that element data represent downcore composites and were not necessarily measured from the core segment on which they are plotted.

Continuous composite profiles $AS10_{prox}$ and $AS10_{dist}$ were constructed by visual correlation in the overlapping parts of parallel core segments (Figs. 3.3 and 3.4). A stratigraphical framework between the resulting composite profiles was established by intra-basin correlation of 107 macroscopic detrital layers of > 1 mm thickness (Fig. 3.4). These lithological markers provide on average every 50 years an isochronous correlation horizon.

Figure 3.4. Correlation of sediment profiles. (**a**) Core-to-core correlation of parallel core segments using lithological marker layers and element profiles (Ti norm). (**b**) Intra-basin correlation of sediment profiles $AS10_{prox}$ and $AS10_{dist}$ based on macroscopic lithological marker layers.

3.3.2. Microfacies analyses

Detailed microfacies analyses of varve and detrital layer properties were performed on two overlapping series of large-scale petrographic thin sections from composite profiles $AS10_{prox}$ and $AS10_{dist}$. Microscopic investigations were carried out applying a ZEISS Axiolab polarization microscope at 12.5x to 500x magnification under various light and optical conditions. Thickness measurements were performed at 25x magnification. Preparation of thin sections from soft and wet sediment blocks followed a standard procedure minimizing process-induced disturbances of sediment micro-structures and includes shock-freezing with liquid nitrogen, freeze-drying for 48 h, and epoxy resin impregnation under vacuum (Brauer and Casanova, 2001).

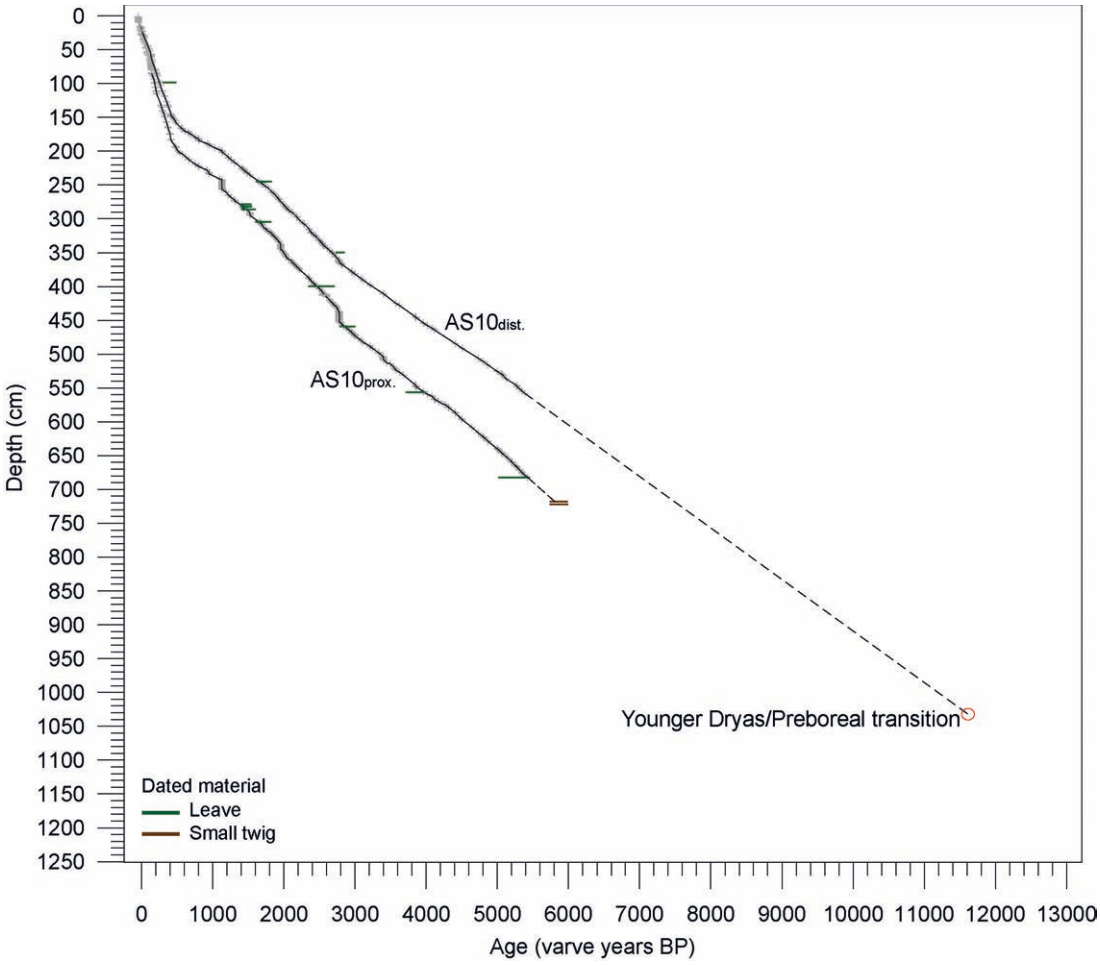

Figure 3.5. Age-depth model for sediment profiles $AS10_{prox}$ and $AS10_{dist}$ constrained by (1) varve dated ages of lithological marker layers (crosses), (2) AMS ^{14}C ages of 14 terrestrial plant macrofossils (bars indicate 2-σ error), and (3) dating of a chronomarker (onset of the Holocene) (von Grafenstein et al., 1999).

3.3.3. Chronology

The age model for the Lake Ammersee detrital layer record was produced (1) by continuous varve counting down to 175 cm in composite profile $AS10_{prox}$ and down to 142 cm in composite profile $AS10_{dist}$ and (2) by construction of a varve-based sedimentation rate chronology for the interval from 175 to 690 cm in $AS10_{prox}$ and from 142 to 357 cm in $AS10_{dist}$. For the latter, varve thickness measurements were carried out in well-preserved sediment sections. Detrital layers in the sediment interval from 357 to 567 cm in $AS10_{dist}$ were dated by transferring ages of correlating deposits in $AS10_{prox}$. Independent age control is provided by accelerator mass spectrometry (AMS) ^{14}C dating of 14 plant macrofossil samples. Of these samples, 9 are leaves and 2 are small twigs from $AS10_{prox}$ and 3 are leaves from $AS10_{dist}$ (Fig. 3.5). Conventional ^{14}C dates were calibrated to years before present (yr BP), *i.e.* AD 1950, applying the CALIB 6.0 program working with the INTCAL09 calibration curve and 2-σ errors (Reimer et al., 2009).

3.3.4. X-ray fluorescence scanning

A set of major element data has been measured from the foil covered surface of splitted cores for composite profiles $AS10_{prox}$ and $AS10_{dist}$ at 200 µm resolution (*i.e.* 5000 data points/meter) using an ITRAX X-ray fluorescence (µ-XRF) core scanner (Cox Analytical, Sweden). The spectrometer has been equipped with a Cr tube and an energy-dispersive SDD detector (Croudace et al., 2006). To reduce sediment matrix effects and ensure predominance of the environmental signal (Francus et al., 2009), the X-ray beam (35 kV, 500 µA, 10 s dwell time) has a width of 8 mm and is orientated parallel to sediment laminations. Continuous downcore element profiles were constructed through multi-parameter correlation of sedimentological and geochemical sediment properties in the overlapping parts (at least 10 cm) of the measured core segments (Fig. 3.4). Micro-XRF data reflect counts per measurement and element normalized (norm) against Cr_{inc} representing relative changes in total element composition. Depth-based µ-XRF data were transferred to the age scale by correlation with varve-dated lithological marker layers, 211 in $AS10_{prox}$ and 156 in $AS10_{dist}$ (Fig. 3.5). Combining high-resolution microfacies and µ-XRF analyses allows evaluating the sedimentological and geochemical properties of each single sediment layer and enables better interpretation and quantification of the data (Brauer et al., 2009).

3.3.5. $CaCO_3$ contents, mineralogy, and grain size distributions

The six thickest detrital layers (E1 to E6) were additionally investigated for intra-layer architecture and composition using $CaCO_3$ contents, mineralogy, and grain size distributions. Varved intervals above and below each detrital layer were analyzed for comparison.

$CaCO_3$ contents were calculated from the total carbon and total organic carbon contents of freeze-dried and homogenized 1 cm sediment slices. Before measuring with an EA-CHNS element analyzer (Eurovector, Milan), aliquots of 3 µg were extracted from the original sample, and for total organic carbon analyzes pre-treated with 20 % HCl at 75°C. After combustion in excess oxygen at 1000°C, total carbon and total organic carbon contents were inferred based on the CO_2 and N_2 contents of the again reduced gases.

Semi-quantitative X-ray diffraction (XRD) analyses were carried out on homogenized bulk sediment samples using a Diffraktometer 5000 (Siemens, Karlsruhe) equipped with a 2 kW X-ray generator working with a Cu tube. The resulting X-ray diffraction pattern is detected by a graphite monochromator and represents the mineralogical composition of the analyzed material.

Grain size distributions of 2 cm sediment samples were measured using a Mastersizer 2000 laser diffraction granulometer (Malvern, Worcestershire). Sample preparation included combustion for 2 hours at 900°C in a muffle furnace to remove the organic fraction and treatment with a dispersant liquid. To ensure representativity of the results, five aliquots from each sample were measured and the final data given as the arithmetic mean of the single measurements.

3.4. Results

3.4.1. Chronology

The age-depth model for Lake Ammersee sediment profiles $AS10_{prox}$ and $AS10_{dist}$ was established back to 5510±161 varve years (vyr) BP. Based on the quality of varve preservation, the chronology can be subdivided into three chronological zones.

Chronological zone A. Back to 400±8 vyr BP (0-175 cm in $AS10_{prox}$/0-142 cm in $AS10_{dist}$) (Fig. 3.3), the chronology for both sediment profiles was constrained by two continuous

counts of distinct varves. Detrital layer seasonality was determined by the microstratigraphic position within an annual sedimentation cycle. A composite chronology was established using counts from the best preserved sediment profile and differs less than 2 % from two previous Lake Ammersee varve chronologies (Alefs, 1997; for details see Czymzik et al., 2010).

Chronological zone B. Due to poor varve preservation, a varve-based sedimentation rate chronology covers the time interval from 400±8 to 5510±161 vyr BP in $AS10_{prox}$ (175-690 cm sediment depth) and to 2820±81 vyr BP in $AS10_{dist}$ (142-357 cm sediment depth) (Fig. 3.3). Years of detrital layer deposition in interpolated sediment intervals were determined based on the calculated sedimentation rate. Annual sedimentation rates have been determined by varve thickness measurements for 55 % of all varves, excluding detrital layers. Comparison of independent varve counts in intervals between two consecutive marker layers in $AS10_{prox}$ and $AS10_{dist}$ (Chapter 3.3.1) revealed a mean chronological error of less than 3 % and enabled to identify the best preserved sediment profile used for the composite chronology.

Chronological zone C. No varves are preserved in sediment profile $AS10_{dist}$ from 2820±81 to 5510±161 vyr BP (357-567 cm core depth). Detrital layers in this interval were dated by transferring ages of correlating deposits in $AS10_{prox}$ (Fig. 3.4).

The composite chronology was anchored to the absolute time-scale using a distinct detrital layer (D2) proven to be formed in June 1993 by sediment trap data (Alefs and Müller, 1999). The onset of the Holocene was defined by a distinct increase in calcite precipitation and a decrease in detrital sedimentation at 1023 cm depth in $AS10_{dist}$ (Fig. 3.3) and dated to 11590 yr BP (von Grafenstein et al., 1999) (Fig. 3.5). The varve chronology is in agreement with 13 AMS ^{14}C dates. One AMS ^{14}C date from fragmented leave particles dated to 340±30 cal. yr BP yielded a ca. 60 years too old age, likely due to redeposition of the material (Fig. 3.5).

3.4.2. Sediment microfacies

The studied sediment interval comprises the upper 690 cm of profile $AS10_{prox}$ and the upper 567 cm of profile $AS10_{dist}$ (Fig. 3.3). Sediment microfacies are biochemical calcite varves and three types of intercalated detrital layers.

3.4.3. Varve microfacies

Characteristic for alpine hardwater lake environments (Swierczynski et al., 2012a), the fine laminated Lake Ammersee deposits (Alefs and Müller, 1999; Czymzik et al., 2010) consist of lighter calcite and darker organic layer couplets (Lotter and Lemcke, 1999) (Fig. 3.6). Calcite layers consist of endogenic precipitated whitish calcite crystals up to 20 µm in size. Typical for low-Mg calcite in freshwater environments like Lake Ammersee (Czymzik et al., 2010) crystal habits are blocky polyhedric and simple rhombic (Folk, 1974; Brauer et al., 2008) (Fig. 3.6). Since calcite precipitation in the epilimnion of lacustrine systems is mainly induced by (1) pH increase due to photosynthetic uptake of dissolved CO_2 by blooming phytoplankton and, (2) because of the retrograde solubity of calcite, during water temperature increase, calcite layers form from late spring to mid-summer (Kelts and Hsü, 1978). Dark organic layers are composed of amorphous organic debris incorporated in a matrix of littoral calcite and dispersed detrital grains. This material is likely eroded at the shoreline by wave activity in fall and redeposited within the lake (Fig. 3.6).

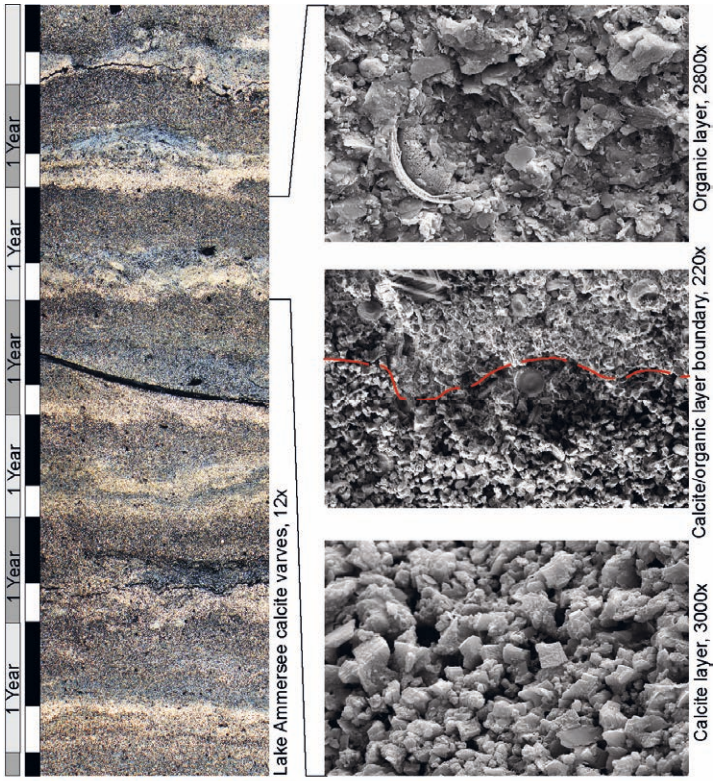

Figure 3.6. (left) Lake Ammersee calcite varves comprising calcite (white) and organic (black) layer couplets (thin section photograph under polarized light). (right) REM-images of (top) an organic layer, (middle) a calcite/organic layer boundary, and (bottom) a calcite layer.

3.4.4. Detrital layer microfacies and geochemistry

Microfacies analyses of the proximal and distal AS10 profiles reveal three main types of detrital microfacies: (1) graded layers, (2) silt/clay layers, and (3) matrix-supported layers (Fig. 3.7). Verifying microscopic observations, all detrital microfacies are accompanied by positive excursions of the elements Ti (Fig. 3.7), Si, K, and Fe, indicative of terrestrial detrital material in Lake Ammersee sediments (Czymzik et al., 2010).

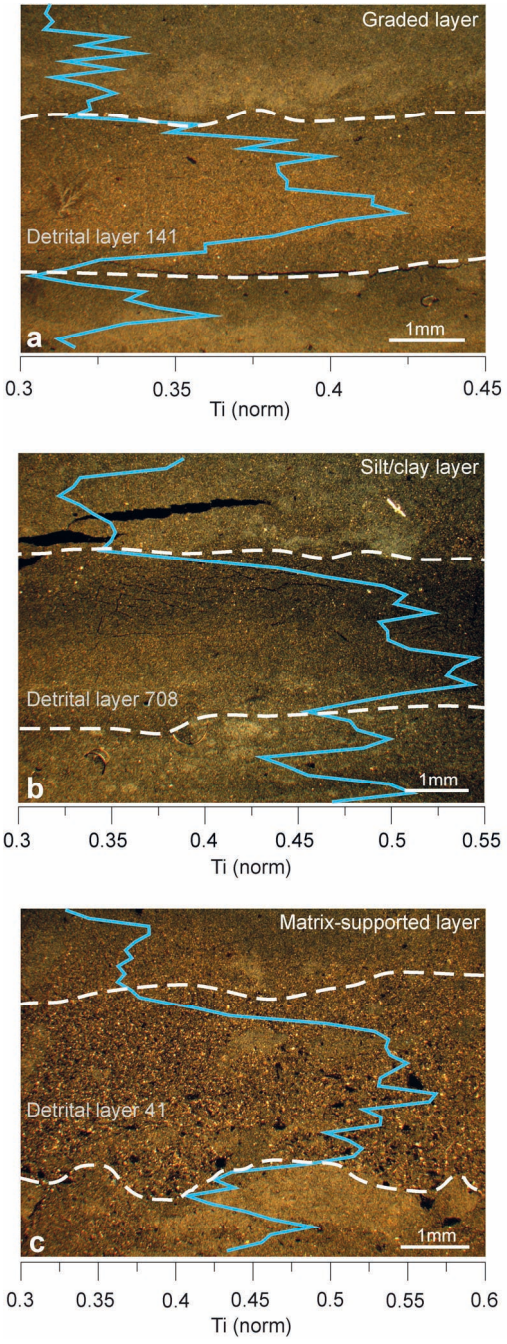

Figure 3.7. Microscope images of detrital microfacies (polarized light) and corresponding µ-XRF Ti (norm) data for (**a**) a graded layer, (**b**) a silt/clay layer, and (**c**) a matrix-supported layer.

1. Graded layers (mean/max. thickness: 1.3 mm/10.8 mm). Layers of this type are characterized by grading from coarse silt (mean grain size 30 µm) to clay (< 2 µm). Some scattered fine sand grains are present in the base of thicker detrital layers. Most thinner graded layers are characterized by an upward fining (Fig. 3.7). Thicker layers of this facies show multiple upward and inverse grading patterns. The predominantly angular detrital grains show a sharp basal contact to the underlying sediment and in some cases an erosional base (Fig. 3.8).

2. Silt/clay layers (mean/max. thickness 1.5 mm/9.6 mm). The very fine, silt to clay, detrital grains that form this lithofacies exhibit no textural organization (Fig. 3.7).

3. Matrix-supported layers (mean/max. thickness: 0.7 mm/135 mm). Matrix-supported layers consist of detrital grains incorporated into a matrix of intraclasts of endogenic calcite both appearing in varying abundances. Plant debris and some littoral diatoms are dispersed throughout these layers (Fig. 3.7).

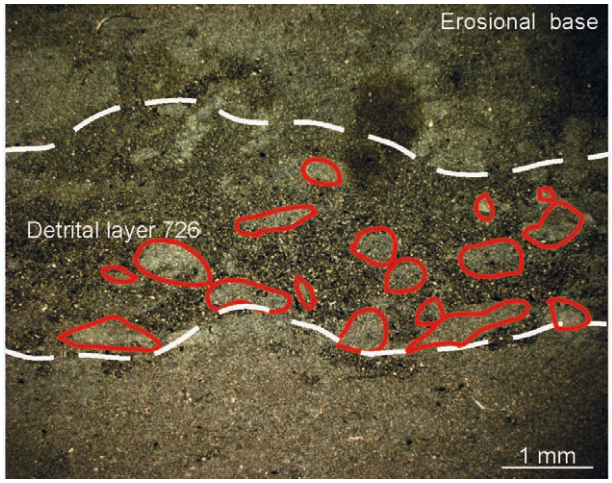

Figure 3.8. Microscope image of a detrital layer with an erosional base (polarized light).

The six thickest matrix-supported layers (E1-E6) deposited at AD 1993, AD 823 (1127 vyr BP), AD 425 (1525 vyr BP), BC 5 (1955 vyr BP), BC 827 (2777 vyr BP), and BC 1446 (3396 vyr BP) were additionally investigated for intra-layer architecture (Fig. 3.9). These layers are from profile $AS10_{prox}$ and vary in thickness between 30 and 135 mm. Thick matrix-supported layers show an increase in median grain size and reduced $CaCO_3$ contents (Fig. 3.9). Main mineral phases are quartz, calcite, and, to a small degree, dolomite. Compositional difference

to thin matrix-supported layers is a higher abundance and coarser grain size of the incorporated plant debris. The thickness of correlating deposits in $AS10_{dist}$ is on average a factor of 8.7 thinner. Five of these correlates are matrix-supported layers and one is a silt/clay layer.

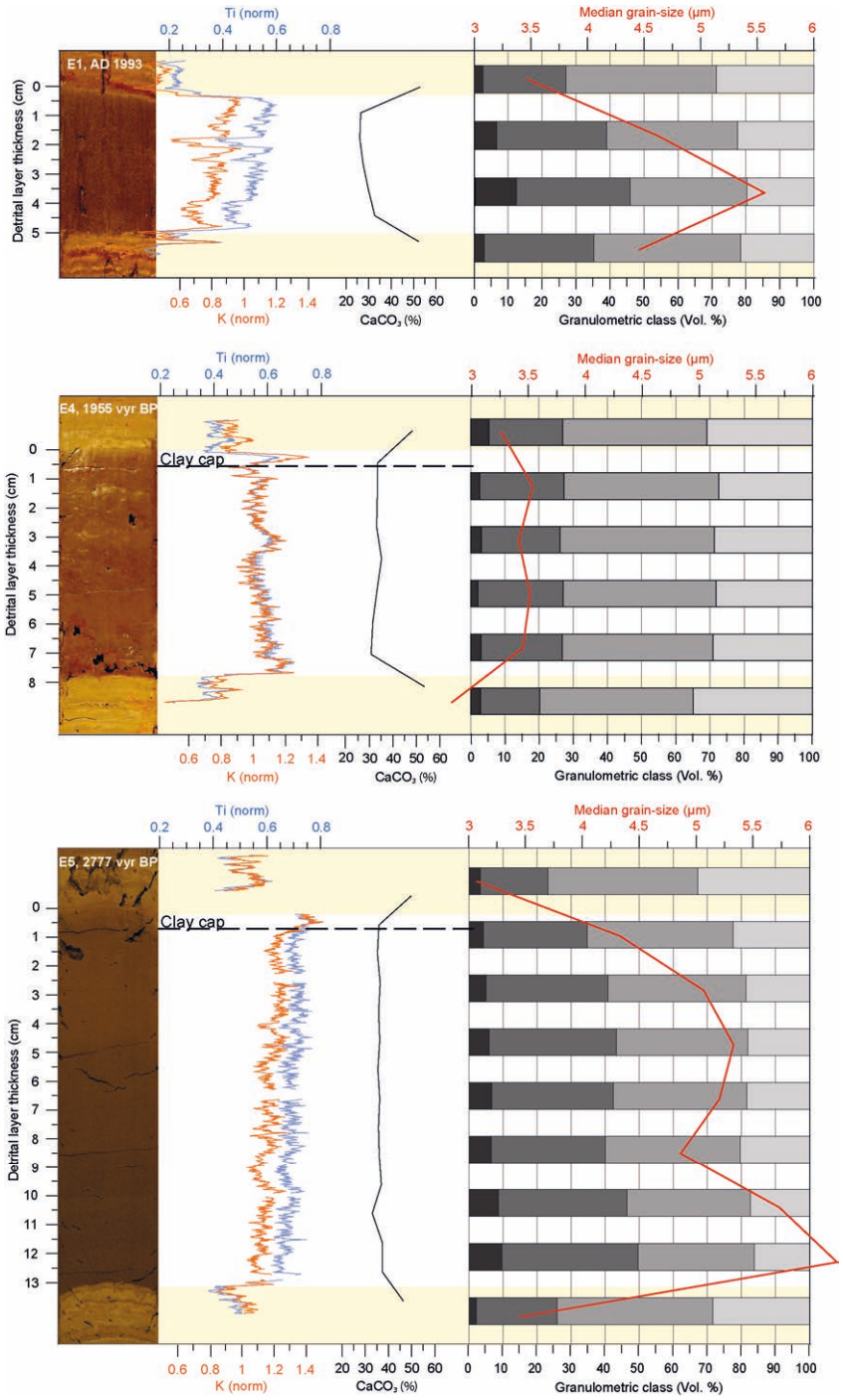

Figure 3.9. Exceptional thick matrix-supported layers E1, E4, and E5 with corresponding µ-XRF Ti and K (norm) data, $CaCO_3$ (%) contents, and median grain size values (µm). Granulometric classes (Vol. %) are: (black) coarse silt, 63 to 20 µm; (dark gray) medium silt, 20 to 6.3 µm; (light gray) fine silt, 6.3 to 2 µm; and (white) clay, 2 to 0.01 µm.

Intra-layer gradients of detrital elements, $CaCO_3$, and grain size vary from layer to layer. Profiles of detrital elements and $CaCO_3$ contents show for 5 out of 6 layers no significant trend within the layer (E2, E3, E4, E5, E6). One layer (E1) indicates upward increasing values for detrital elements and decreasing $CaCO_3$ contents. Median grain size exhibits an upward fining for 3 layers (E1, E2, E5), no trend for layer E4, and an upward coarsening for layer E6. The thickness of layer E3 was too thin to extract more than one sample for grain size measurements. Five of six thick matrix-supported layers (E2, E3, E4, E5, E6) are covered by a clay cap of about 5 mm thickness (Fig. 3.9).

3.4.5. Detrital layer stratigraphy

Since ~5500 vyr BP, in total 1573 detrital layers varying in thickness between 0.2 and 135 mm have been found in either one or both of the investigated Lake Ammersee sediment profiles. Before that time detrital layer deposition was very low in $AS10_{prox}$ and $AS10_{dist}$. The detrital layer record can be subdivided into three depositional units (I-III) ranging from ~5500 to 2800 vyr BP, ~2800 to 500 vyr BP, and from ~500 vyr BP until today, characterized by different mean layer frequency and thickness (Figs. 3.10 and 3.11).

Depositional unit I (~5500-2800 vyr BP). In total 780 detrital layers have been found in this depositional unit. All of these layers were detected in $AS10_{prox}$, but only 39 in $AS10_{dist}$. Frequency of detrital layers is 29 layers/100 yr in $AS10_{prox}$ and 1 layer/100 yr in $AS10_{dist}$. Mean detrital layer thickness is 0.4 mm in $AS10_{prox}$. Due to the low sample size, no representative detrital layer thickness can be given for $AS10_{dist}$ (Figs. 3.10 and 3.11).

Depositional unit II (~2800-500 vyr BP). In comparison to depositional unit I, most conspicuous features of depositional unit II are thicker detrital layers in $AS10_{prox}$ and more frequent detrital layers in $AS10_{dist}$. In total 633 detrital layers have been found in this depositional unit, 571 in $AS10_{prox}$ and 406 in $AS10_{dist}$. Mean frequency and thickness of detrital layers is higher in $AS10_{prox}$ (24 layers/100 yr and 1.2 mm) than in $AS10_{dist}$ (17 layers/100 yr and 0.6 mm) (Figs. 3.10 and 3.11).

Depositional unit III (~500 vyr BP–today). The detrital layer stratigraphy in this depositional unit is characterized by an increase in mean layer thickness and frequency in $AS10_{prox}$ and $AS10_{dist}$, compared to depositional unit II. In total 160 detrital layers have been found in this depositional unit, 150 in $AS10_{prox}$ and 110 in $AS10_{dist}$. Mean detrital layer frequency and

thickness is higher in $AS10_{prox}$ (33 layers/100 yr and 1.4 mm) than in $AS10_{dist}$ (24 layers/100 yr and 1 mm) (Figs. 3.10 and 3.11).

Previous studies on a short Lake Ammersee sediment core (AS07-P1) from the position of $AS10_{dist}$ revealed 13 less detrital layers for depositional unit III (Czymzik et al., 2010). This difference does not change the detrital layer frequency distribution significantly and is due to poorer varve preservation in core AS07-P1 between ~400 and 100 vyr BP.

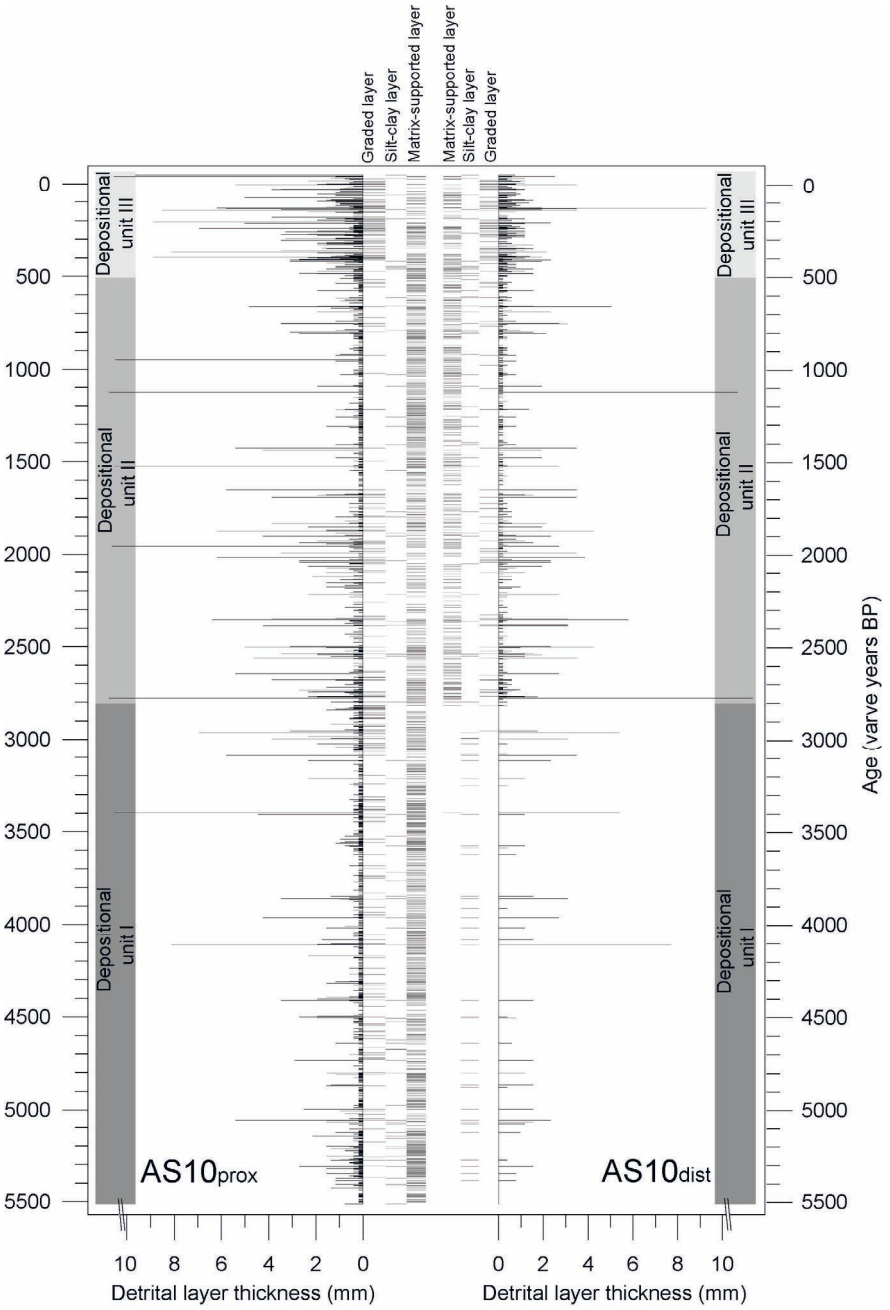

Figure 3.10. Frequency, thickness, and microfacies of detrital layers in $AS10_{prox}$ and $AS10_{dist}$ for depositional units I to III. For a better overview, detrital layer thickness is cut off at 10 mm.

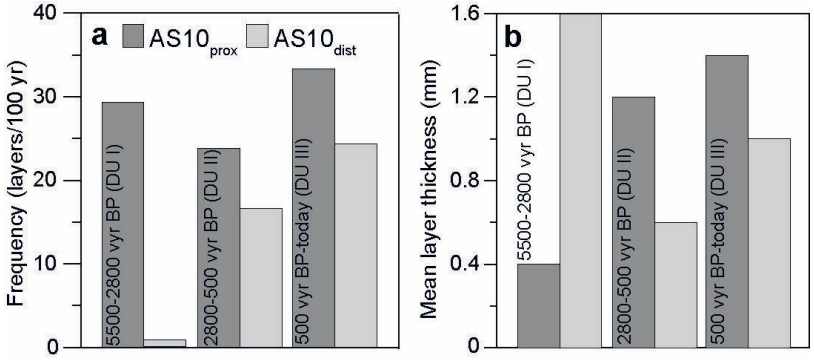

Figure 3.11. Detrital layer deposition pattern for depositional units I to III (DU I-III). (**a**) Frequency of detrital layers (layers/100 yr), and (**b**) mean detrital layer thickness (mm).

3.4.6. Differences in microfacies between $AS10_{prox}$ and $AS10_{dist}$

Throughout the complete ~5500 years, 73 of 483 correlating detrital layers show different microfacies in $AS10_{prox}$ and $AS10_{dist}$. 32 of these deposits are either graded or matrix-supported layers in the proximal profile correlating to silt/clay layers in the distal profile and 31 are graded layers in the proximal profile correlating to matrix-supported layers in the distal profile. Furthermore, eight matrix-supported layers in the proximal profile correlate to graded layers in the distal profile. One graded and one matrix-supported layer in the distal profile correlates to a silt/clay layer in the proximal profile (Fig. 3.10).

3.5. Discussion

3.5.1. Mechanisms of detrital layer formation

The three detrital microfacies are interpreted in terms of different event-type deposition processes (Fig. 3.7).

1. Graded layers. Grading and a proximal-distal layer thickness and frequency pattern (Figs. 3.7 and 3.10) point to deposition of hyperpycnal turbidity currents commonly interpreted to reflect river floods (Sturm and Matter, 1978; Mulder and Alexander, 2001). The sediment/water effluent discharging into the lake is of higher density than the ambient water body and travels, keeping the transported material in suspension by fluid turbulences, as a subaqueous continuation of the river flow along the lake floor. Mixing at the turbidite/lake

water interface leads to a gradual decrease in turbulence affecting differential setting of the transported material (Siegenthaler and Sturm, 1991; Mulder and Alexander, 2001).

2. Silt/clay layers. The fine-grained nature of the deposited detrital material is indicative of meso- or hypopycnal flows (Sturm and Matter, 1978; Mulder and Alexander, 2001) (Fig. 3.7). After entering the lake, the detrital grains are dispersed into a buoyant plume far into the basin and distributed within the water column relative to the density of the travelling gravity current and that of the surrounding water body (Sturm and Matter, 1978). This is reflected by a rather homogenous occurrence of silt/clay layers throughout the basin (Fig. 3.10). The fine particles aggregate and fall out of the water column within few days (Siegenthaler and Sturm, 1991). Alternatively, as demonstrated by 32 silt/clay layers in $AS10_{dist}$ correlating to graded- or matrix-supported layers in $AS10_{prox}$, this lithofacies might reflect distal deposits of high-density flows from which the coarser fraction already deposited (Mangili et al., 2005).

3. Matrix-supported layers. This microfacies reflects high-density currents in which particle interaction is the dominant transport mechanism and enhanced sediment concentrations inhibit graded setting of the material (Mulder and Alexander, 2001). The proximal-distal thickness pattern, incorporated littoral material, and 31 matrix-supported layers in $AS10_{dist}$ correlating to graded layers in $AS10_{prox}$ (Fig. 3.10) suggest deposition after Ammer flood events causing erosion of unconsolidated sediments.

A likely prerequisite for exceptional thick matrix-supported layers (Fig. 3.9) is additional sediment load in the tributary river system of Lake Ammersee. Observations in the Ammer catchment and sediment trap data from Lake Ammersee proved the exceptional thick matrix-supported layer deposited in AD 1993 to reflect a flood induced breakup of the armor layer in a River Ammer tributary (Czymzik et al., 2010). Additional trigger for thick matrix-supported layers might be slope failure in the river catchment.

To summarize, all detrital layers are very likely triggered by River Ammer floods. This interpretation is confirmed by calibration studies comparing the detrital layer record with instrumental River Ammer runoff data from AD 1926 to 1999. The agreement between flood events and flood layers proves the record to represent a time-series of high-magnitude River Ammer floods in spring and summer, the flood seasons in the Ammer catchment (Czymzik et al., 2010).

3.5.2. Uncertainty in flood layer time-series

Establishment of flood layer time-series might be biased by several processes.

Major source of uncertainty are missing flood layers, whether not deposited, not preserved, or not detected (Czymzik et al., 2010; Kämpf et al., 2012b). However, errors of this type can be to a degree detected, quantified, and minimized by comparison of detrital layers in two sediment profiles: For 1018 flood layers only present in $AS10_{prox}$, missing correlates in $AS10_{dist}$ can be explained by reduced detrital sedimentation in more remote positions from the Ammer river mouth (Fig. 3.10). Dispersed detrital grains have been frequently observed in $AS10_{dist}$ at positions where detrital layers occur in $AS10_{prox}$. For 72 flood layers only present in $AS10_{dist}$, however, missing correlates in $AS10_{prox}$ are more difficult to explain. Mean thickness of these deposits in $AS10_{dist}$ is very thin (0.3 mm). Possible explanations for missing deposits in $AS10_{prox}$ might be (1) local erosion by the turbidity stream causing removal of already deposited material (Mulder and Alexander, 2001), (2) inhomogeneous spatial distribution of detrital material on the lake floor, and (3) sediment micro-disturbances. Sediment supply into Lake Ammersee from the western and eastern shores by other minor tributaries is negligible (Müller and Sigl, 1977) and, therefore, as trigger for these layers unlikely.

Since detrital layers in Lake Ammersee represent flood events of River Ammer, flood layers should successively get thinner as function of increasing distance towards the Ammer river inlet (Sturm and Matter, 1978; Mangili et al., 2005). Nevertheless, 225 correlating flood layers are either of equal thickness in both sediment profiles or even slightly thicker in sediment profile $AS10_{dist}$. Equally thick deposits are on average very thin (0.3 mm). In the range of noise, thickness measurements for most of these correlates are not significant. Few slightly thicker flood layers in $AS10_{dist}$ might be explained by inhomogeneous spatial sedimentation and local erosion by the turbidity stream (Mulder and Alexander, 2001).

Human interferences in the lake catchment might obscure the climate induced flood layer signal through land use change modifying sediment mobility (Lauterbach et al., 2012). Located 4.4 km and 6.2 km away from the introductory source River Ammer, supply of detrital material to the locations of sediment profiles $AS10_{prox}$ and $AS10_{dist}$ requires strong floods (Czymzik et al. 2010). Human influences on sediment mobility might, therefore, predominantly amplify the amount of sediment transported into the lake during a flood, and thereby layer thickness, but should not significantly affect layer frequency.

As derived from pollen data, human activity in the Ammersee region first starts at ~4000 yr BP, intensifies synchronous with widespread deforestation and construction of a road net during the Roman Period at ~2000 yr BP, and reaches a maximum at ~1200 yr BP, when several monasteries were founded in the Ammer catchment (Kleinmann, 1995). The lack of synchronous changes in the flood layer record suggests that human contributions to flood layer deposition were likely minor (see Fig. 3.14). This result is in agreement with studies from lakes Lac du Bourget, Silvaplana, and Mondsee (Swierczynski et al., 2012b) suggesting that detrital layer deposition in larger lakes is not strongly affected by human impacts on sediment supply.

Changes in the availability of erodible detrital material in the catchment caused by varying local weathering rates are a further source of uncertainty in flood layer time-series. The Ammer catchment is covered by wide spread late moraine, flysch, and molasse formations since the last deglaciation that all provide abundant erodible fine material (Fig. 3.1). Therefore, changes in weathering rates are unlikely to influence the availability of erodible material at Lake Ammersee throughout the last 5500 years.

3.5.3. Mid- to Late Holocene changes in flood layer deposition

The Mid- to Late Holocene Lake Ammersee record is punctuated by three major shifts in mean flood layer frequency and thickness at ~5500, ~2800, and ~500 vyr BP of different manifestation in $AS10_{prox}$ and $AS10_{dist}$.

After the onset of detrital layer deposition at ~5500 vyr BP, most significant feature of the flood layer record is a conspicuous increase in flood frequency in $AS10_{prox}$ resulting in a 29-fold higher flood layer frequency than in $AS10_{dist}$ (Fig. 3.11). The onset of flood layer deposition in $AS10_{prox}$ might be ascribed to an increase in mean flood intensity. Mean transport capacity of the water/sediment suspension in the lake at that time became sufficient to deliver sediment to the proximal coring location, but was not strong enough to transport sediment to the distal coring location (Fig. 3.12). Exceptions to this pattern are few flood layers in $AS10_{dist}$. Correlating to the thickest deposits in $AS10_{prox}$, these layers might be interpreted in terms of extreme floods (Fig. 3.10).

The second shift in flood layer deposition at ~2800 vyr BP is manifested by a 3-fold increase in flood layer thickness in $AS10_{prox}$ and a 17-fold increase in flood layer frequency in $AS10_{dist}$

(Fig. 3.11). These changes in flood layer distribution might be explained by a further increase in mean flood intensity enhancing the amount of sediment transported to the proximal coring position and leading to a more frequent deposition of detrital material at the distal coring location (Fig. 3.12).

The third shift in flood layer deposition around ~500 vyr BP is marked by an increase in flood layer thickness in $AS10_{prox}$ and $AS10_{dist}$ (Fig. 3.11), suggesting a further enhancement of mean flood intensity. The mean transport capacity of the flood triggered turbidity stream became sufficient to again enhance the amount of detrital material transported to the proximal and distal coring locations (Fig. 3.12).

To conclude, the emerging flood layer deposition pattern in Lake Ammersee sediments during the last ~5500 years is best explained by three stepwise shifts towards higher flood intensities. Similar trends found in flood archives from mid-latitude regions around the globe point to a larger spatial significance of the signal (Fig. 3.13).

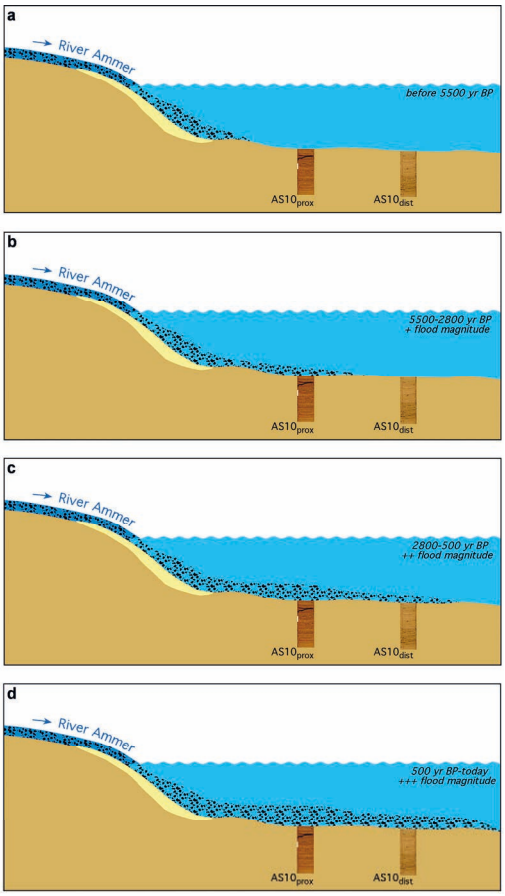

Figure 3.12. Schematic diagram of flood layer deposition in Lake Ammersee at the positions of sediment profiles $AS10_{prox}$ and $AS10_{dist}$ (**a**) before ~5500, (**b**) between ~5500 and 2800, (**c**) between ~2800 and 500 vyr BP, and (**d**) from ~500 vyr BP until today.

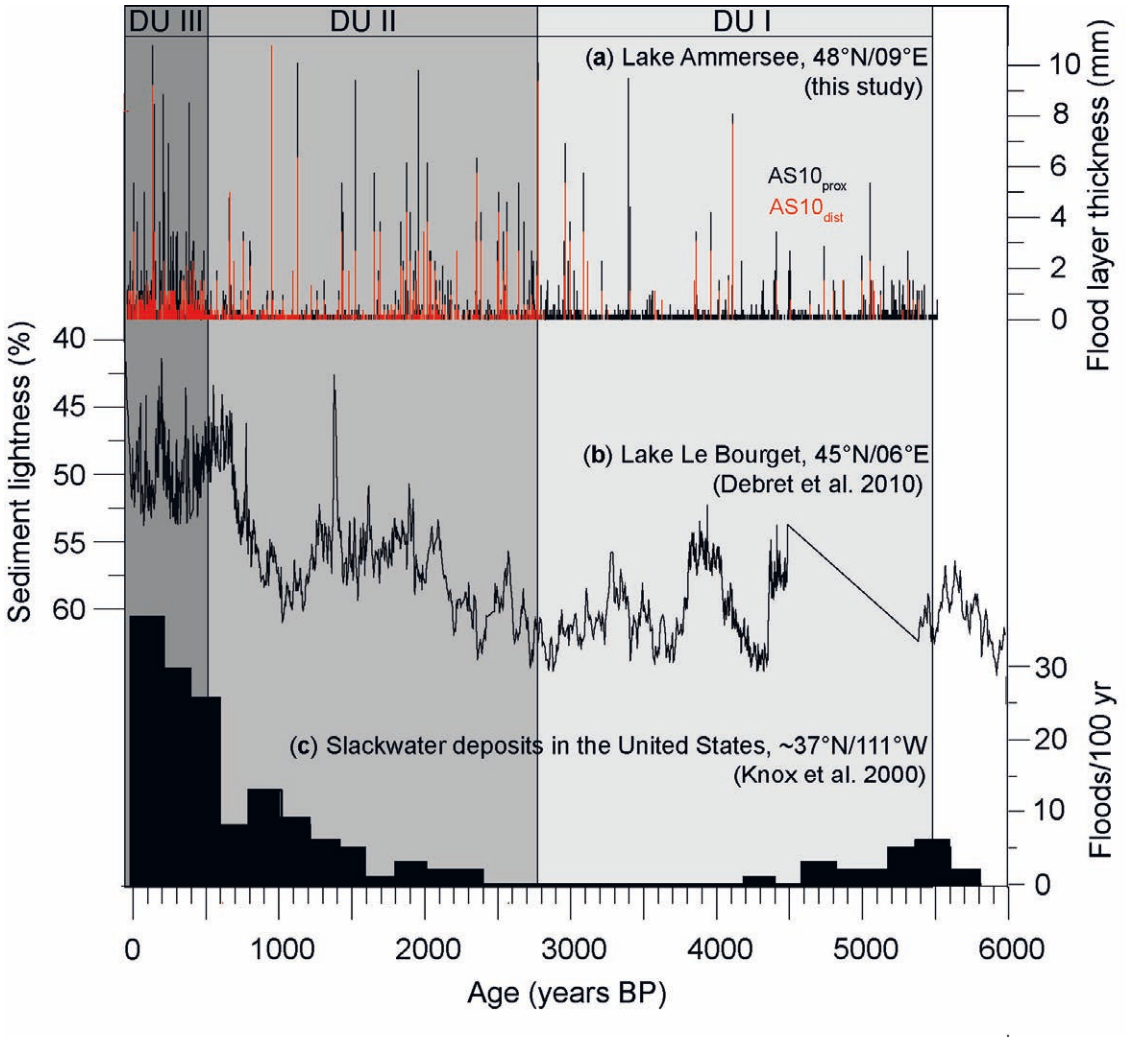

Figure 3.13. Comparison of the (**a**) Lake Ammersee flood layer record (cut off at 10 mm) to mid-latitude paleoflood records. (**b**) Sediment lightness from Lake Le Bourget in the French Alps (Debret et al., 2010) and (**c**) paleofloods from slackwater deposits in Arizona and southern Utah, United States (Knox, 2000). Depositional units (DU) I to III are marked.

Today, flood events in the Ammer catchment are induced by cyclonic westerly weather regimes transporting moisture from the North Atlantic across continental Europe from late spring to summer (Czymzik et al., 2010). In order to increase the mean amount of deposited material on the lake floor after a flood event, rain intensity must have shifted towards extremer events. Anthropogenic influences as well as effects of changes in the availability of erodible material on flood layer deposition are likely of minor importance at Lake Ammersee (chapter 3.5.2).

Westerly cyclone intensity is strengthened by hemispheric cooling acting to enhance potential energy in the troposphere by higher pole-to-equator temperature gradients and, consequently, strengthened baroclinicity (Gill, 1982; Raible et al., 2007; Lamy et al., 2010). Gradually reduced orbital forcing during Northern Hemisphere summer from the Mid-Holocene until today (Laskar, 1990) provoked progressive cooling in the Northern Hemisphere (Wanner et al., 2008) (Fig. 3.14). The regional relevance of this trend is verified by $\delta^{18}O$ of precipitation reconstructed from ostracods in Lake Ammersee sediments, a proxy record of past air temperature (von Grafenstein 1996; 1999) (Fig. 3.14). Thus, orbital forcing might have contributed to the stepwise shifts towards increased mean flood intensity throughout the last ~5500 years.

However, as indicated by the stepwise increasing character, the recorded shifts in flood magnitude throughout the Mid- to Late Holocene are unlikely to be triggered by gradual changes in orbital forcing alone (Fig. 3.14). Timing of shifts in flood intensity coincides with centennial-scale solar minima (Hallstatt minima) (Damon and Sonett, 1991), as reflected in the low-pass filtered record of total solar irradiation (Steinhilber et al., 2009) (Fig. 3.14). A solar influence on climate has been repeatedly proposed based on correlations between paleoclimate records and solar activity. Hypothesized mechanism is a large change in UV radiation affecting polar vortex activity by modification of ozone chemistry and heating in the stratosphere. These disturbances communicate downwards to the surface via wave-mean flow interactions to influence position and strength of the tropospheric westerly storm tracks from winter to early spring (Gray et al., 2010; Martin-Puertas et al., 2012). In addition, shifts towards higher flood intensity at Lake Ammersee are in broad agreement with phases of higher lake level in central Europe interpreted to reflect wetter conditions (Magny, 2004) and cooling in the North Atlantic realm (Denton and Karlén, 1973; Bond et al., 2001; Magny, 2004; Mayewski et al., 2004) (Fig. 3.14). Records of aeolian sand flux in raised bogs from southwest Sweden offer information on increased storminess in the Northern Hemisphere at ~5500, ~2800, and ~500 yr BP (de Jong et al., 2006) (Fig. 3.14). These coincidences might associate the recorded shifts in flood magnitude at Lake Ammersee to strengthened westerlies and potentially hint to a solar influence on atmospheric circulation not only during winter, but also during summer. It is hypothesized that cryospheric processes in spring including sea ice cover of the Barents Sea and snow over Eurasia provide a memory allowing winter climate conditions, potentially affected by the Sun, to transfer into summer (Ogi et al., 2004).

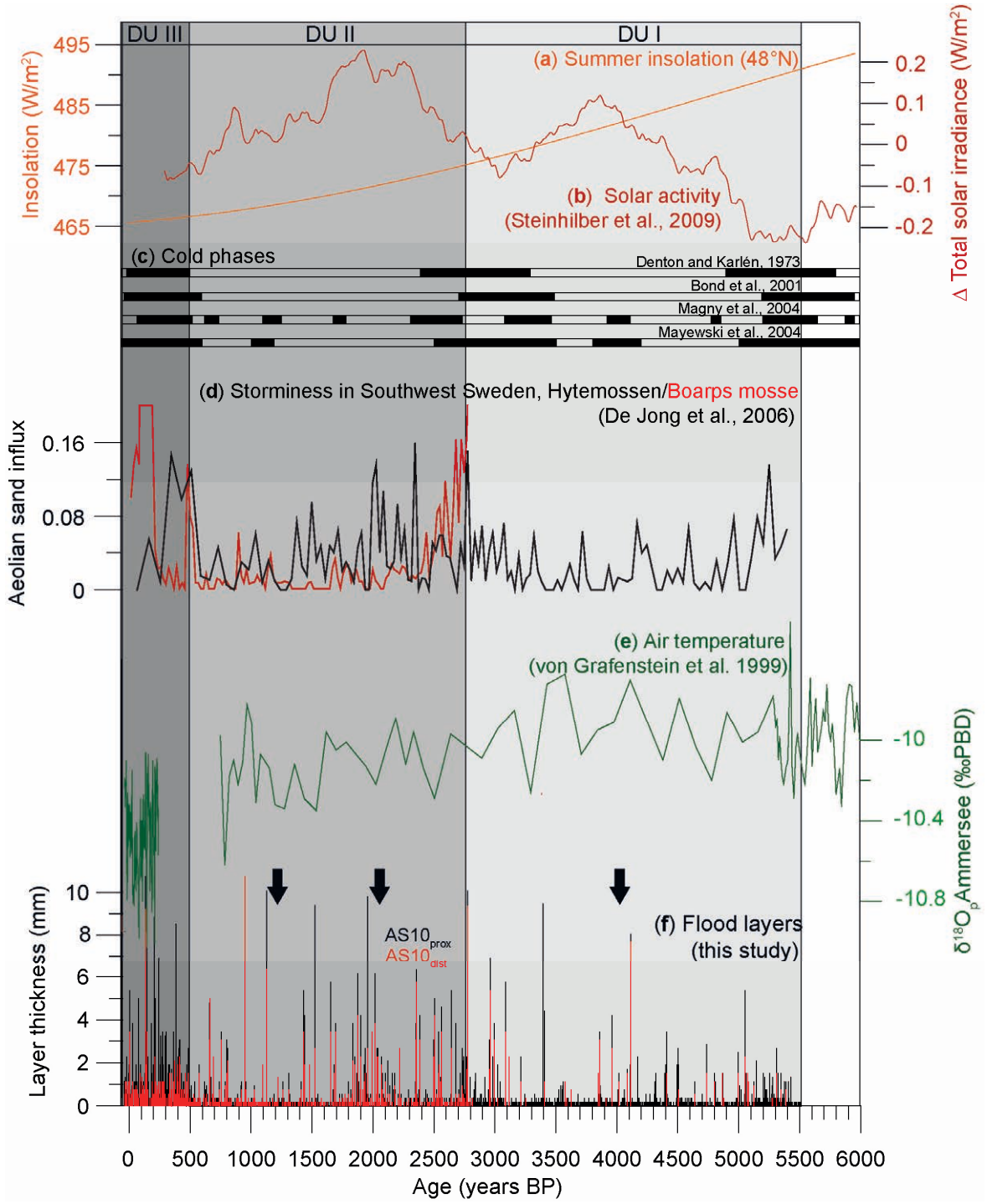

Figure 3.14. Comparison of the Lake Ammersee flood layer time-series with selected Mid- to Late Holocene climate forcing and paleoclimate records. (**a**) Summer insolation (15. July) at 48°N (Laskar, 1990), (**b**) Δ total solar irradiance (Steinhilber et al., 2009) on a 151-year running mean as low-pass filtered record of solar variability, (**c**) cold phases selected from the literature (see the figure for references), (**d**) aeolian sand influx (grains cm^2/yr) reflecting wind strength (de Jong et al., 2006), (**e**) $\delta^{18}O$ of precipitation inferred from benthic ostracods in Lake Ammersee sediments indicating air temperature (von Grafenstein et al., 1999), (**f**) flood layer frequency and thickness (cut off at 10 mm) in Lake Ammersee sediment profiles $AS10_{prox}$ and $AS10_{dist}$. Timing of major human catchment interferences at Lake Ammersee is marked by arrows. Depositional units (DU) I to III are marked by gray shading.

On millennial time-scales, it appears that shifts in flood intensity at Lake Ammersee are induced by gradually reduced orbital summer forcing and centennial-scale solar activity minima affecting a strengthening of flood-prone atmospheric circulation patterns at the mid-latitude location of Lake Ammersee (Fig. 3.15). Proposed response to this forcing is hemispheric cooling enhancing potential energy in the troposphere by strengthened meridional temperature gradients. This energy is translated into intensified cyclonic disturbances, extremer precipitation events and stronger floods at Lake Ammersee.

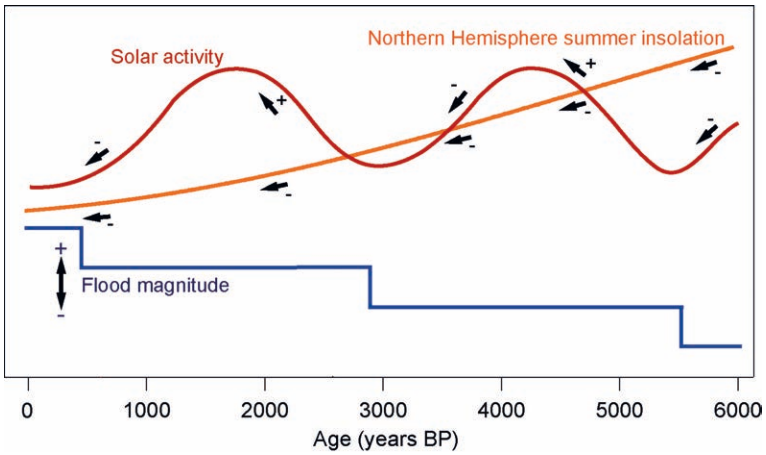

Figure 3.15. Hypothesized forcing of shifts towards higher mean flood intensity at Lake Ammersee by gradually reduced Northern Hemisphere summer insolation and centennial-scale solar activity minima.

3.6. Conclusions

Tracing detrital layer microfacies in two sediment profiles located in a proximal and distal position towards the main tributary of Lake Ammersee and correlating them by means of a varve chronology shed light on flood triggered depositional processes within the lake. Based on their microfacies, geochemistry, and proximal-distal deposition pattern, detrital layers were interpreted as flood deposits of the main tributary River Ammer, predominantly deposited in late spring and summer.

In total 1573 flood layers were detected in the Lake Ammersee sediment record back to ~5500 vyr BP. The flood layer record is punctuated by three stepwise shifts in flood layer thickness and frequency at ~5500, ~2800, and ~500 vyr BP. Combining information from

both sediment profiles allowed to interpret these shifts in terms of stepwise increases in mean flood intensity.

Shifts towards higher flood intensities are likely triggered by gradual orbital and superimposed centennial-scale solar forcing. Likely atmospheric response to these forcing is latitude dependent cooling in the Northern Hemisphere that causes enhanced baroclinicity, stronger mid-latitude cyclones, and enhanced flood intensities at Lake Ammersee.

Acknowledgements

This study is a contribution to the climate initiatives REKLIM Topic 8 ‘Rapid climate change derived from proxy data’ and TERENO of the Helmholtz Association (HGF). We are grateful to B. Brademann (GFZ-Potsdam), M. Köhler (MK Factory), and R. Niederreiter (UWITEC) for their support during the coring campaign and would like to thank D. Berger and G. Arnold (GFZ-Potsdam) for preparing high-quality thin sections. Finally, we would like to acknowledge the Bayerische Verwaltung der staatlichen Schlösser, Gärten und Seen, the LRA Landsberg am Lech, and the WWA-Weilheim for their generous support and permission for conducting coring on Lake Ammersee. A. Hendrich helped with the layout of the figures.

(4) Atmospheric control of flood frequency in central Europe throughout the past 5500 years

Markus Czymzik,[1] Achim Brauer,[1] Gerrit Lohmann,[2] Norel Rimbu,[2] Peter Dulski[1]

[1] GFZ German Research Centre for Geosciences, Section 5.2 Climate Dynamics and Landscape Evolution, Telegrafenberg, 14473 Potsdam, Germany

[2] AWI Alfred Wegener Institute for Polar and Marine Research, Bussestraße 24, 28334 Bremerhaven, Germany

Manuscript in preparation

Modern societies are highly vulnerable to the effects of hydrological extremes like floods on lifes and economy, and thermodynamic increase in atmospheric water vapor is expected to increase the likelihood of such events when Earth warms (Milly et al., 2002; Min et al., 2011). To adequately anticipate the response of floods to climate change it is crucial to understand the receptiveness of these events to natural climate forcing on short and long time-scales and on a regional basis (Knox, 1993; Mudelsee et al., 2003; Czymzik et al., 2010). Instrumental runoff time-series, however, rarely extend the last 100 years and are too short for satisfactory assessing flood responses to changing climate boundary conditions. Flood triggered detrital layers in annually laminated (varved) lake sediments provide natural flood records extending instrumental runoff time-series for millennia, down to seasonal resolution (Czymzik et al., 2010; Swierczynski et al., 2012a). Here, we report a 5500-year record of spring-summer floods based on the frequency of detrital layers in a varved sediment core from Lake Ammersee. Our findings demonstrate that recurrences of floods resemble variability in the East Atlantic-Western Russia (EA-WR) atmospheric pattern, which is commonly not considered for climate studies in this region, as well as decadal to millennial-scale changes in solar activity. Maxima in flood frequency correspond to the negative EA-WR phase and reduced solar activity. We propose a central role of changes in large-scale atmospheric circulation over Europe for the frequency of floods in the Ammersee region and suggest that these atmospheric changes, in turn, are likely influenced by solar variability throughout the past 5500 years.

Extreme river floods have profound effects on society and environment (IPCC, 2012). On seasonal to multi-decadal scales, flood variability in Europe has been repeatedly linked to the prevalent phase of the North Atlantic Oscillation (NAO) (Hurrel, 1995) influencing low-frequency atmospheric circulation, regional precipitation and temperature (Rimbu et al., 2002; Moreno et al., 2008). Much less attention has been paid to hydrometeorological effects of other prominent atmospheric modes like the EA-WR pattern, a zonal symmetric seesaw of atmospheric pressure with centers of action over Western Europe and North of the Caspian Sea (Fig. 4.1) (Barnston and Livezey, 1987; Krichak and Alpert, 2005). Variations of these atmospheric patterns, in turn, are affected by various climate forcing (Nichols and Huang, 2012; Martin-Puertas et al., 2012). Enhanced radiative forcing caused by global warming increases atmospheric water-holding capacity and is expected to enhance the likelihood of stronger floods (Milly et al., 2002; Min et al., 2011). Natural climate variability may affect the frequency and magnitude of such events on time-scales from years to millennia (Knox, 1993; Mudelsee et al., 2003; IPCC, 2012). To date, however, understanding of flood responses to varying climate boundary conditions is limited due to the scarcity of hydrological data in space and time (IPCC, 2012). Exploring paleoclimate archives like varved lake sediments helps to fill this gap in knowledge offering precise dated time-series of flood variability for millennia, at seasonal resolution (Czymzik et al., 2010; 2012a; Swierczynski et al., 2012a).

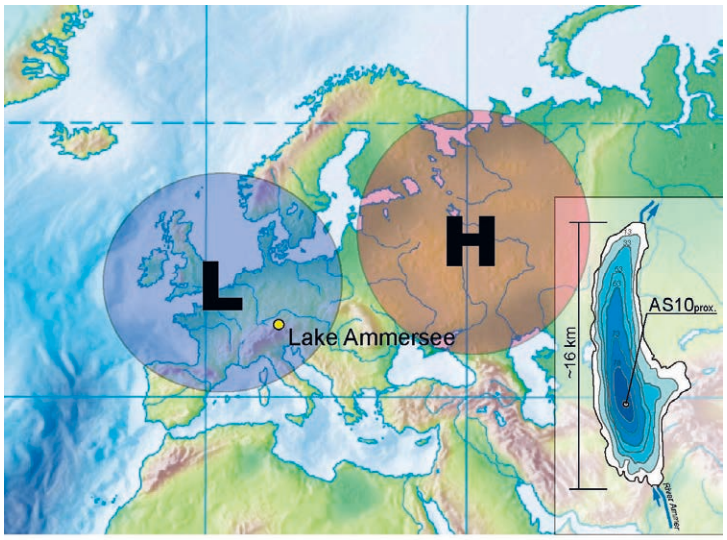

Figure 4.1. East Atlantic-Western Russia (EA-WR) atmospheric pattern and Lake Ammersee. Schematic sketch of pressure anomalies for the negative phase of the EA-WR atmospheric pattern projecting lower pressure over Western Europe and higher pressure north of the Caspian Sea. (inset) Bathymetric map of Lake Ammersee with positions of sediment profile $AS10_{prox}$ and the Ammer river inlet.

Here, we provide a ~5500-year record of recurrences of major floods applying the frequency of detrital layers intercalated into a varved sediment profile from pre-alpine Lake Ammersee in southern Germany (48°00'N, 11°07'E, 533 m above sea level) (Fig. 4.1). During river floods, detrital catchment material is eroded and transported in suspension by fluid turbulence into downstream lakes. In the water body the transport capacity of the inflowing turbidity current successively diminishes leading to the deposition of detrital layers on the lake floor (Fig. 4.2) (Sturm and Matter, 1987; Mulder and Alexander, 2001).

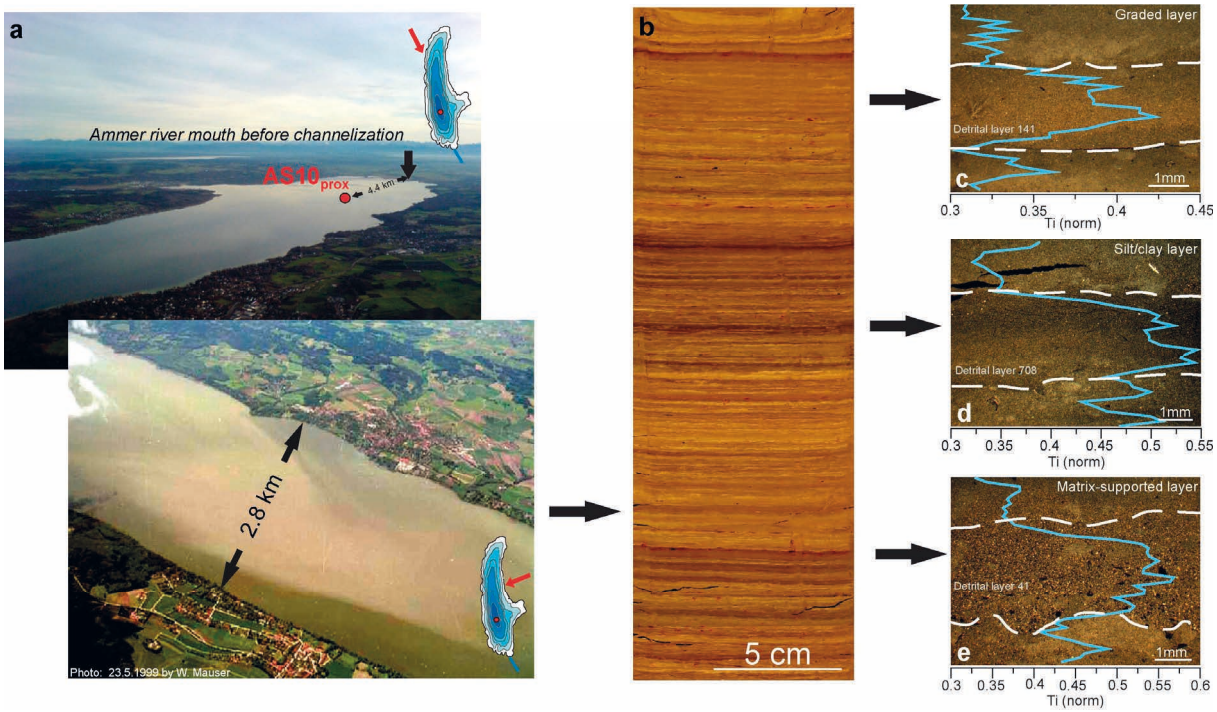

Figure 4.2. Lake Ammersee flood layers. (**a**) Aerial photographs of Lake Ammersee during normal conditions and on 23.5.1999, one day after the crest of the Whitsun flood (22.5.1999; daily mean River Ammer runoff 535 m³/s) exhibiting large amounts of suspended sediments in the water column deposited as a conspicuous flood layer of 10 mm thickness (Czymzik et al., 2010). Red arrows indicate viewing directions. The locations of sediment core $AS10_{prox}$ and the Ammer river mouth before channelization between AD 1920 and 1924 are marked. **(b)** Core photograph of Lake Ammersee sediments showing lighter calcite varves and darker flood layers. **(c-e)** Micrographs (polarized light) of flood layer microfacies in Lake Ammersee sediments overlain by µ-XRF Ti (normalized) data showing **(c)** a graded layer, **(d)** a silt/clay layer, and **(e)** a matrix-supported layer.

Today, major floods in the Ammer catchment are generated by exceptional cyclonic rainfall events from late-spring to summer (Czymzik et al., 2010). High water tables in the northern catchment and low water holding capacity of the alpine soils favor direct translation of

extreme precipitation events into floods by saturation excess overland flow. Late moraine, flysch, and molasse formations in the lake catchment provide abundant erodible fine material for downstream transport into the gully shaped lake by only one main tributary, River Ammer (Czymzik et al., 2012a).

From two Ammersee sediment profiles along a proximal-distal transect, the one closer (~4.5 km) to the Ammer river mouth ($AS10_{prox}$) has been selected for flood reconstruction because of its more complete flood layer record (Czymzik et al., 2012a). The detrital layer time-series was constructed conducting complementary microfacies and X-ray fluorescence analyses (200 µm step size) on sediment profile $AS10_{prox}$ allowing reliable detection of even fractions of a mm thick sediment layers based on their sedimentological and geochemical properties (Czymzik et al., 2012a). Detrital layers were dated by varve counting and their position within an annual sedimentation cycle at seasonal resolution back to 400±8 vyr BP and, due to poorer varve preservation, by means of a varve-based sedimentation rate chronology at annual resolution from 400±8 to 5510±161 vyr BP, in agreement with 14 accelerator mass spectrometry ^{14}C dates (Czymzik et al., 2012a).

In total 1501 detrital layers varying in thickness between 0.19 and 135 mm (mean thickness 0.9 mm) were deposited during the past ~5500 years. These layers form three types of detrital microfacies explained in terms of fluxes of detrital catchment material into the lake after extreme runoff events (Fig. 4.2c-e) (Sturm and Matter, 1978; Mulder and Alexander, 2001; Mangili et al., 2005). Distinct Ti peaks for all detrital layers confirm this interpretation, indicative of terrestrial detrital material in Lake Ammersee sediments (Fig. 4.2c-e) (Czymzik et al., 2012a). River Ammer has been proven as source of the detrital material by the intra-basin deposition pattern of correlating flood layers (Czymzik et al., 2012a). Calibration studies with instrumental River Ammer runoff data confirmed the succession of flood layers to represent a time-series of major River Ammer floods during spring and summer (Czymzik et al., 2010). We consider the annual flood layer succession of the complete ~5500 years to represent a significant flood time-series during spring and summer, the flood season in the Ammer region (Czymzik et al., 2010), because 89 % of all flood layers in the seasonally resolved section back to ~400 vyr BP are deposited in these seasons (Czymzik et al., 2012a). A substantial human impact on flood layer deposition at Lake Ammersee can be ruled out since we do not observe an increase in detrital sedimentation synchronous to major human interferences in the Ammer catchment (Czymzik et al., 2012a).

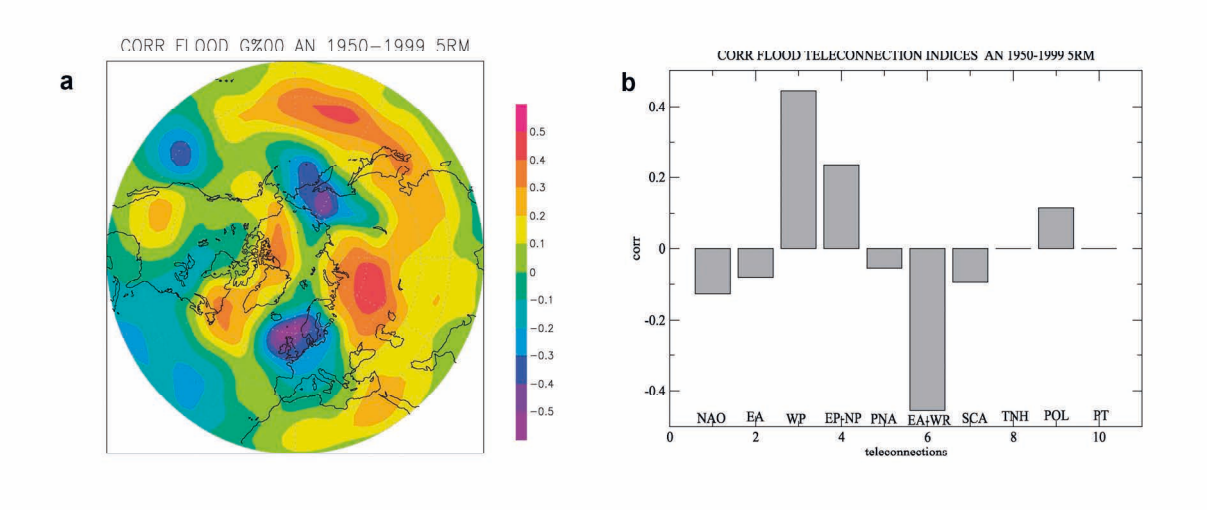

Figure 4.3. Relationship of flood layer frequency to 500 mb geopotential height anomalies and teleconnection patterns. (a) Correlation between flood layer frequency and annual mean 500 mb geopotential high (Kalnay et al., 1996) for the period AD 1950-1999. **(b)** Correlation of annual flood frequency and annual indices of atmospheric teleconnection patterns for the same period. All datasets were filtered with a 5-year running mean prior to the analyses.

For identifying flood-prone large-scale atmospheric circulation at Lake Ammersee, we correlated annual flood layer frequency and annual mean 500 mb geopotential height both filtered with a 5-year running mean for the period AD 1950-1999 using each grid-point of the NCEP/NCAR reanalysis model (Kalnay et al., 1996), working at 2.5 lon x 2.5 lat resolution (Fig. 4.3a). The correlation map depicts a coherent northern hemispheric pattern. For periods of high (low) flood frequency, this pattern projects well on the negative (positive) phase of the EA-WR pattern (Fig. 4.3a). This result is consistent with correlations between flood layer frequency and selected teleconnection pattern indices for the period AD 1950-1999 revealing the highest negative correlation for the EA-WR pattern (Fig. 4.3b).

To test the relationship between flood frequency and the EA-WR atmospheric pattern in the longer term we computed sea level pressure (AD 1750-1999) (Küttel et al., 2010) and 500 mb geopotential height (AD 1766-1999) (Luterbacher et al., 2002) anomalies for years with a flood layer. Indicative of the negative EA-WR phase, both anomaly maps project lower pressure over Western Europe (Fig. 4.4).

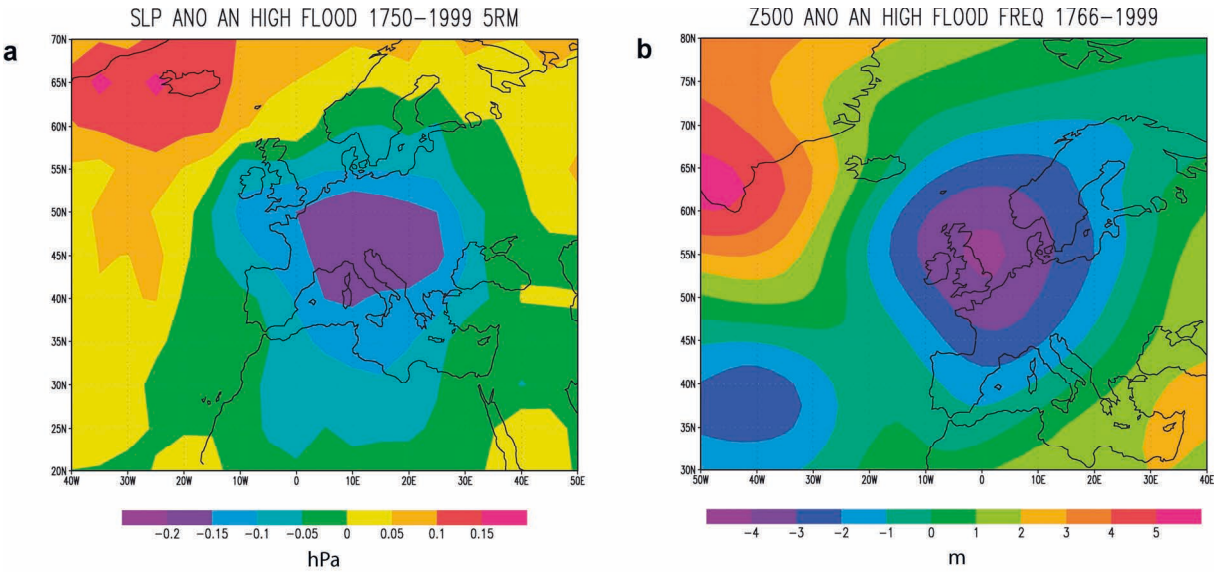

Figure 4.4. Flood layer frequency and atmospheric circulation. (a) Sea level pressure (Küttel et al., 2010) anomaly pattern associated to years with a flood layer for the period AD 1750-1999. **(b)** 500 mb geopotential height (Luterbacher et al., 2002) anomaly pattern associated to years with a flood layer for the period AD 1766-1999.

Instrumental mean daily River Ammer runoff data allow to investigate flood triggering atmospheric circulation at Lake Ammersee in more detail. We calculated mean 500 mb geopotential height anomalies 6, 3, and 0 days prior to River Ammer floods with a daily runoff ≥ 130 m^3/s for the period 1948-2006 using NCEP/NCAR reanalysis data (Fig. 4.5). The atmospheric circulation pattern represent an average of the circulation causing major River Ammer floods and reflect a Rossby wave-breaking phenomenon (Rivère et al., 2010). According to this, major floods at Lake Ammersee are predominantly triggered by atmospheric blocking over Eastern Europe and Rossby wave breaking by a high-pressure ridge over the Iberian Peninsula causing quasi-stationary orogenic precipitation in the Ammersee region by a low-pressure system transporting moisture from the North Atlantic to the northern Alps (Fig. 4.5). We propose that the EA-WR atmospheric pattern modulates the frequency of daily circulation patterns associated to floods in the Ammersee region.

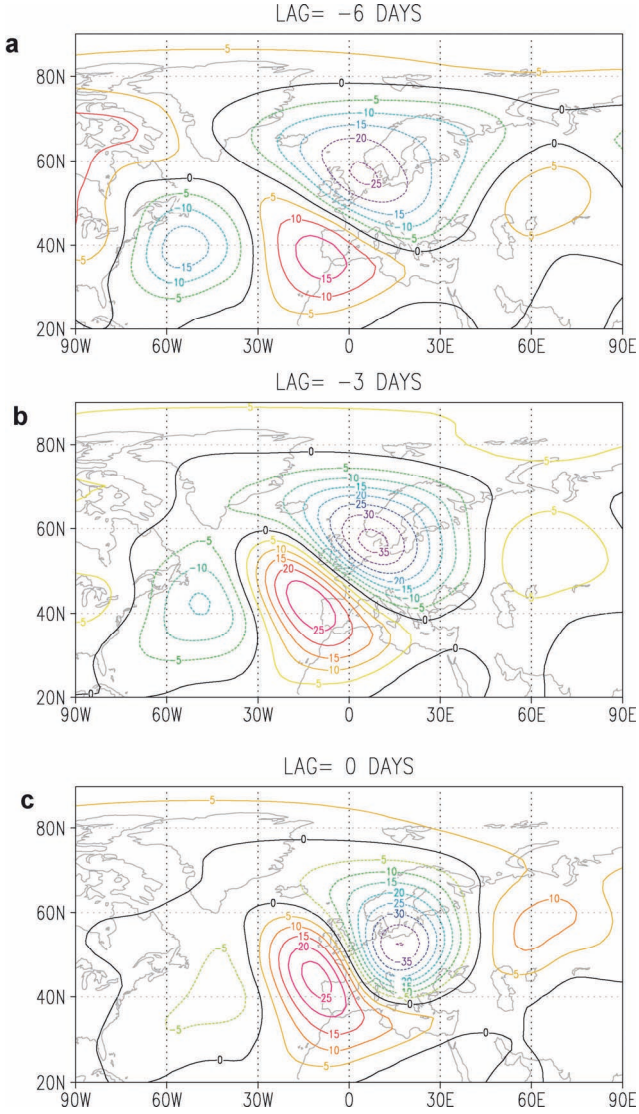

Figure 4.5. Mean atmospheric circulation during major River Ammer floods. 500 mb geopotential height (m) (Kalnay et al., 1996) anomaly maps **(a)** 6 days, **(b)** 3 days, and **(c)** 0 days prior to River Ammer floods ≥ 130 m^3/s daily runoff for the period 1948-2006. The atmospheric circulation patterns represent an average of the circulation causing major River Ammer floods.

In addition, flood layer frequency trends throughout the past 5500 years resemble decadal-scale fluctuations in reconstructed total solar irradiance (TSI) (Steinhilber et al., 2009), increases in flood frequency correspond to reduced TSI (r=-0.47; p=<0.001) (Fig. 4.6a). This linkage remains valid when the flood layer record is compared to multiple other solar activity proxy records (Fig. 4.7). While the influence of the Sun appears to be small on global scale, significant impacts were reported particularly for the mid-latitude areas of Europe and Asia (Martin-Puertas et al., 2012; Lockwood, 2012). Hypothesized mechanism amplifying the small changes in total solar irradiation is the large change in UV emission affecting polar

vortex activity by modification of ozone chemistry and heating in the stratosphere. These disturbances communicate downwards to the surface by mean wave activity flow to influence position and strength of the tropospheric westerly storm tracks in winter (Haigh, 1996; Gray et al., 2010). However, since the Ammersee flood record is representative for spring and summer, the correlation between flood layer frequency and solar activity suggests a solar influence on climate also for these seasons. Possible memory mechanisms transferring the potentially solar induced winter climate signal into summer might be cryospheric processes in spring like ice cover in the Barents Sea and snow in Siberia (Ogi et al., 2004).

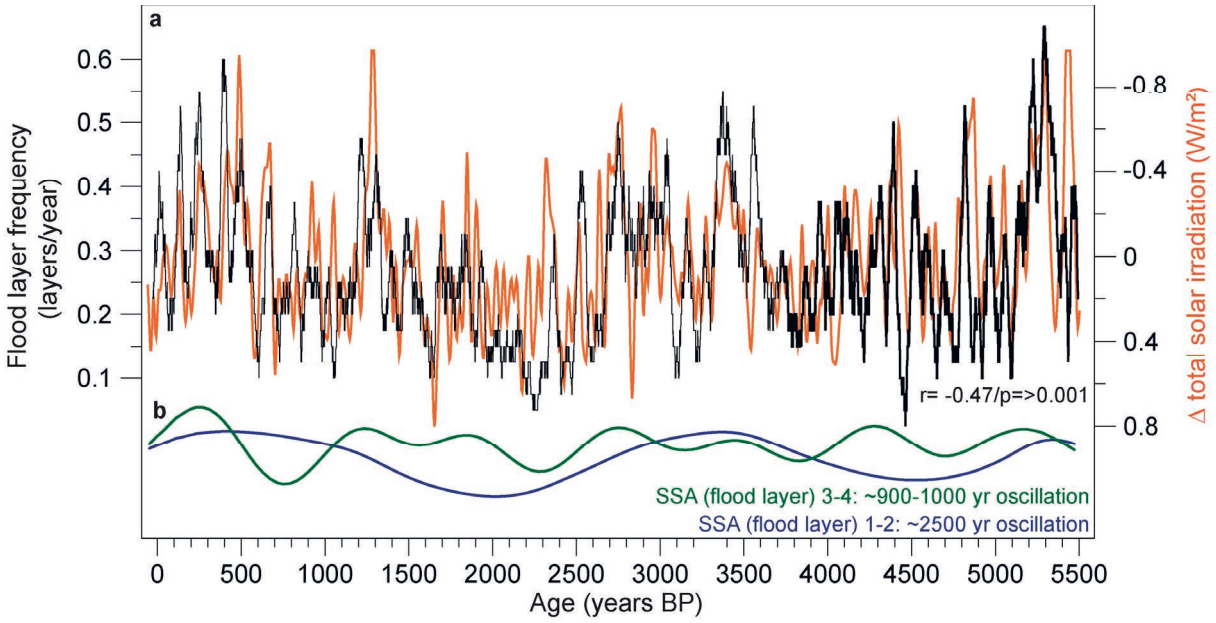

Figure 4.6. Flood layer frequency and solar activity during the past 5500 years. (a) Frequency of flood layers in sediment profile $AS10_{dist.}$ and Δ total solar irradiance (Steinhilber et al., 2009) filtered with a 40-year running mean. **(b)** SSA analysis of the filtered flood layer time-series revealing oscillations of 2500 years for SSA 1-2 and 900-1000 years for SSA 3-4.

In order to isolate longer-term quasi-periodic components, we applied singular spectrum analysis (SSA) (Ghil et al., 2002) to the 5500-year flood layer record filtered with a 40-year running mean. Paired eigenvalues 1-2 reveal a ~2500 year and paired eigenvalues 3-4 a ~900-1000 year oscillation (Fig. 4.6b). Both oscillations have been previously detected in the solar activity record (Dima and Lohmann, 2009) and suggest a solar influence on flood frequency not only on decadal, but also on up to multi-millennial time-scales.

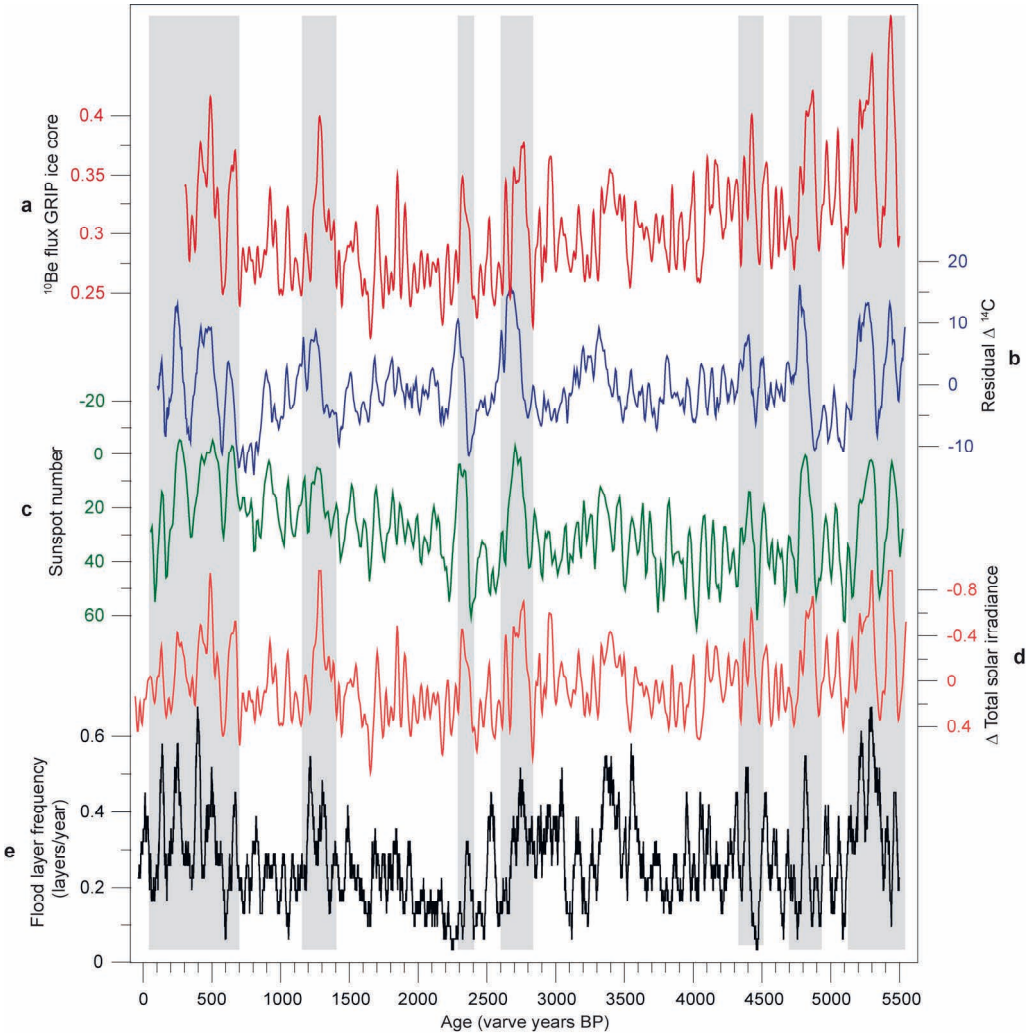

Figure 4.7. Agreement between flood layer frequency and multiple solar activity proxy records. Graphic correlation between **(a)** ^{10}Be flux in GRIP ice core (Vonmoos et al., 2006), **(b)** residual $\Delta^{14}C$ (Reimer et al., 2004), **(c)** reconstructed sunspot number (Solanki et al., 2004), **(d)** Δ total solar irradiation (Steinhilber et al., 2009), and **(e)** flood layer frequency filtered using a 40-year running mean.

This study highlights the great potential of detrital layers in varved lake sediments as long-term flood records at seasonal resolution allowing to deduce flood triggering climate mechanisms on time-scales from years to millennia. Based on robust correlations, our results implicate that the frequency of floods in the Ammersee region is not controlled by temperature, but by changes in large-scale atmospheric circulation over Europe. The additional link between flood frequency and the varying Sun suggests, in line with the hypothesis of a solar influence on mid-latitude tropospheric circulation via changes in UV emission, that these changes in atmospheric circulation, in turn, are likely induced by solar variability.

Acknowledgements

This study is a contribution to the Helmholtz Association (HFG) climate initiatives REKLIM Topic 8 'Rapid climate change derived from proxy data' and TERENO. We thank B. Brademann, M. Köhler, and R. Niederreiter for participating in the coring campaign, as well as D. Berger and G. Arnold for preparation of petrographic thin-sections. We gratefully acknowledge the Bayerische Verwaltung der staatlichen Schlösser, Gärten und Seen, the Landratsamt Landsberg am Lech, and the Wasserwirtschaftsamt Weilheim for providing coring permission for Lake Ammersee. The Bayerisches Landesamt für Umwelt is acknowledged for supplying River Ammer runoff data. We thank U. von Grafenstein for constructive comments on the manuscript.

(5) Summary

5.1 Main results

Primary scientific objectives of this PhD thesis were (1) to explore the potential of varved lake sediments as archives of flood activity and (2) to evaluate climate influences on frequency and magnitude of floods at Lake Ammersee.

To address these objectives a detrital layer record covering the last ~5500 years has been established from two varved Lake Ammersee sediment profiles retrieved in a proximal ($AS10_{prox}$) and distal ($AS10_{dist}$) position towards the main tributary River Ammer. The sedimentological and geochemical features of even microscopic detrital layers have been examined using microscopic microfacies analyses on petrographic thin sections and µ-XRF measurements with a step size of 200 µm. Detrital layers have been dated down to the season by varve counting and determination of the microstratigraphic position within an annual sedimentation cycle. The floating chronology is anchored to the absolute time-scale using a distinct detrital layer of which the deposition in June 1993 is confirmed by sediment trap data and validated by 14 AMS ^{14}C dates from terrestrial plant macrofossils. Intra-basin correlation of detrital layers in both sediment profiles has been performed by means of varve chronology and stratigraphy (Czymzik et al., 2012a).

5.1.1 The potential of detrital layers in varved Lake Ammersee sediments as flood archive

Detrital layers. Detrital layers in Lake Ammersee sediment profiles form three types of microfacies: *(1) Graded layers* consist of clay to coarse silt detrital grains, predominantly organized in a thin upward fining sequence or in a thicker unit built-up by multiple regular and inverse graded beds. *(2) Silt/clay layers* are exclusively formed by very fine detrital grains exhibiting no clear indications of a textural organization. *(3) Matrix-supported layers* are composed of detrital grains and dispersed littoral debris incorporated into a matrix of endogenic calcite. All three detrital microfacies are explained by fluxes of detrital catchment material into the lake after extreme surface runoff events (Czymzik et al., 2010; 2012a).

Confirming the origin of the material, detrital microfacies are accompanied by distinct increases in the elements Ti, Si, K, and Fe, indicative of terrestrial detrital material in Lake Ammersee sediments (Czymzik et al., 2012a).

Due to a successive reduction of transport capacity in the water body, the thickness of flood deposits on the lake floor gets thinner, or deposition even ceases, as function of increasing distance towards the introductory source. Analyzing detrital layers in two sediment profiles along a proximal-distal transect towards the Ammer river mouth revealed 63 % more and 55 % thicker detrital layers in the proximal sediment profile. This proximal-distal deposition pattern enabled to trace River Ammer as source of the material (Czymzik et al., 2012a). Thus, from their microfacies, geochemistry, and proximal-distal deposition pattern, it can be inferred that the succession of detrital layers in Lake Ammersee sediments represents a time-series of River Ammer floods.

Calibration of the flood layer stratigraphy using instrumental runoff data. In order to evaluate the flood time-series in terms of triggering mechanisms and completeness, and to confirm the microscopic determined layer seasonality, the flood layer record was calibrated with instrumental mean daily River Ammer runoff data from AD 1926 to 1999, the time-span covered by flood layer and runoff data (Czymzik et al., 2010).

First, this calibration showed that all layers are triggered by River Ammer floods and confirmed the microstratigraphic determined flood layer seasonality. For 15 of 22 flood layers the season has been determined exactly. Three flood layers designated as “summer” layers correspond to May floods and two designated “spring” layers correspond to February floods. Flood layer seasonality is defined by the position relative to the calcite layer. A spring flood layer is positioned directly under, and a summer flood layer above the calcite layer. The slight uncertainties in flood layer seasonality might be explained by inter-annual variability in the timing of calcite precipitation caused by varying onset and magnitude of summer warming. Further, two designated spring layers reflect a June flood. This uncertainty might be due to micro-erosion that displaced the thin calcite layer (Czymzik et al., 2010).

Second, comparing the flood layer record to instrumental River Ammer floods of different runoff thresholds allowed to define a kind of runoff threshold below which flood layer deposition becomes very unlikely and to evaluate the completeness of the flood layer record. 12 of 17 (71 %) of the strongest floods (≥ 125 m^3/s daily mean runoff) are covered by spring-summer flood layers. For the remaining 5 floods ≥ 125 m^3/s no corresponding flood layer has been found (see the following paragraph for a discussion of possible biases in flood layer time-series). Below the threshold of 125 m^3/s the deposition of a flood layer becomes very unlikely. From 21 floods with a daily runoff between 100 and 125 m^3/s only 2 are represented by a flood layer (Czymzik et al., 2010).

However, including the latter two layers, the comparison also revealed 10 flood layers that are deposited by lower magnitude floods (< 125 m^3/s). Six of these layers are deposited during fall or winter and are not considered for our spring-summer flood time-series. The production of fall flood layers during lower magnitude floods might be explained by enhanced sediment redistribution due to wave triggered shoreline erosion in fall. Two of these layers are deposited in spring-summer and are triggered by floods close to the defined threshold value of 125 m^3/s daily runoff. Two are spring-summer layers only present in $AS10_{prox}$ related to a flood clearly below 125 m^3/s daily runoff (Czymzik et al., 2010).

To conclude, the flood layer stratigraphy in Lake Ammersee sediments represents a significant time-series of the frequency of spring-summer floods ≥ 125 m^3/s daily runoff. The lack of a clear link between the thickness of individual flood layers and flood magnitude suggests non-linearity in the erosion-transport-deposition process cascade (Czymzik et al., 2010).

Uncertainty in flood layer time-series. Several processes might bias flood layer time-series. Main source are missing flood layers, whether not deposited, not preserved, or not detected. Comparison of detrital layers in two sediment profiles allows to a degree to detect, quantify, and minimize this type of error: For 1018 flood layers only present in $AS10_{prox}$, missing correlates in $AS10_{dist}$ might be due to reduced detrital sedimentation in more remote positions from the Ammer river mouth. Dispersed detrital grains have been frequently observed in $AS10_{dist}$ at positions where detrital layers occur in $AS10_{prox}$. For 72 flood layers only present in $AS10_{dist}$, however, missing correlates in $AS10_{prox}$ are more difficult to explain. Mean thickness of these deposits in $AS10_{dist}$ is very thin (0.3 mm). Possible explanations for missing deposits in $AS10_{prox}$ might be (1) local erosion by the turbidity stream causing removal of already deposited material, (2) inhomogeneous spatial distribution of detrital material on the lake floor, and (3) sediment micro-disturbances. Sediment supply into Lake Ammersee from the western and eastern shores by other minor tributaries is negligible and, therefore, as trigger for these layers unlikely (Czymzik et al., 2012a).

Human interferences in the lake catchment might obscure the climate induced flood layer signal through land use change modifying sediment mobility. Located 4.4 km and 6.2 km away from the introductory source River Ammer, supply of detrital material to the locations of sediment profiles $AS10_{prox}$ and $AS10_{dist}$ requires strong floods (Czymzik et al., 2010). Human influences on sediment mobility might, therefore, predominantly amplify the amount

of sediment transported into the lake during a flood, and thereby layer thickness, but should not significantly affect layer frequency (Czymzik et al., 2012a).

As derived from pollen data, human activity in the Ammersee region first starts at ~4000 yr BP, intensifies synchronous with widespread deforestation and construction of a road net during the Roman Period at ~2000 yr BP, and reaches a maximum at ~1200 yr BP, when several monasteries were founded in the Ammer catchment. The lack of synchronous changes in the flood layer record suggests that human contributions to flood layer deposition were likely minor. In agreement with studies from lakes Lac du Bourget, Silvaplana, and Mondsee, this result might imply that detrital layer deposition in larger lakes is not strongly affected by human impacts on sediment supply (Czymzik et al., 2012a).

Further source of uncertainty in flood layer time-series are varying weathering rates changing the availability of erodible material in the catchment. The Ammer catchment is covered by wide spread late moraine, flysch, and molasse formations since the last deglaciation that all provide abundant fine detrital material for erosion and downstream transport into the lake during a flood. Therefore, changes in weathering rates are unlikely to influence the availability of erodible material at Lake Ammersee throughout the last 5500 years (Czymzik et al., 2012a).

5.1.2 Climatic influences on flood frequency and intensity at Lake Ammersee

Mid- to Late Holocene changes in flood frequency. Correlation maps of flood layer frequency with 500 mb geopotential height from the NCEP/NCAR reanalysis model as well as with long-term sea level pressure and 500 mb geopotential height reconstructions project well on the East Atlantic-Western Russia (EA-WR) atmospheric pattern, while flood frequency at Lake Ammersee is enhanced when the EA-WR is in its negative phase. The EA-WR pattern is a zonal symmetric seesaw of atmospheric pressure over Europe. During its negative phase, low-pressure anomalies dominate over Western Europe and high-pressure anomalies dominate north of the Caspian Sea. This result is consistent with correlations between flood layer frequency and selected teleconnection pattern indices for the period AD 1950-1999 revealing the highest negative correlation for the EA-WR pattern. These correlations indicate that flood frequency at Lake Ammersee is apparently modified by the prevalent phase of the EA-WR atmospheric pattern (Czymzik et al., 2012b).

Furthermore, flood frequency resembles decadal to millennial-scale solar activity changes throughout the past ~5500 years, with more floods associated to reduced solar activity. A solar influence on Earth's climate variability has been repeatedly suggested based on correlations between climate variables and the activity of the Sun. While the influence of the Sun appears to be small on global scale, significant impacts were reported for mid-latitudinal areas of the European and Asian continents. Proposed mechanism amplifying the small changes in total solar irradiation is the large change in UV emission affecting polar vortex activity by modification of ozone chemistry and heating in the stratosphere. These disturbances communicate downwards to the surface by mean wave activity flow to influence position and strength of the tropospheric westerly storm tracks from winter to early spring. However, valid for spring and summer, the Lake Ammersee flood layer record suggests a solar influence on climate also for these seasons. It is hypothesized that cryospheric processes in spring including sea ice cover of the Barents Sea and snow over Eurasia transfer winter climate conditions potentially affected by the Sun into summer (Czymzik et al., 2012b).

Summarizing, the presented links suggest that flood frequency at Lake Ammersee in spring and summer is controlled by the prevalent phase of the EA-WR pattern, and that changes in this pattern might, in turn, might be influenced by solar variability throughout the past 5500 years (Czymzik et al., 2012b).

Mid- to Late Holocene changes in flood intensity. Combining flood layer frequency and thickness data from $AS10_{prox}$ and $AS10_{dist}$ allowed to distinguish three shifts towards higher mean flood intensity at Lake Ammersee at ~5500, 2800, and 500 vyr BP (Czymzik et al., 2012a).

Strong floods at Lake Ammersee are triggered by cyclonic weather regimes from the North Atlantic during late-spring and summer (Czymzik et al., 2010). The intensity of such weather regimes is strengthened by hemispheric cooling acting to enhance potential energy and baroclinicity in the troposphere by higher pole-to-equator temperature gradients. Gradually reduced orbital forcing during Northern Hemisphere summer from the Mid-Holocene until today provoked progressive cooling. Hence, orbital forcing might have contributed to the stepwise shifts towards increased mean flood intensity throughout the last ~5500 years (Czymzik et al., 2012a).

However, as indicated by the stepwise increasing character, the recorded shifts in flood intensity are unlikely to be triggered by gradual reduction in orbital forcing alone. Timing of

shifts in flood intensity is synchronous with centennial-scale solar minima, as reflected in the low-pass filtered record of total solar irradiation. In addition, shifts towards higher flood intensity at Lake Ammersee are in broad agreement with phases of higher lake level in central Europe interpreted to reflect wetter conditions, cooling in the North Atlantic realm, and increased storminess in southwest Sweden. These coincidences presumably associate the shifts in flood intensity at Lake Ammersee to strengthened westerlies and potentially hint to a solar forcing of these changes (Czymzik et al., 2012a).

To conclude, stepwise shifts towards higher flood intensity at Lake Ammersee at ~5500, ~2800, and ~500 vyr BP are likely triggered by gradually reduced orbital summer forcing and centennial-scale solar activity minima. Proposed atmospheric response to this forcing is hemispheric cooling enhancing potential energy in the troposphere by strengthened meridional temperature gradients. This energy is translated into intensified cyclonic disturbances, extremer precipitation, and intensified floods at Lake Ammersee (Czymzik et al., 2012a).

5.2 Conclusions

Analyzing detrital layers in two varved sediment profiles from Lake Ammersee located in a proximal and distal position towards the main tributary River Ammer and correlating them by means of varve chronology enabled to establish a 5500-year record of flood triggered detrital sedimentation, down to seasonal resolution. Based on their microfacies, geochemistry, and proximal-distal deposition pattern, detrital layers were interpreted in terms of River Ammer flood deposits predominantly deposited in spring and summer. Calibration with instrumental River Ammer runoff data has proven the flood layer succession to represent a significant time-series of major River Ammer floods during spring and summer, the flood season in the Ammersee region. Interpretation of flood layer data in combination with reanalysis models and time-series analysis indicates that flood frequency and intensity at Lake Ammersee is not stationary, but modified by multi-causal climate forcing on time-scales from years to millennia influencing large-scale atmospheric circulation over Europe. These results challenge future projections that hypothesize an increase in floods when Earth warms based only on the assumption of an enhanced hydrological cycle.

A crucial prerequisite for establishing flood records from lake sediments is a favorable lake/catchment setting. Referring to this, various environmental features in the Ammersee setting can be addressed:

- Varved sediments enable to precisely detect flood layers and date them at seasonal precision by varve counting and the microstratigraphic position within an annual sedimentation cycle.

- A well-developed delta signifies River Ammer as an introductory source of detrital input into the lake throughout the past.

- The gully shaped basin morphology provides a well-defined deposition center for fluxes of detrital material into the lake. The absence of sub-basins that may prevent the turbidity stream to reach the coring locations reduces morphological effects on flood layer deposition and favors predominance of the climate induced flood signal.

- Detrital material is transported into Lake Ammersee by only one main tributary at its southern front side. This allows comparably undisturbed deposition of flood layers without competing lake internal currents and reduces erosion of already deposited detrital material. Additionally, the transport of detrital sediment into the lake by one main tributary enables to better trace the introductory source of flood deposits by their proximal-distal deposition pattern.

- Anthropogenic land use change, glacier fluctuations, and varying weathering rates might bias the climate driven flood layer signal by changing the availability of erodible detrital material in the catchment. These effects are likely of minor importance for detrital sedimentation at Lake Ammersee throughout the past 5500 years.

- Available local runoff and meteorological time-series allow to calibrate the flood layer record in terms of completeness as well as to disentangle climate and environmental impacts on flood triggered detrital sedimentation on a single layer basis.

The novel methodological approach for flood reconstruction combining microfacies analyses and high-resolution μ-XRF measurements on two varved sediment profiles allowed to establish a paleoflood record of a new quality:

- Mean thickness of flood layers in the investigated Lake Ammersee sediments is 0.9 mm. Thus, most of these layers would have remained undetected using traditional geochemical, physical, and biological analyses on discrete samples.

- Investigating flood layers by means of microfacies analyses allows to interpret depositional processes by the micro-sedimentological features of the individual layer itself. This information enables an improved process-orientated understanding of flood layer deposition.

- Comparing flood layer time-series in two varved sediment profiles allows to reduce uncertainties in the chronology and biases in the flood layer time-series produced by missing layers. Correlation of flood layer microfacies in two sediment profiles enables to better infer depositional processes behind flood layer deposition and to trace the introductory source of the detrital material by the proximal-distal deposition pattern.

- To adequately calibrate the flood layer record with instrumental runoff data requires comparable time-concepts. The application of varved sediments reduces the usually decadal to multi-decadal resolution of lake sediment records to the season. This reduction of the time gap between geological and instrumental data allows to more directly compare both data.

- Seasonal varying soil moisture and vegetation cover in the lake catchment bias flood layer deposition by modifying sediment erosion and transport processes (Istanbulluogluras and Bras, 2006). To disentangle these environmental effects on flood layer deposition requires seasonal resolved records.

- Intra-annual climate variability affects regional flood characteristic with regard to triggering atmospheric circulation pattern (Mudelsee et al., 2003; Sivapalan et al., 2005). To isolate this effect requires seasonal resolved chronologies.

5.3 Outlook

The presented results highlight the value of detrital layers in varved Lake Ammersee sediments for better understanding flood triggered detrital deposition in lakes and to deduce climate influences on flood frequency and intensity, but also point to potential for future studies.

Calibration of the Lake Ammersee flood layer stratigraphy with instrumental River Ammer runoff data reveals strong floods that are not represented by a flood layer. Comparing the results from both Lake Ammersee sediment profiles to each other and to instrumental Ammer runoff data allowed to deduce causes for missing layers. In few cases, however, these explanations remain rather speculative. Recently, at Lake Mondsee in upper Austria a holistic observation network was installed integrating in-depth monitoring in the catchment and the lake and a dense net of surface sediment cores. Preliminary results indicate that the observatory is able to trace, follow, and quantify flood-triggered fluxes of detrital material from the tributary river system using automated turbidity sensors and water samplers to the lake using sediment traps. A similar approach at Lake Ammersee will permit to better understand the complete cascade of processes behind flood layer deposition.

The results presented within this thesis suggest a solar influence on flood frequency and magnitude at Lake Ammersee. However, time-scale differences are presently a major source of uncertainty in paleoclimate studies. To investigate the solar/flood link in more detail requires proxy records based on the same chronology. First results on solar activity proxy ^{10}Be in varved lake sediments showed the potential of these archives for solar activity reconstruction, but also pointed to potential biases through contamination with 'old' ^{10}Be by sediment redeposition (Berggren et al., 2009; Mann et al., 2012). Therefore, measuring ^{10}Be in Lake Ammersee sediments might provide a more comprehensive insight into solar/flood relationships. However, it has to be assured that the samples for ^{10}Be measurements are free of detrital material.

Keeping the time-scale issue in mind, analyses of δ^{18}O from benthic ostracods in Lake Ammersee sediments allowed a high-resolution paleotemperature reconstruction for the period from 15500 to 5000 yr BP (von Grafenstein et al., 1999). Extending this record into the present based on the now existing varve chronology will allow to directly compare flood and temperature data for a better understanding of flood-triggering climate boundary conditions.

The Lake Ammersee paleoflood record shed light on regional flood triggering climate mechanisms working on multiple time-scales throughout the last 5500 years. However, flood-generating mechanisms vary in space and time (Petrow and Merz, 2009). A network of long flood time-series from varved lake sediments will help to better understand and predict flood triggering climate mechanisms in continental areas around the globe.

(6) References

Alefs, J. (1997). Feinstratigraphie und Diatomeensukzession in den Profundalsedimenten des Ammersees und Starnberger Sees (Oberbayern). Dissertation an der *Fakultät für Chemie, Biologie und Geowissenschaften der Technischen Universität München*, Hieronymus, München, Deutschland.

Alefs, J., Müller, J., Lenhart, B. (1996). Year to year changes of the diatom assemblage since 1958 in dated varves of a sediment core from Lake Ammersee (Bavaria). *Limnologica* **26**, 39-48.

Alefs, J., Müller, J. (1999). Differences in eutrophication dynamics of Ammersee and Starnberger See (Southern Germany), reflected by the diatom succession in varve-dated sediments. *J. Paleolimnol.* **21**, 395-407.

Arnaud, F., Revel, M., Chapron, E., Desmet, M., Tribovillard, N. (2005). 7200 years of Rhône river flooding activity in Lake Le Bourget, France: a high-resolution sediment record of NW Alps hydrology. *Holocene* **15**, 420-428.

Baker, V.R. (2006). Palaeoflood hydrology in a global context. *Catena* **66**, 161-168.

Baker, V.R. (2008). Paleoflood hydrology: origin, progress, prospects. *Geomorphology* **101**, 1-13.

Barnston, A.G. Livezey, R.E. (1987). Classification, seasonality and persistence of low-frequency atmospheric circulation pattern. *Mon. Weather Rev.* **115**, 1083-1126.

Berggren, A.M., Aldahan, A., Possnert, G., Haltia-Hovi, E., Saarinen, T. (2010). ^{10}Be and solar activity cycles in varved sediments, AD 1900-2006. *J. Paleolimnol.* **44**, 559-569.

Beniston, M., Jungo, P. (2002). Shifts in the distributions of pressure, temperature and moisture and changes in the typical weather patterns in the Alpine region in response to the behavior of the North Atlantic Oscillation. *Theor. Appl. Climatology* **71**, 29-42.

Bond, G., Kromer, B., Beer, J., Muscheler, R., Evans, M.N., Showers, W., Hoffmann, S., Lotti-Bond, R., Hajdas, I., Bonani, G. (2001). Persistent solar influence on the North Atlantic climate during the Holocene. *Science* **294**, 2130-2136.

Binder, H.H. (1999). Lexikon der chemischen Elemente. Das Periodensystem in Fakten, Zahlen und Daten. S. *Hirzel Verlag,* Stuttgart/Leipzig.

Bluszcz, P., Kirilova, E.P., Lotter, A.F., Ohlendorf, C., Zolitschka, B. (2008). Global radiation and onset of stratification as forcing factors of seasonal carbonate and organic matter flux dynamics in a hypertrophic hardwater lake (Sacrower See, northeastern Germany). *Aquat. Geochem.* **14**, 73-98.

Brauer, A. (2004). Annually laminated lake sediments and their palaeoclimatic relevance. In *The Climate in Historical Times. Towards a Synthesis of Holocene Proxy Data and Climate Models*, edited by Fischer, H., Kumke, T., Lohmann, G., Flöser, G., Miller, H., von Storch, H., Negendank, J.F.W. 487 pp., Springer Verlag.

Brauer, A., Casanova, J. (2001). Chronology and depositional processes of the laminated sediment record from Lac d'Annecy, French Alps. *J. Paleolimnol.* **25**, 163-177.

Brauer, A., Mangili, C., Moscariello, A., Witt, A. (2008). Palaeoclimatic implications from micro-facies data of a 5900 varve time series from the Piànico interglacial sediment record, southern Alps. *Palaeogeogr. Palaeocl.* **259**, 121-135.

Brauer, A., Dulski, P., Mangili, C., Mingram, J., Liu, J. (2009). The potential of varves in high-resolution paleolimnological studies. *PAGESnews* **17**, 96-98.

Chapron, E., Desmet, M., De Putter, T., Loutre, M.F., Beck, C., Deconinck, J.F. (2002). Climatic variability in the northwestern Alps, France, as evidenced by 600 years of terrigenous sedimentation in Lake Le Bourget. *Holocene* **12**, 177-185.

Croudace, I.W., Rindby, A., Rothwell, R.G. (2006). ITRAX: description and elevation of a new multi-function X-ray core scanner. In: Rothwell, R.G. (Eds.), *New techniques in sediment core analysis. Geological Society, London, special Publications* **367**, 51-63.

Czymzik, M., Dulski, P., Plessen, B., von Grafenstein, U., Naumann, R., Brauer, A. (2010). A 450 year record of spring-summer flood layers in annually laminated sediments from Lake Ammersee (southern Germany). *Water Resour. Res.* **46**, W11528.

Czymzik, M., Brauer, A., Dulski, P., Plessen, B., Naumann, R., von Grafenstein, U., Scheffler, R. (2012a). Shifts of Mid- to Late Holocene flood magnitude in detrital layers from varved sediments of pre-alpine Lake Ammersee (southern Germany). *Quat. Sci. Rev.* **submitted**.

Czymzik, M., Brauer, A., Lohmann, G., Rimbu, N., Dulski, P. (2012b). Atmospheric control of flood frequency in central Europe throughout the past 5500 years. **in prep**.

Damon, P.E., Sonett, C.P. (1991). Solar and terrestrial components of the atmospheric ^{14}C variation spectrum. In: Sonett, C.P., Giampapa, M.S., Matthews, M.S. (Eds.), *The sun in time*. University of Arizona, Tucson, pp. 360-388.

de Jong, R., Björck, S., Björkman, L., Clemmensen, L.B. (2006). Storminess variation during the last 6500 years as reconstructed from an omrbotrophic peat bog in Halland, southwest Sweden. *J. Quaternary Sci.* **21**, 905-919.

Dearing, J.A. (1991). Lake sediment records of erosional processes. *Hydrobiologica* **214**, 99-106.

Dearing, J.A., Hu, Y., Doody, P., James, P.A., Brauer, A. (2001). Preliminary reconstruction of sediment-source linkages from the past 6000 yr at the Petit Lac d'Annecy, France, based on mineral magnetic data. *J. Paleolimnol.* **25**, 245-248.

Debret, M., Chapron, E., Desmet, M., Rolland-Revel, M., Magand, O., Trentesaux, A., Bout-Roumazeille, V., Nomade, J., Arnaud, F. (2010). North western Alps Holocene paleohydrology recorded by flooding activity in Lake Le Bourget, France. *Quat. Sci. Rev.* **29**, 2185-2200.

Denton, G.H., Karlén, W. (1973). Holocene climate variations - Their pattern and possible cause. *Quaternary Res.* **3**, 155-174.

Dima, M., Lohmann, G. (2009). Conceptual model for millennial climate variability: a possible combined solar-thermohaline circulation origin for the ~1500-year cycle. *Clim. Dyn.* **32**, 301-311.

Folk R.L. (1974). The natural history of crystalline calcium carbonate: effect of magnesium content and salinity. *J. Sediment. Petrol.* **44**, 40-53.

Francus, P., Lamb, H., Nakagawa, T., Marshall, M., Brown, E., Suigetsu 2006 Project Members (2009). The potential of high-resolution X-ray fluorescence core scanning: Applications in paleolimnology. *PAGESnews* **17**, 93-95.

Gerstengarbe, F.-W., Werner, P.C. (2005). Katalog der Großwetterlagen Europas (1881-2004). Nach Paul Hess und Helmut Brezowsky, 6. verbesserte und ergänzte Auflage.

Ghil, M., Allen, M.R., Dettinger, M.D., Ide, K., Kondrashov, D., Mann, M.E., Robertson, A.W., Saunders, A., Tian, Y., Varadi, F., Yiou, P. (2002). Advanced spectral methods for climatic time series. *Rev. Geophys.* **40**, 1-41 (2002).

Gilbert, R., Crookshanks, S. (2009). Sediment waves in a modern high-energy glacilacustrine environment. *Sedimentology* **56**, 645-659.

Gill, A.E. (1982). Atmosphere-ocean dynamics. *International Geophysics Series* **30**, Academic Press, New York.

Gilli, A., Anselmetti, F.S., Ariztegui, D., McKenzie, J.A. (2003). A 600-year sedimentary record of flood events from two sub-alpine lakes (Schwendiseen, Northeastern Switzerland). *Eclogae Geol. Helv.* **96**, 49-58.

Gilli, A., Anselmetti, F.S., Glur, L., Wirth, S.B. (2013). Lake sediments as archives of recurrence rates and intensities of past flood events. *Advances in global change research* **47**, 225-242.

Glaser, R., Stangl, H. (2004). Climate and floods in Central Europe since AD 1000: data, methods, results and consequences. *Surv. Geophys.* **25**, 485-510.

Gray, L.J., Beer, J., Geller, M., Haigh, J.D., Lockwood, M., Matthes, K., Cubasch, U., Fleitmann, D., Harrison, G., Hood, L., Luterbacher, J., Meehl, G.H., Shindell, D., van Geel, B., White, W. (2010). Solar influences on climate. *Rev. Geophys*. **48**, RG4001.

Haigh, J.D. (1994). The role of stratospheric ozone in modulating the solar radiative forcing of climate. *Nature* **370**, 544-546.

Haigh, J.D. (1996). The impact of solar variability on climate. *Science* **272**, 981-984.

Haug, G.H., Hughen, K.A., Sigman, D.M., Peterson, L.C., Röhl, U. (2001). Southward migration of the Intertropical Convergence Zone through the Holocene. *Science* **293**, 1304-1308.

Hurrel, H.W. (1995). Decadal trends in the North Atlantic Oscillation: Regional temperatures and precipitation. *Science* **269**, 676-679.

IPCC (2007). Climate Change 2007: The Physical Science Basis. Contribution of Working Group I to the Fourth Assessment Report of the Intergovernmental Panel on Climate Change (Solomon, S., Qin, D., Manning, M., Chen, Z., Marquis, M., Averyt, K.B., Tignor, M., Miller, H.L. (eds.)). Cambridge University Press, Cambridge, United Kingdom and New York, NY, USA, 996 pp.

IPCC (2012). Managing the Risks of Extreme Events and Disasters to Advance Climate Change Adaptation. A Special Report of Working Groups I and II of the

Intergovernmental Panel on Climate Change (Field, C.B., Barros, V., Stocker, T.F., Qin, D., Dokken, D.J., Ebi, K.L., Mastrandrea, M.D., Mach, K.J., Plattner, G.K., Allen, S.K., Tignor, T., Midgley, P.M. (eds.)). Cambridge University Press, Cambridge, UK, and New York, NY, USA, 582 pp.

Istanbulluoglu, E., Bras, R.L. (2006). On the dynamics of soil moisture, vegetation, and erosion: Implications of climate variability and change. *Water Resour. Res.* **42**, W06418.

Kämpf, L., Brauer, A., Dulski, P., Lami, A., Marchetto, A., Gerli, S., Ambrosetti, W., Guilizzoni, P. (2012a). Detrital layers marking flood events in recent sediments of Lago Maggiore (N. Italy) and their comparison with instrumental data. *Freshwater Biol.* **published online**.

Kämpf, L., Brauer, A., Dulski, P., Feger, K.H., Jacob, F., Klemt, E. (2012b). Sediment imprint of the severe 2002 summer flood in the Lehnmühle reservoir, eastern Erzgebirge (Germany). *Quaternary Science Journal* **61**, 3-15.

Kalnay, E., Kanamitsu, M., Kistler, R., Collins, W., Deaven, D., Gandin, L., Iredell, M., Saha, S., White, G., Woollen, J., Zhu, Y., Chelliah, M., Ebisuzaki, W., Higgins, W., Janowiak, J., Mo, K.C., Ropelewski, C., Wang, J., Leetmaa, A., Reynolds, R., Jenne, R., Joseph, D. (1996). The NCEP/NCAR 40-year reanalysis project. *Bull. Am. Meteorol. Soc.* **77**, 437-471.

Kelts, K., Hsü, K. (1978). Freshwater carbonate sedimentation. In *Lakes: Chemistry*, *Geology, Physics*, edited by Lerman, A., pp. 295-323, Springer, New York.

Kleinmann, A. (1995). Seespiegelschwankungen am Ammersee. Ein Beitrag zur spät- und postglazialen Klimageschichte Bayerns. *Geologica Bavarica* **99**, 253-367.

Knox, J.C. (1993). Large increases in flood magnitude in response to modest changes in climate. *Nature* **361**, 430-432.

Knox, J.C., Kundzewicz, Z.W. (1997). Extreme hydrological events, palaeo-information and climate change. *Hydrolog. Sci. J.* **42**, 765-779.

Knox, J.C. (2000). The sensitivity of modern and Holocene floods to climate change. *Quat. Sci. Rev.* **19**, 439-457.

Kochel, R.C., Baker, V.R. (1982). Paleoflood hydrology. *Science* **22**, 353-361.

Krichak S.O., Alpert, P. (2005). Decadal trends in the east Atlantic-west Russia pattern and Mediterranean precipitation. *Int. J. Climatol.* **25**, 183-192.

Küttel, M., Xoplaki, E., Gallego, D., Luterbacher, J., Garrcía-Herrera, R., Allan, R., Barriendos, M., Jones, P.D., Wheeler, D., Wanner, H. (2010). The importance of ship log data: reconstructing North Atlantic, European and Mediterranean sea level pressure fields back to 1750. *Clim. Dyn.* **34**, 1115-1128.

LfW (Bayerisches Landesamt für Wasserwirtschaft) (2005). Seelitorale in Bayern: Ammersee, Untersuchung benthischer Diatomeen 2001. *Materialienbände des Bayerischen Landesamt für Wasserwirtschaft* **120**.

LfU (Bayerisches Landesamt für Umwelt) (2007). Daily River Ammer runoff data from 1926 to 2005. *Bayerisches Landesamt für Umwelt*, München.

Lamb, M.P., Mohrig, D. (2009). Do hyperpycnal-flow deposits record river-flood dynamics? *Geology* **37**, 1067-1070.

Lambert, A.M., Kelts, K.R., Marshall, N.F. (1976). Measurements of density underflows from Walensee, Switzerland. *Sedimentology* **23**, 87-105.

Lamy, F., Kilian, R., Arz, H.W., Francois, J.P., Kaiser, J., Prange, M., Steinke, T. (2010). Holocene changes in the position and intensity of the southern westerly wind belt. *Nat. Geosci.* **3**, 695-699.

Laskar, J. (1990). The chaotic motion of the solar system: A numerical estimate of the size of the chaotic zones. *Icarus* **88**, 266-291.

Lauterbach, S., Chapron, E., Hüls, M., Gilli, A., Arnaud, F., Piccin, A., Nomade, J., Desmet, M., von Grafenstein, U., DecLakes Participants (2012). A sediment record of Holocene surface runoff events and earthquake activity from Lake Iseo (Southern Alps, Italy). *Holocene* **22**, 749-760.

Leng, M.J., Marshall, J.D. (2004). Palaeoclimate interpretation of stable isotope data from lake sediment archives. *Quat. Sci. Rev.* **23**, 811-831.

Lockwood, M. (2012). Solar influence on global and regional climates. *Surv. Geophys.* **33**, 503-534.

Lotter, A.F., Lemcke, G. (1999). Methods for preparing and counting biochemical varves. *Boreas* **28**, 243-252.

Ludwig, R., Taschner, S., Mauser, W. (2003). Modelling floods in the Ammer catchment: limitations and challenges with a coupled meteo-hydrological model approach. *Hydrol. Earth Syst. Sci.* **7**, 833-847.

Luterbacher. J., Xoplaki, E., Diedrich, D., Rickli, R., Jacobeit, J., Beck, C., Gyaliastras, D., Schmutz, C., Wanner, H. (2002). Reconstruction of sea level pressure fields over the Eastern North Atlantic and Europe back to 1500. *Clim. Dyn.* **18**, 545-561.

Magny, M. (2004). Holocene climate variability as reflected by mid-European lake-level fluctuations and its probable impact on prehistoric human settlements. *Quatern. Int*. **113**, 65-79.

Mangelsdorf, J., Zelinka, K. (1973). Zur Hydrochemie der Ammer (Oberbayern) und ihrer Zuflüsse. *Wasserwirtschaft* **63**, 1-5.

Mangili, C., Brauer, A., Moscariello, A., Naumann, R. (2005). Microfacies of detrital event layers deposited in Quaternary varved lake sediments of the Piànico-Sèllere Basin (northern Italy). *Sedimentology* **52**, 927-943.

Mangili, C., Brauer, A., Plessen, B., Dulski, P., Moscariello, A., Naumann, R. (2010). Effects of detrital carbonate on stable oxygen and carbon isotope data from varved sediments of the interglacial Piànico palaeolake (Southern Alps, Italy). *J. Quaternary Sci.* **25**, 135-145.

Mann, M., Beer, J., Steinhilber, F., Christl, M. (2012). ^{10}Be in lacustrine sediments-a record of solar activity? *J. Atmos. Sol-Terr. Phys.* **80**, 92-99.

Mann, M.E. (2002). Little Ice Age. In *Encyclopedia of Global Environmental Change* **1***, The Earth system: physical and chemical dimensions of global environmental change,* edited by MacCracken, M.C. Perry, J.S., pp 504-509, John Wiley and Sons, Ltd, Chichester.

Martin-Puertas, C., Matthes, K., Brauer, A., Muscheler, R., Hansen, F., Petrick, C., Aldahan, A., Possnert, G., van Geel, B. (2012). Regional atmospheric circulation shifts induced by a grand solar minimum. *Nat. Geosci.* **5**, 397-401.

Mayewski, P.A., Rohling, E.E., Stager, J.C., Karlén, W., Maasch, K.A., Meeker, L.D., Meyerson, E.A., Gasse, F., van Krefeld, S., Holmgren, K., Lee-Thorp, J., Rosqvist, G., Rack, F., Staubwasser, M., Schneider, R.R., Steig, E.J. (2004). Holocene climate variability. *Quaternary Res.* **62**, 243-255.

McEwen, L.J. (2006). Flood seasonality and generating conditions in the Tay catchment, Scotland from 1200 to present. *Area* **38**, 47-64.

Middleton, G.V. (1993). Sediment deposition from turbidity currents. *Annu. Rev. Earth Planet. Sci.* **21**, 89-114.

Milly, P.C.D., Wetherald, R.T., Dunne, K.A., Delworth, T.L. (2002). Increasing risk of great floods in a changing climate. *Nature* **415**, 514-517.

Min, S.-K., Zhang, X., Zwiers, F.W., Hegerl, G.C. (2011). Human contribution to more-intense precipitation extremes. *Nature* **470**, 378-381.

Moreno, A., Valero-Garcés, B.L., González-Sampéritz, P., Rico, M. (2008). Flood response to rainfall variability during the last 2000 years inferred from the Taravilla Lake record (Central Iberian Range, Spain). *J. Paleolim.* **40**, 943-961.

Mudelsee, M., Börngen, M., Tetzlaff, G., Grünewald, U. (2003). No upward trends in the occurence of extreme floods in central Europe. *Nature* **425**, 166-169.

Müller, J., Sigl, W. (1977). Morphologie und rezente Sedimentation des Ammersees. *N. Jahrbuch für Geologie und Paläontologie* **154**, 155-185.

Mulder, T., Alexander J. (2001). The physical character of subaqueous sedimentary density flows and their deposits. *Sedimentology* **48**, 269-299.

Nesje, A., Dahl, S.O., Matthews, J.A., Berrisford, M.S. (2001). A ~4500-yr record of river floods obtained from a sediment core in Lake Atnsjoen, eastern Norway. *J. Paleolimnol.* **25**, 329-342.

Nichols, J.E., Huang, Y. (2012). Hydroclimate of the northeastern United States is highly sensitive to solar forcing. *Geophys. Res. Lett.* **39**, L04707.

Noren, A.J., Bierman, P.R., Steig, E.J., Lini, A., Southon, J. (2002). Millennial-scale storminess variability in the northeastern United States during the Holocene epoch, *Nature* **417**, 821-824.

Ogi, M., Yamazaki, K., Tachibana, Y. (2004). The summertime annular mode in the Northern Hemisphere and its linkage to the winter mode. *J. Geophys. Res.* **109**, D20114.

Osleger, D.A., Heyvaert, A.C., Stoner, J.S., Verosub, K.L. (2009). Lacustrine turbidites as indicators of Holocene storminess and climate: Lake Tahoe, California and Nevada. *J. Paleolimnol.* **42**, 103-122.

Petrow, T., Merz, B. (2009). Trends in flood magnitude, frequency and seasonality in Germany in the period 1951-2002. *J. Hydrol.* **371**, 129-141.

Raible, C.C., Yoshimori, M., Stocker, T.F., Casty, C. (2007). Extreme midlatitude cyclones and their implications for precipitation and wind speed extremes in simulations of the Maunder Minimum versus present day conditions. *Clim. Dyn.* **28**, 409-423.

Reimer, P.J., Baillie, M.G.L., Bard, E., Bayliss, A., Beck, J.W., Bertrand, C.J.H., Blackwell, P.G., Buck, C.E., Burr, G.S., Cutler, K.B., Damon, P.E., Edwards, R.L., Fairbanks, R.G., Friedrich, M., Guilderson, T.P., Hughen, K.A., Kromer, B., McCormac, F.G., Manning, S., Ramsey, C.B., Reimer, R.W., Remmele, S., Southon, J.R., Stuiver, M., Talamo, S., Taylor, F.W., van der Plicht, J., Weyhenmeyer, C.E. (2004). Residual $\Delta^{14}C$ around 1000 year moving average of IntCal04. *Radiocarbon* **46**, 1029-1058.

Reimer, P.J., Baillie, M.G.L., Bard, E., Bayliss, A., Beck, J.W., Blackwell, P.G., Bronk Ramsey, C., Buck, C.E., Burr, G.S., Edwards, R.L., Friedrich, M., Grootes, P.M., Guilderson, T.P., Hajdas, I., Heaton, T.J., Hogg, A.G., Hughen, K.A., Kaiser, K.F., Kromer, B., McCormac, F.G., Manning, S.W., Reimer, R.W., Richards, D.A., Southon, J.R., Talamo, S., Turney, C.S.M., van der Plicht J., Weyhenmeyer, C.E. (2009). IntCal09 and Marine09 radiocarbon age calibration curves, 0-50000 years cal BP. *Radiocarbon* **51**, 1111-1150.

Rimbu, N., Boroneant, C., Buta, C., Dima, M. (2002). Decadal variability of the Danube river flow in the lower basin and its relation to the North Atlantic Oscillation. *Int. J. Climatol.* **22**, 1169-1179.

Rivère, G., Laîné, A., Lapeyre, G., Salas-Mélia, D., Kageyama, M. (2010). Links between rossby wave breaking and the North Atlantic Oscillation-Arctic Oscillation in present day and last glacial maximum simulations. *J. Climate* **23**, 2987-3008.

Schiefer, E., Gibert, R., Hassan, M.A. (2011). A lake sediment-based proxy of floods in the Rocky Mountain Front Ranges, Canada. *J. Paleolimnol.* **45**, 137-149.

Siegenthaler, C., Sturm, M. (1991). Die Häufigkeit von Ablagerungen extremer Reusshochwasser. Die Sedimentationsgeschichte im Urnersee seit dem Mittelalter. *Mitt. Bundesamt für Wasserwirtschaft* **4**, 127-139.

Sivapalan, M., Blöschl, G., Merz, R., Gutknecht, D. (2005). Linking flood frequency to long-term water balance: Incorporating effects of seasonality. *Water Resour. Res.* **41**, W06012.

Solanki, S.K., Usoskin, I.G., Kromer, B., Schüssler, M., Beer, J. (2004). Unusual activity of the Sun during recent decades compared to the previous 11,000 years. *Nature* **431**, 1084-1087.

Spötl, C., Vennemann, T.W. (2003). Continuous-flow isotope ratio mass spectrometric analysis of carbonate minerals. *Rapid Commun. Mass Sp.* **17**, 1004-1006.

Stabel, H.H. (1986). Calcite precipitation in Lake Constance: Chemical equilibrium, sedimentation, and nucleation by algae. *Limnol. Oceanogr.* **31**, 1081-1094.

Steinhilber, F., Beer, J., Fröhlich, C. (2009). Total solar irradiance during the Holocene. *Geophys. Res. Lett.* **36**, L19704.

Stewart, M.M., Grosjean, M., Kuglitsch, F.G., Nussbaumer, S.U., von Gunten, L. (2011). Reconstruction of late Holocene paleofloods and glacier length changes in the Upper Engadin, Switzerland (ca. 1450 BC-AD 420). *Palaeogeogr. Palaeocl.* **311**, 215-223.

Støren, E.N., Dahl, S.O., Nesje, A., Paasche, Ø. (2010). Identifying the sedimentary imprint of high-frequency Holocene river floods in lake sediments: developement and application of a new method. *Quat. Sci. Rev.* **29**, 3021-3033.

Stuiver, M., Polach, H.A. (1977). Discussion: Reporting of ^{14}C Data, *Radiocarbon* **19**, 355-363.

Sturm, M., Matter, A. (1978). Turbidites and varves in Lake Brienz (Switzerland): deposition of clastic detritus by density currents. *Spec. Publs. int. Ass. Sediment* **2**, 147-168.

Svensmark, H., Friis-Christensen, E. (1997). Variation of cosmic ray flux and global cloud coverage - a missing link in solar-climate relationships. *J. Atmos. Sol-Terr. Phys.* **59**, 1225-1232.

Svensmark, H. (2000). Cosmic rays and Earth's climate. *Space Sci. Rev.* **93**, 175-185.

Swierczynski, T., Lauterbach, S., Dulski, P., Brauer, A. (2009). Die Sedimentablagerungen des Mondsees (Oberösterreich) als ein Archiv extremer Abflussereignisse der letzten 100 Jahre. In *Alpine Space – Man & Environment* **6***: Klimawandel in Österreich*, pp. 115-126, Innsbruck University Press.

Swierczynski, T., Brauer, A., Lauterbach, S., Martin-Puertas, C., Dulski, P., von Grafenstein, U., Rohr, C. (2012a). A 1600-year seasonally resolved record of decadal-scale flood variability from the Austrian pre-Alps. *Geology* **accepted**.

Swierczynski, T., Lauterbach, S., Dulski, P., Delgado, J., von Grafenstein, U., Merz, B., Brauer, A. (2012b). Late Holocene paleohydrological changes in the northeastern Alps: A 4000-year flood record from varved sediments of Lake Mondsee (Upper Austria). *Quat. Sci. Rev*. **in prep**.

Thorndycraft, V.R., Hu, Y., Oldfield, F., Crooks, P.R.J., Appleby, P.G. (1998). Individual flood events detected in the recent sediments of the Petit Lac d'Annecy, eastern France. *Holocene* **8**, 714-746.

Thorndycraft, V.R., Benito, G. (2006). The Holocene fluvial chronology of Spain: evidence from a newly compiled radiocarbon database. *Quat. Sci. Rev*. **25**, 223-234.

Usoskin, I.G., Solanki, S.K., Schüssler, M., Mursula, K., Alanko, K. (2003). Millennium-scale sunspot number reconstruction: Evidence for an unusual active sun since the 1940s. *Phys. Rev. Lett.* **91**, 211101.

van Geel, B., Raspopov, O.M., Renssen, H., van der Plicht, J., Dergachev, V.A., Meijer, H.A.J. (1999). The role of solar forcing upon climate change. *Quat. Sci. Rev.* **18**, 331-338.

von Grafenstein, U., Erlenkeuser, H., Müller, J., Kleinmann-Eisenmann, A. (1992). Oxygen isotope records of benthic ostracods in Bavarian lake sediments. *Naturwissenschaften* **79**, 145-152.

von Grafenstein, U., Erlenkeuser, H., Müller, J., Trimborn, P., Alefs, J. (1996). A 200 year mid-European air temperature record preserved in lake sediments: An extension of the $\delta^{18}O_P$-air-temperature relation into the past. *Geochim. Cosmochim. Ac.* **60**, 4025-4036.

von Grafenstein, U., Erlenkeuser, H., Brauer, A., Jouzel, J., Johnson, S.J. (1999). A mid-European decadal isotope-climate record from 15,500 to 5000 years BP. *Science* **284**, 1654-1657.

Vonmoos, M., Beer, J., Muscheler, R. (2006). Large variations in Holocene solar activity: Constrains from ^{10}Be in the Greenland Ice Core Project ice core. *J. Geophys. Res.* **111**, A10105.

Wanner, H., Beer, J., Bütikofer, J., Crowley, T.J., Cubasch, U., Flückiger, J., Goose, H., Grosjean, M., Joos, F., Kaplan, J.O., Küttel, M., Müller, S.A., Prentice, I.C., Solomina, O., Stocker, T.F., Tarasov, P., Wagner, M., Widmann, M. (2008). Mid- to Late Holocene climate change: an overview. *Quat. Sci. Rev.* **27**, 1791-1828.

Waple, A.M., Mann, M.E., Bradley, R.S. (2002). Long-term patterns of solar irradiance forcing in model experiments and proxy based surface temperature reconstructions. *Clim. Dynam.* **18**, 563-578.

Wilhelm, B., Arnaud, F., Sabatier, P., Crouzet, C., Brisset, E., Chaumillon, E., Disnar, J.R., Guiter, F., Malet, E., Reyss, J.L., Tachikawa, K., Bard, E., Delannoy, J.J. (2012). 1400 years of extreme precipitation patterns over the Mediterranean French Alps and possible forcing mechanisms. *Quaternary Res.* **78**, 1-12.

Wirth, S.B., Girardclos, S., Rellstab, C., Anselmetti, F.S. (2011). The sedimentary response to a pioneer geo-project: Tracking the Kander River deviation in the sediments of Lake Thun (Switzerland). *Sedimentology* **58**, 1737-1761.

(7) Data appendix

Appendix A. Flood layer data from sediment profiles $AS10_{prox}$ and $AS10_{dist}$. Back to 400 vyr BP flood layers are dated to the season. From 400 to 5510 vyr BP the resolution is annual. Microfacies are: 1, graded layers; 2, silt/clay layers; 3, matrix-supported layers.

Year BP	Year AD	Sediment profile	Flood layer thickness (mm)	Spring	Summer	Fall	Winter	Microfacies	Annual	Sediment profile	Flood layer thickness (mm)	Spring	Summer	Fall	Winter	Microfacies	Annual
-49	1999	AS10dist	1.73565		1			2	1	AS10prox	9.6425		1			2	1
-43	1993	AS10dist	2.50705		1			3	1	AS10prox	47.0554		1			3	1
-40	1990	AS10dist	0.57855	1				3	1	AS10prox	1.1571	1				3	1
-31	1981	AS10dist	1.1571		1			2	1	AS10prox	1.34995		1			2	1
-29	1979	AS10dist	0.3857	1				3	1	AS10prox	0.7714	1				1	1
-28	1978	AS10dist	0							AS10prox	0.57855	1				1	1
-26	1976	AS10dist	0.3857		1			3	1	AS10prox	0.57855		1			3	1
-22	1972	AS10dist	0.57855			1		1	1	AS10prox	0						
-18	1968	AS10dist	1.1571			1		1	1	AS10prox	2.3142			1		1	1
-15	1965	AS10dist	0.96425		1			1	1	AS10prox	0.3857		1			1	1
-9	1959	AS10dist	0							AS10prox	0.57855	1				1	1
-4	1954	AS10dist	1.1571		1			1	1	AS10prox	0.57855		1			1	1
-2	1952	AS10dist	0.7714				1	1	1	AS10prox	1.5428				1	1	1
0	1950	AS10dist	0							AS10prox	0.7714			1		3	1
1	1949	AS10dist	0.7714		1			1	1	AS10prox	1.9285		1			1	1
3	1947	AS10dist	0.3857			1		3	1	AS10prox	0.57855			1		3	1
4	1946	AS10dist	3.4713		1			1	1	AS10prox	5.3998		1			1	1
12	1938	AS10dist	0.3857			1		1	1	AS10prox	0.3857			1		1	1
13	1937	AS10dist	0							AS10prox	0.57855		1			1	1
15	1935	AS10dist	0							AS10prox	0.57855	1				1	1
18	1932	AS10dist	0.57855		1			1	1	AS10prox	0						
20	1930	AS10dist	0.57855		1			3	1	AS10prox	0.7714		1			3	1
22	1928	AS10dist	0							AS10prox	0.7714		1			3	1
25	1925	AS10dist	0							AS10prox	0.96425		1			1	1
26	1924	AS10dist	0.7714		1			1	1	AS10prox	0.7714		1			1	1
27	1923	AS10dist	1.1571		1			3	1	AS10prox	1.5428		1			1	1
28	1922	AS10dist	1.1571		1			1	1	AS10prox	3.4713		1			1	1
30	1920	AS10dist	1.1571		1			1	1	AS10prox	3.857		1			1	1
39	1911	AS10dist	0							AS10prox	0.96425		1			1	1
40	1910	AS10dist	0.7714		1			1	1	AS10prox	1.1571		1			1	1
43	1907	AS10dist	0							AS10prox	0.7714			1		3	1
44	1906	AS10dist	0							AS10prox	0.96425		1			3	1
49	1901	AS10dist	0.7714			1		3	1	AS10prox	1.1571			1		1	1
57	1893	AS10dist	0.96425		1			3	1	AS10prox	1.9285		1			3	1
62	1888	AS10dist	0.7714		1			2	1	AS10prox	1.1571		1			2	1
63	1887	AS10dist	0.3857		1			3	1	AS10prox	0.3857		1			3	1
65	1885	AS10dist	0.3857	1				3	1	AS10prox	1.1571	1				1	1
67	1883	AS10dist	0.7714	1				3	1	AS10prox	0						
72	1878	AS10dist	0.57855			1		3	1	AS10prox	0						
76	1874	AS10dist	0.3857		1			1	1	AS10prox	0						
78	1872	AS10dist	0.3857		1			3	1	AS10prox	5.0141		1			3	1
83	1867	AS10dist	0							AS10prox	0.3857		1			3	1
88	1862	AS10dist	1.1571		1			3	1	AS10prox	1.34995		1			1	1
91	1859	AS10dist	1.5428	1				3	1	AS10prox	1.5428	1				3	1
95	1855	AS10dist	0.3857	1				3	1	AS10prox	1.9285	1				3	1
99	1851	AS10dist	0.57855		1			1	1	AS10prox	1.1571		1			1	1
105	1845	AS10dist	1.34995		1			1	1	AS10prox	1.1571		1			1	1
109	1841	AS10dist	0.57855	1				3	1	AS10prox	0.7714	1				3	1
110	1840	AS10dist	0.7714		1			3	1	AS10prox	0.96425		1			3	1
119	1831	AS10dist	0.96425		1			1	1	AS10prox	1.1571		1			1	1

123	1827	AS10dist	0						AS10prox	0.3857		1		1	1
124	1826	AS10dist	0.57855	1			1	1	AS10prox	0.3857	1			1	1
125	1825	AS10dist	0						AS10prox	0.57855		1		1	1
128	1822	AS10dist	0.7714		1		1	1	AS10prox	1.5428		1		1	1
129	1821	AS10dist	0.3857	1			3	1	AS10prox	0.3857	1			1	1
131	1819	AS10dist	0						AS10prox	1.1571		1		1	1
132	1818	AS10dist	1.9285	1			3	1	AS10prox	6.1712	1			3	1
135	1815	AS10dist	9.2568		1		1	1	AS10prox	10.7996		1		1	1
136	1814	AS10dist	3.4713		1		1	1	AS10prox	5.7855		1		1	1
137	1813	AS10dist	1.5428		1		1	1	AS10prox	3.4713		1		1	1
138	1812	AS10dist	0						AS10prox	0.57855		1		1	1
139	1811	AS10dist	0						AS10prox	0.57855		1		1	1
140	1810	AS10dist	1.9285		1		2	1	AS10prox	3.4713		1		2	1
144	1806	AS10dist	3.4713		1		1	1	AS10prox	8.4854		1		1	1
145	1805	AS10dist	0						AS10prox	0.3857		1		1	1
150	1800	AS10dist	0						AS10prox	0.19285	1			3	1
152	1798	AS10dist	0						AS10prox	0.3857		1		3	1
153	1797	AS10dist	0.7714		1		3	1	AS10prox	2.3142		1		1	1
155	1795	AS10dist	0						AS10prox	0.3857	1			1	1
156	1794	AS10dist	0						AS10prox	1.1571		1		1	1
164	1786	AS10dist	0						AS10prox	0.3857		1		3	1
172	1778	AS10dist	0.3857		1		3	1	AS10prox	0.3857		1		3	1
180	1770	AS10dist	0						AS10prox	0.3857		1		1	1
181	1769	AS10dist	0						AS10prox	0.96425		1		1	1
182	1768	AS10dist	0.3857		1		3	1	AS10prox	3.857		1		1	1
188	1762	AS10dist	0.3857	1			3	1	AS10prox	1.5428	1			1	1
189	1761	AS10dist	0						AS10prox	0.3857			1	3	1
190	1760	AS10dist	1.1571		1		2	1	AS10prox	0.7714		1		2	1
195	1755	AS10dist	0						AS10prox	0.3857		1		1	1
197	1753	AS10dist	0.57855		1		1	1	AS10prox	1.9285		1		1	1
205	1745	AS10dist	0						AS10prox	0.7714		1		1	1
207	1743	AS10dist	0.57855			1	1	1	AS10prox	8.8711			1	1	1
212	1738	AS10dist	2.3142		1		1	1	AS10prox	0.19285		1		3	1
215	1735	AS10dist	0						AS10prox	1.5428		1		3	1
216	1734	AS10dist	1.1571		1		1	1	AS10prox	5.0141		1		1	1
217	1733	AS10dist	0						AS10prox	0.3857		1		1	1
219	1731	AS10dist	1.1571			1	1	1	AS10prox	0.7714			1	1	1
222	1728	AS10dist	0						AS10prox	0.19285		1		1	1
225	1725	AS10dist	0.57855	1			1	1	AS10prox	0					
226	1724	AS10dist	0.57855	1			1	1	AS10prox	0.3857	1			1	1
229	1721	AS10dist	0						AS10prox	0.3857		1		3	1
233	1717	AS10dist	0.96425		1		3	1	AS10prox	0.19285		1		3	1
235	1715	AS10dist	0.57855			1	1	1	AS10prox	0.3857			1	1	1
237	1713	AS10dist	0.3857		1		3	1	AS10prox	0.57855		1		3	1
239	1711	AS10dist	0.3857		1		3	1	AS10prox	0.3857		1		3	1
240	1710	AS10dist	0.7714		1		3	1	AS10prox	0.3857		1		3	1
241	1709	AS10dist	0.3857		1		1	1	AS10prox	0.3857		1		1	1
242	1708	AS10dist	1.1571		1		1	1	AS10prox	1.1571		1		1	1
243	1707	AS10dist	0.96425		1		3	1	AS10prox	6.9426		1		3	1
244	1706	AS10dist	0.7714		1		1	1	AS10prox	0.3857		1		1	1
246	1704	AS10dist	0.3857			1	3	1	AS10prox	0.19285			1	3	1
248	1702	AS10dist	0						AS10prox	0.57855		1		1	1
251	1699	AS10dist	0						AS10prox	0.3857		1		3	1
255	1695	AS10dist	0						AS10prox	0.3857	1			1	1
256	1694	AS10dist	1.1571		1		1	1	AS10prox	1.9285		1		1	1
258	1692	AS10dist	0						AS10prox	0.3857		1		3	1
260	1690	AS10dist	0						AS10prox	0.3857		1		3	1
261	1689	AS10dist	0.3857	1			3	1	AS10prox	3.27845	1			3	1
263	1687	AS10dist	0						AS10prox	0.3857		1		3	1
265	1685	AS10dist	1.1571			1	3	1	AS10prox	0.19285			1	3	1
266	1684	AS10dist	0.7714	1			1	1	AS10prox	0.7714	1			1	1
268	1682	AS10dist	0.7714			1	2	1	AS10prox	0.19285			1	3	1

272	1678	AS10dist	1.1571		1		1	1	AS10prox	2.3142		1		1	1
274	1676	AS10dist	0.3857		1		1	1	AS10prox	3.4713		1		1	1
278	1672	AS10dist	0.3857	1			3	1	AS10prox	0.7714	1			3	1
281	1669	AS10dist	1.1571		1		1	1	AS10prox	1.9285		1		1	1
284	1666	AS10dist	0.7714		1		3	1	AS10prox	0.3857		1		3	1
286	1664	AS10dist	0						AS10prox	0.3857		1		3	1
288	1662	AS10dist	0.57855		1		3	1	AS10prox	0					
289	1661	AS10dist	1.1571		1		1	1	AS10prox	0					
290	1660	AS10dist	0.57855	1			3	1	AS10prox	0.3857	1			3	1
294	1656	AS10dist	0.57855		1		3	1	AS10prox	1.1571		1		3	1
297	1653	AS10dist	0						AS10prox	3.27845	1			1	1
299	1651	AS10dist	0.3857		1		3	1	AS10prox	0					
300	1650	AS10dist	0.19285		1		3	1	AS10prox	1.1571		1		3	1
305	1645	AS10dist	0						AS10prox	3.4713		1		1	1
310	1640	AS10dist	0						AS10prox	0.7714		1		3	1
313	1637	AS10dist	0.3857	1			1	1	AS10prox	0.3857	1			1	1
316	1634	AS10dist	0						AS10prox	0.3857		1		3	1
319	1631	AS10dist	0						AS10prox	1.5428	1			1	1
323	1627	AS10dist	0.57855	1			3	1	AS10prox	1.9285	1			3	1
324	1626	AS10dist	0.57855		1		3	1	AS10prox	0.7714		1		1	1
326	1624	AS10dist	0						AS10prox	1.5428		1		3	1
332	1618	AS10dist	1.5428		1		3	1	AS10prox	1.9285		1		3	1
338	1612	AS10dist	0.3857		1		3	1	AS10prox	0.3857		1		3	1
340	1610	AS10dist	0						AS10prox	0.3857		1		1	1
343	1607	AS10dist	0.7714			1	1	1	AS10prox	0.19285			1	1	1
349	1601	AS10dist	1.1571		1		3	1	AS10prox	1.73565		1		3	1
350	1600	AS10dist	1.5428	1			1	1	AS10prox	1.5428	1			1	1
354	1596	AS10dist	0.7714	1			1	1	AS10prox	0					
357	1593	AS10dist	0						AS10prox	0.19285		1		1	1
363	1587	AS10dist	1.1571		1		1	1	AS10prox	3.4713		1		1	1
370	1580	AS10dist	2.12135	1	1		1	2	AS10prox	8.0997	1	1		1	2
374	1576	AS10dist	0.7714		1		1	1	AS10prox	1.9285		1		1	1
375	1575	AS10dist	0						AS10prox	0.7714		1		3	1
381	1569	AS10dist	0.3857		1		3	1	AS10prox	0.3857		1		3	1
382	1568	AS10dist	0.57855		1		3	1	AS10prox	0.3857		1		3	1
384	1566	AS10dist	0.3857	1			3	1	AS10prox	0.19285	1			3	1
387	1563	AS10dist	0						AS10prox	0.7714			1	1	1
388	1562	AS10dist	0.3857		1		3	1	AS10prox	0.3857		1		3	1
390	1560	AS10dist	0.57855		1		1	1	AS10prox	1.1571		1		1	1
393	1557	AS10dist	1.3857	1	1		3	2	AS10prox	1.34995	1	1		3	2
394	1556	AS10dist	0.7714		1		1	1	AS10prox	0.57855		1		1	1
396	1554	AS10dist	0						AS10prox	0.26999		1		3	1
397	1553	AS10dist	0.3857		1		1	1	AS10prox	0.3857		1		1	1
398	1552	AS10dist	1.9285	1			1	1	AS10prox	8.8711	1			1	1
399	1551	AS10dist	0						AS10prox	2.3142		1		1	1
401	1549	AS10dist	1.1571				1	1	AS10prox	1.9285				1	1
402	1548	AS10dist	0.57855				1	1	AS10prox	1.5428				1	1
403	1547	AS10dist	0						AS10prox	0.19285				3	1
405	1545	AS10dist	0						AS10prox	0.19285				3	1
406	1544	AS10dist	0.19285				3	1	AS10prox	0.96425				1	1
407	1543	AS10dist	0						AS10prox	2.6999				1	1
408	1542	AS10dist	0.3857				3	1	AS10prox	0.7714				3	1
410	1540	AS10dist	0.57855				3	1	AS10prox	2.6999				3	1
412	1538	AS10dist	2.3142				1	1	AS10prox	3.0856				1	1
417	1533	AS10dist	0.19285				3	1	AS10prox	0.3857				3	1
418	1532	AS10dist	1.9285				2	1	AS10prox	3.0856				2	1
423	1527	AS10dist	0.19285				3	1	AS10prox	0.19285				3	1
424	1526	AS10dist	0.3857				3	1	AS10prox	0.7714				3	1
427	1523	AS10dist	0						AS10prox	0.19285				3	1
428	1522	AS10dist	0.7714				3	1	AS10prox	1.5428				3	1
431	1519	AS10dist	0.3857				1	1	AS10prox	0					
432	1518	AS10dist	0.3857				3	1	AS10prox	0					

438	1512	AS10dist	0.7714	3	1	AS10prox	0.7714	3	1
446	1504	AS10dist	0.3857	2	1	AS10prox	1.1571	2	1
449	1501	AS10dist	0.19285	3	1	AS10prox	0.19285	3	1
450	1500	AS10dist	0.7714	2	1	AS10prox	1.1571	2	1
451	1499	AS10dist	0.19285	3	1	AS10prox	0		
455	1495	AS10dist	0			AS10prox	0.19285	3	1
458	1492	AS10dist	0.19285	3	1	AS10prox	0.19285	3	1
459	1491	AS10dist	0.3857	3	1	AS10prox	0.57855	3	1
460	1490	AS10dist	1.5428	2	1	AS10prox	1.5428	2	1
465	1485	AS10dist	0.3857	3	1	AS10prox	0.3857	3	1
466	1484	AS10dist	0.3857	3	1	AS10prox	0.3857	3	1
468	1482	AS10dist	0.19285	3	1	AS10prox	0.19285	3	1
473	1477	AS10dist	0			AS10prox	0.3857	3	1
474	1476	AS10dist	1.1571	1	1	AS10prox	1.9285	1	1
476	1474	AS10dist	0.57855	3	1	AS10prox	0.3857	3	1
484	1466	AS10dist	1.5428	2	1	AS10prox	2.6999	3	1
485	1465	AS10dist	0.57855	3	1	AS10prox	0.57855	3	1
486	1464	AS10dist	0.19285	3	1	AS10prox	0		
487	1463	AS10dist	1.5428	3	1	AS10prox	1.9285	3	1
488	1462	AS10dist	0.19285	3	1	AS10prox	0.19285	3	1
489	1461	AS10dist	0			AS10prox	0.3857	3	1
494	1456	AS10dist	0.19285	3	1	AS10prox	0.19285	3	1
496	1454	AS10dist	0			AS10prox	0.19285	3	1
497	1453	AS10dist	0.3857	2	1	AS10prox	0.7714	3	1
499	1451	AS10dist	0.3857	3	1	AS10prox	0.3857	3	1
502	1448	AS10dist	0.3857	3	1	AS10prox	0.19285	3	1
505	1445	AS10dist	0			AS10prox	0.3857	3	1
507	1443	AS10dist	0			AS10prox	0.3857	3	1
508	1442	AS10dist	0			AS10prox	0.19285	3	1
509	1441	AS10dist	0			AS10prox	0.3857	3	1
511	1439	AS10dist	0.19285	3	1	AS10prox	0.96425	3	1
512	1438	AS10dist	0			AS10prox	0.19285	3	1
517	1433	AS10dist	0.19285	2	1	AS10prox	0.3857	1	1
522	1428	AS10dist	0			AS10prox	0.19285	3	1
523	1427	AS10dist	0			AS10prox	0.3857	3	1
527	1423	AS10dist	0.19285	3	1	AS10prox	0.3857	3	1
529	1421	AS10dist	0			AS10prox	0.19285	3	1
532	1418	AS10dist	0.57855	1	1	AS10prox	0.19285	1	1
536	1414	AS10dist	0.3857	1	1	AS10prox	1.1571	1	1
541	1409	AS10dist	0			AS10prox	0.19285	3	1
544	1406	AS10dist	0.3857	3	1	AS10prox	0.19285	3	1
549	1401	AS10dist	0.19285	3	1	AS10prox	0.19285	3	1
550	1400	AS10dist	0.19285	3	1	AS10prox	0.19285	3	1
555	1395	AS10dist	0			AS10prox	0.19285	3	1
557	1393	AS10dist	0.19285	1	1	AS10prox	0		
558	1392	AS10dist	0.19285	3	1	AS10prox	0.19285	1	1
559	1391	AS10dist	0.19285	3	1	AS10prox	0		
562	1388	AS10dist	0.3857	3	1	AS10prox	0.19285	3	1
565	1385	AS10dist	0.19285	3	1	AS10prox	0.3857	3	1
570	1380	AS10dist	0			AS10prox	0.19285	3	1
575	1375	AS10dist	1.5428	2	1	AS10prox	1.9285	3	1
576	1374	AS10dist	0			AS10prox	0.19285	3	1
578	1372	AS10dist	0.3857	3	1	AS10prox	0.19285	3	1
581	1369	AS10dist	0.3857	3	1	AS10prox	0.19285	3	1
586	1364	AS10dist	0.19285	3	1	AS10prox	0.19285	3	1
602	1348	AS10dist	0			AS10prox	0.19285	3	1
609	1341	AS10dist	0.3857	2	1	AS10prox	0		
613	1337	AS10dist	0.19285	1	1	AS10prox	0		
614	1336	AS10dist	0.57855	2	1	AS10prox	0.57855	2	1
615	1335	AS10dist	0.3857	3	1	AS10prox	0		
618	1332	AS10dist	0			AS10prox	0.19285	3	1
619	1331	AS10dist	0			AS10prox	1.1571	3	1

626	1324	AS10dist	0.19285	3	1	AS10prox	0		
627	1323	AS10dist	0.3857	3	1	AS10prox	0.7714	3	1
630	1320	AS10dist	0.19285	3	1	AS10prox	0.19285	3	1
633	1317	AS10dist	0.57855	3	1	AS10prox	0.96425	3	1
639	1311	AS10dist	0			AS10prox	0.3857	3	1
642	1308	AS10dist	0.19285	3	1	AS10prox	0.19285	3	1
644	1306	AS10dist	0.19285	3	1	AS10prox	0.57855	3	1
657	1293	AS10dist	0.19285	3	1	AS10prox	0		
658	1292	AS10dist	1.5428	2	1	AS10prox	1.9285	2	1
659	1291	AS10dist	0.19285	3	1	AS10prox	0.19285	3	1
660	1290	AS10dist	0.19285	3	1	AS10prox	0.19285	3	1
661	1289	AS10dist	3.0856	1	1	AS10prox	4.82125	1	1
662	1288	AS10dist	5.0141	1	1	AS10prox	4.2427	1	1
663	1287	AS10dist	0.3857	3	1	AS10prox	0.57855	3	1
664	1286	AS10dist	0.3857	3	1	AS10prox	0.3857	3	1
667	1283	AS10dist	0			AS10prox	0.19285	3	1
669	1281	AS10dist	0			AS10prox	0.19285	3	1
670	1280	AS10dist	0.19285	3	1	AS10prox	1.34995	3	1
672	1278	AS10dist	0			AS10prox	0.19285	3	1
674	1276	AS10dist	0			AS10prox	0.3857	3	1
679	1271	AS10dist	0			AS10prox	0.3857	3	1
683	1267	AS10dist	0.57855	3	1	AS10prox	0.57855	3	1
689	1261	AS10dist	0.19285	3	1	AS10prox	0		
690	1260	AS10dist	0.19285	3	1	AS10prox	0.19285	3	1
691	1259	AS10dist	2.3142	2	1	AS10prox	1.9285	3	1
700	1250	AS10dist	0.19285	3	1	AS10prox	0.19285	3	1
701	1249	AS10dist	0.19285	3	1	AS10prox	0.19285	3	1
705	1245	AS10dist	0			AS10prox	0.3857	3	1
709	1241	AS10dist	0.3857	3	1	AS10prox	0.3857	3	1
717	1233	AS10dist	0.19285	3	1	AS10prox	0.3857	3	1
721	1229	AS10dist	0			AS10prox	0.19285	1	1
725	1225	AS10dist	0.19285	3	1	AS10prox	0.3857	3	1
729	1221	AS10dist	0.19285	3	1	AS10prox	0		
734	1216	AS10dist	0.19285	3	1	AS10prox	0.3857	3	1
741	1209	AS10dist	0.7714	3	1	AS10prox	1.1571	3	1
742	1208	AS10dist	0.19285	1	1	AS10prox	0		
751	1199	AS10dist	0			AS10prox	0.19285	3	1
753	1197	AS10dist	0			AS10prox	0.19285	3	1
755	1195	AS10dist	2.6999	2	1	AS10prox	3.4713	1	1
757	1193	AS10dist	3.0856	1	1	AS10prox	3.4713	1	1
758	1192	AS10dist	0.3857	3	1	AS10prox	0.3857	3	1
764	1186	AS10dist	0.19285	3	1	AS10prox	0.19285	3	1
768	1182	AS10dist	0.19285	1	1	AS10prox	0.19285	1	1
771	1179	AS10dist	0.19285	3	1	AS10prox	0.19285	3	1
777	1173	AS10dist	0.19285	3	1	AS10prox	0		
785	1165	AS10dist	0.3857	3	1	AS10prox	0.7714	3	1
790	1160	AS10dist	0.96425	2	1	AS10prox	1.1571	2	1
792	1158	AS10dist	0.19285	3	1	AS10prox	0.19285	3	1
794	1156	AS10dist	0.19285	3	1	AS10prox	0.19285	3	1
797	1153	AS10dist	0			AS10prox	0.19285	1	1
800	1150	AS10dist	1.5428	2	1	AS10prox	3.0856	3	1
805	1145	AS10dist	0			AS10prox	0.57855	3	1
807	1143	AS10dist	2.12135	2	1	AS10prox	2.6999	3	1
808	1142	AS10dist	0.19285	3	1	AS10prox	0.3857	3	1
812	1138	AS10dist	0.19285	3	1	AS10prox	0.3857	3	1
817	1133	AS10dist	0			AS10prox	0.3857	3	1
821	1129	AS10dist	0.19285	3	1	AS10prox	0.19285	3	1
824	1126	AS10dist	0.19285	3	1	AS10prox	0.3857	3	1
826	1124	AS10dist	0.3857	3	1	AS10prox	0.19285	3	1
830	1120	AS10dist	0			AS10prox	0.19285	3	1
832	1118	AS10dist	0.19285	3	1	AS10prox	0.19285	3	1
834	1116	AS10dist	0			AS10prox	0.3857	3	1

835	1115	AS10dist	0.3857	3	1	AS10prox	0.3857	3	1
836	1114	AS10dist	0.3857	3	1	AS10prox	0.3857	3	1
839	1111	AS10dist	0			AS10prox	0.19285	3	1
848	1102	AS10dist	0			AS10prox	0.19285	3	1
854	1096	AS10dist	0			AS10prox	0.19285	3	1
864	1086	AS10dist	0			AS10prox	0.19285	3	1
870	1080	AS10dist	0.19285	3	1	AS10prox	0.3857	3	1
879	1071	AS10dist	0			AS10prox	0.19285	3	1
881	1069	AS10dist	0.19285	3	1	AS10prox	0		
882	1068	AS10dist	0.3857	3	1	AS10prox	0.3857	3	1
883	1067	AS10dist	0.3857	3	1	AS10prox	0.3857	3	1
885	1065	AS10dist	0.19285	3	1	AS10prox	0.19285	3	1
891	1059	AS10dist	0.3857	3	1	AS10prox	0.57855	3	1
895	1055	AS10dist	0.19285	3	1	AS10prox	0		
897	1053	AS10dist	0			AS10prox	0.19285	3	1
898	1052	AS10dist	0.3857	3	1	AS10prox	0.3857	3	1
902	1048	AS10dist	0.19285	3	1	AS10prox	0.19285	3	1
905	1045	AS10dist	0.19285	3	1	AS10prox	0.19285	3	1
910	1040	AS10dist	0.19285	3	1	AS10prox	0.19285	3	1
914	1036	AS10dist	0.19285	3	1	AS10prox	0.19285	3	1
918	1032	AS10dist	0.3857	2	1	AS10prox	0.96425	3	1
922	1028	AS10dist	0.19285	3	1	AS10prox	0.19285	3	1
924	1026	AS10dist	0.7714	1	1	AS10prox	1.1571	1	1
928	1022	AS10dist	0			AS10prox	0.19285	3	1
936	1014	AS10dist	0.19285	3	1	AS10prox	0.19285	3	1
940	1010	AS10dist	0.19285	3	1	AS10prox	0.19285	3	1
944	1006	AS10dist	0			AS10prox	0.19285	3	1
949	1001	AS10dist	10.7996	3	1	AS10prox	22.3706	3	1
951	999	AS10dist	0.19285	3	1	AS10prox	0.19285	3	1
955	995	AS10dist	0			AS10prox	0.3857	3	1
956	994	AS10dist	0.7714	3	1	AS10prox	1.1571	3	1
959	991	AS10dist	0			AS10prox	0.19285	3	1
963	987	AS10dist	0.19285	3	1	AS10prox	0.19285	3	1
970	980	AS10dist	0			AS10prox	0.19285	3	1
973	977	AS10dist	0.19285	3	1	AS10prox	0.19285	3	1
977	973	AS10dist	0.3857	1	1	AS10prox	0		
981	969	AS10dist	0.19285	3	1	AS10prox	0		
984	966	AS10dist	0.19285	3	1	AS10prox	0.19285	3	1
987	963	AS10dist	0.19285	3	1	AS10prox	0.19285	3	1
996	954	AS10dist	0.19285	3	1	AS10prox	0.19285	3	1
1004	946	AS10dist	0.19285	3	1	AS10prox	0.3857	3	1
1007	943	AS10dist	0.19285	3	1	AS10prox	0.3857	3	1
1011	939	AS10dist	0			AS10prox	0.19285	3	1
1017	933	AS10dist	0.19285	3	1	AS10prox	0.19285	3	1
1019	931	AS10dist	0.19285	3	1	AS10prox	0.3857	3	1
1020	930	AS10dist	0.3857	3	1	AS10prox	0.3857	1	1
1024	926	AS10dist	0.19285	3	1	AS10prox	0.19285	3	1
1028	922	AS10dist	0.7714	2	1	AS10prox	0.96425	2	1
1030	920	AS10dist	0.19285	3	1	AS10prox	0.19285	3	1
1032	918	AS10dist	0.3857	3	1	AS10prox	0		
1038	912	AS10dist	0.19285	3	1	AS10prox	0.19285	3	1
1041	909	AS10dist	0.19285	3	1	AS10prox	0.19285	3	1
1044	906	AS10dist	0.19285	3	1	AS10prox	0		
1056	894	AS10dist	0.19285	3	1	AS10prox	0		
1060	890	AS10dist	0.19285	3	1	AS10prox	0.19285	3	1
1067	883	AS10dist	0.19285	3	1	AS10prox	0.19285	3	1
1074	876	AS10dist	0.19285	3	1	AS10prox	0.19285	3	1
1078	872	AS10dist	0.19285	3	1	AS10prox	0.19285	3	1
1082	868	AS10dist	0.19285	3	1	AS10prox	0.19285	3	1
1085	865	AS10dist	0			AS10prox	0.19285	3	1
1088	862	AS10dist	0			AS10prox	0.19285	3	1
1093	857	AS10dist	0.19285	3	1	AS10prox	0.3857	3	1

1095	855	AS10dist	1.9285	2	1	AS10prox	1.9285	2	1
1097	853	AS10dist	0			AS10prox	0.19285	3	1
1102	848	AS10dist	0.19285	3	1	AS10prox	0.19285	3	1
1103	847	AS10dist	0.19285	3	1	AS10prox	0		
1107	843	AS10dist	0.19285	1	1	AS10prox	0		
1112	838	AS10dist	0.19285	3	1	AS10prox	0.19285	3	1
1116	834	AS10dist	0.19285	3	1	AS10prox	0.19285	3	1
1117	833	AS10dist	0.19285	3	1	AS10prox	0		
1122	828	AS10dist	0.19285	3	1	AS10prox	0.19285	3	1
1124	826	AS10dist	0.19285	3	1	AS10prox	0		
1127	823	AS10dist	14.2709	3	1	AS10prox	125	3	1
1132	818	AS10dist	0.19285	3	1	AS10prox	0.19285	3	1
1136	814	AS10dist	0.19285	3	1	AS10prox	0.19285	3	1
1140	810	AS10dist	0			AS10prox	0.19285	3	1
1141	809	AS10dist	0			AS10prox	0.19285	3	1
1150	800	AS10dist	0.19285	3	1	AS10prox	0.19285	3	1
1156	794	AS10dist	0			AS10prox	0.19285	3	1
1157	793	AS10dist	0.19285	3	1	AS10prox	0.3857	3	1
1160	790	AS10dist	0			AS10prox	0.19285	3	1
1166	784	AS10dist	0			AS10prox	0.19285	3	1
1168	782	AS10dist	0			AS10prox	0.19285	3	1
1169	781	AS10dist	0			AS10prox	0.19285	3	1
1176	774	AS10dist	0.3857	3	1	AS10prox	0		
1181	769	AS10dist	0			AS10prox	0.19285	3	1
1186	764	AS10dist	0			AS10prox	0.19285	3	1
1187	763	AS10dist	0.19285	3	1	AS10prox	0.57855	3	1
1192	758	AS10dist	0			AS10prox	0.19285	3	1
1196	754	AS10dist	0			AS10prox	0.19285	3	1
1198	752	AS10dist	0.19285	3	1	AS10prox	0		
1199	751	AS10dist	0.19285	3	1	AS10prox	0.19285	3	1
1202	748	AS10dist	0.19285	3	1	AS10prox	0.19285	3	1
1204	746	AS10dist	0.19285	2	1	AS10prox	0.19285	3	1
1205	745	AS10dist	0			AS10prox	0.19285	3	1
1207	743	AS10dist	0			AS10prox	0.19285	3	1
1210	740	AS10dist	0			AS10prox	0.19285	3	1
1211	739	AS10dist	0.19285	3	1	AS10prox	0.19285	3	1
1213	737	AS10dist	0			AS10prox	0.19285	3	1
1214	736	AS10dist	0			AS10prox	0.19285	3	1
1217	733	AS10dist	0.19285	3	1	AS10prox	0.19285	3	1
1219	731	AS10dist	0			AS10prox	0.19285	3	1
1220	730	AS10dist	1.1571	3	1	AS10prox	0.3857	3	1
1221	729	AS10dist	1.34995	1	1	AS10prox	0.7714	1	1
1222	728	AS10dist	0.3857	1	1	AS10prox	1.1571	1	1
1226	724	AS10dist	0			AS10prox	0.19285	3	1
1228	722	AS10dist	0			AS10prox	0.19285	3	1
1229	721	AS10dist	0			AS10prox	0.3857	3	1
1232	718	AS10dist	0			AS10prox	0.19285	3	1
1238	712	AS10dist	0			AS10prox	0.19285	3	1
1241	709	AS10dist	0			AS10prox	0.19285	3	1
1242	708	AS10dist	0			AS10prox	0.19285	3	1
1245	705	AS10dist	0			AS10prox	0.19285	3	1
1249	701	AS10dist	0			AS10prox	0.19285	3	1
1251	699	AS10dist	0			AS10prox	0.19285	3	1
1253	697	AS10dist	0			AS10prox	0.3857	3	1
1256	694	AS10dist	0.19285	3	1	AS10prox	0.19285	3	1
1260	690	AS10dist	0.7714	2	1	AS10prox	1.1571	2	1
1266	684	AS10dist	0			AS10prox	0.19285	3	1
1270	680	AS10dist	0			AS10prox	0.3857	3	1
1274	676	AS10dist	0.19285	3	1	AS10prox	0.19285	3	1
1275	675	AS10dist	0.19285	3	1	AS10prox	0.19285	3	1
1277	673	AS10dist	0.19285	3	1	AS10prox	0.19285	3	1
1280	670	AS10dist	0.19285	3	1	AS10prox	0.19285	3	1

1284	666	AS10dist	0.19285	3	1	AS10prox	0		
1286	664	AS10dist	0			AS10prox	0.19285	3	1
1288	662	AS10dist	0			AS10prox	0.19285	3	1
1289	661	AS10dist	0			AS10prox	0.19285	3	1
1290	660	AS10dist	0			AS10prox	0.19285	3	1
1291	659	AS10dist	0.19285	3	1	AS10prox	0.19285	3	1
1298	652	AS10dist	0			AS10prox	0.19285	3	1
1299	651	AS10dist	0			AS10prox	0.19285	3	1
1300	650	AS10dist	0			AS10prox	0.19285	3	1
1301	649	AS10dist	0.19285	3	1	AS10prox	0		
1305	645	AS10dist	0.19285	3	1	AS10prox	0.19285	3	1
1309	641	AS10dist	0			AS10prox	0.19285	3	1
1311	639	AS10dist	0.7714	2	1	AS10prox	1.5428	2	1
1313	637	AS10dist	0.19285	3	1	AS10prox	0.19285	3	1
1314	636	AS10dist	0.19285	3	1	AS10prox	0		
1315	635	AS10dist	0			AS10prox	0.19285	3	1
1316	634	AS10dist	0.19285	3	1	AS10prox	0.19285	3	1
1317	633	AS10dist	0			AS10prox	0.57855	3	1
1318	632	AS10dist	0.19285	3	1	AS10prox	0.19285	3	1
1320	630	AS10dist	0			AS10prox	0.19285	3	1
1322	628	AS10dist	0.19285	3	1	AS10prox	0.19285	3	1
1327	623	AS10dist	0.19285	3	1	AS10prox	0.19285	3	1
1330	620	AS10dist	0			AS10prox	0.19285	3	1
1333	617	AS10dist	0			AS10prox	0.19285	3	1
1337	613	AS10dist	0			AS10prox	0.19285	3	1
1343	607	AS10dist	0			AS10prox	0.19285	3	1
1344	606	AS10dist	0.19285	3	1	AS10prox	0.19285	3	1
1351	599	AS10dist	0			AS10prox	0.19285	3	1
1357	593	AS10dist	0.19285	3	1	AS10prox	0		
1360	590	AS10dist	0.19285	3	1	AS10prox	0		
1361	589	AS10dist	0.19285	3	1	AS10prox	0.19285	3	1
1370	580	AS10dist	0			AS10prox	0.19285	3	1
1371	579	AS10dist	0			AS10prox	0.19285	3	1
1376	574	AS10dist	0			AS10prox	0.19285	3	1
1382	568	AS10dist	0			AS10prox	0.19285	3	1
1384	566	AS10dist	0.19285	3	1	AS10prox	0.19285	3	1
1386	564	AS10dist	0			AS10prox	0.19285	3	1
1387	563	AS10dist	0			AS10prox	0.19285	3	1
1392	558	AS10dist	0.19285	3	1	AS10prox	0		
1393	557	AS10dist	0.19285	3	1	AS10prox	0		
1395	555	AS10dist	0			AS10prox	0.19285	3	1
1398	552	AS10dist	0.3857	2	1	AS10prox	0.19285	3	1
1401	549	AS10dist	0			AS10prox	0.19285	3	1
1405	545	AS10dist	0			AS10prox	0.3857	3	1
1407	543	AS10dist	0			AS10prox	0.19285	3	1
1410	540	AS10dist	0.7714	2	1	AS10prox	1.1571	2	1
1414	536	AS10dist	0.19285	3	1	AS10prox	0.19285	3	1
1418	532	AS10dist	0			AS10prox	0.19285	3	1
1423	527	AS10dist	0			AS10prox	0.19285	3	1
1429	521	AS10dist	3.4713	1	1	AS10prox	5.3998	1	1
1433	517	AS10dist	0			AS10prox	0.19285	3	1
1439	511	AS10dist	1.9285	3	1	AS10prox	4.2427	3	1
1449	501	AS10dist	0			AS10prox	0.19285	3	1
1453	497	AS10dist	0.19285	3	1	AS10prox	0.3857	3	1
1457	493	AS10dist	0			AS10prox	0.3857	3	1
1463	487	AS10dist	0.19285	3	1	AS10prox	0.19285	3	1
1468	482	AS10dist	0.19285	3	1	AS10prox	0.19285	3	1
1473	477	AS10dist	0			AS10prox	0.19285	3	1
1479	471	AS10dist	0.19285	3	1	AS10prox	0.19285	3	1
1481	469	AS10dist	1.9285	2	1	AS10prox	1.1571	3	1
1484	466	AS10dist	0			AS10prox	0.19285	3	1
1485	465	AS10dist	0			AS10prox	0.19285	3	1

1486	464	AS10dist	0			AS10prox	0.19285	3	1
1488	462	AS10dist	0			AS10prox	0.19285	3	1
1490	460	AS10dist	0.19285	3	1	AS10prox	0.19285	3	1
1492	458	AS10dist	0			AS10prox	0.19285	3	1
1498	452	AS10dist	0			AS10prox	0.3857	1	1
1501	449	AS10dist	0.19285	3	1	AS10prox	0.19285	3	1
1502	448	AS10dist	0			AS10prox	0.19285	3	1
1503	447	AS10dist	0.19285	3	1	AS10prox	0.19285	3	1
1515	435	AS10dist	0.19285	3	1	AS10prox	0.19285	3	1
1516	434	AS10dist	0			AS10prox	0.19285	3	1
1522	428	AS10dist	0.19285	3	1	AS10prox	0.3857	3	1
1523	427	AS10dist	0.3857	3	1	AS10prox	0		
1525	425	AS10dist	2.6999	2	1	AS10prox	30.4703	3	1
1527	423	AS10dist	0			AS10prox	0.19285	3	1
1530	420	AS10dist	0			AS10prox	0.19285	3	1
1532	418	AS10dist	0.19285	3	1	AS10prox	0.3857	3	1
1536	414	AS10dist	0			AS10prox	0.19285	3	1
1546	404	AS10dist	0			AS10prox	0.3857	2	1
1549	401	AS10dist	0.19285	3	1	AS10prox	0.57855	2	1
1557	393	AS10dist	0			AS10prox	0.19285	3	1
1559	391	AS10dist	0			AS10prox	0.19285	3	1
1561	389	AS10dist	0			AS10prox	0.19285	3	1
1565	385	AS10dist	0.19285	3	1	AS10prox	0.19285	3	1
1569	381	AS10dist	0			AS10prox	0.19285	3	1
1574	376	AS10dist	0.19285	3	1	AS10prox	0.19285	3	1
1578	372	AS10dist	0.3857	3	1	AS10prox	0.19285	3	1
1591	359	AS10dist	0.19285	3	1	AS10prox	0.19285	3	1
1592	358	AS10dist	0			AS10prox	0.19285	3	1
1595	355	AS10dist	0			AS10prox	0.19285	3	1
1601	349	AS10dist	0.19285	3	1	AS10prox	0.19285	3	1
1604	346	AS10dist	0.19285	3	1	AS10prox	0.19285	3	1
1617	333	AS10dist	0			AS10prox	0.19285	3	1
1624	326	AS10dist	0.19285	3	1	AS10prox	0.19285	3	1
1630	320	AS10dist	0			AS10prox	0.19285	3	1
1632	318	AS10dist	0			AS10prox	0.19285	3	1
1651	299	AS10dist	0			AS10prox	0.19285	3	1
1652	298	AS10dist	3.4713	1	1	AS10prox	5.7855	1	1
1656	294	AS10dist	0			AS10prox	0.19285	3	1
1670	280	AS10dist	0.19285	3	1	AS10prox	0.19285	3	1
1673	277	AS10dist	0			AS10prox	0.19285	3	1
1674	276	AS10dist	0.19285	3	1	AS10prox	0.7714	1	1
1678	272	AS10dist	0			AS10prox	0.19285	3	1
1679	271	AS10dist	0.19285	3	1	AS10prox	0.19285	1	1
1680	270	AS10dist	1.1571	3	1	AS10prox	1.5428	1	1
1681	269	AS10dist	1.5428	3	1	AS10prox	1.9285	1	1
1689	261	AS10dist	0			AS10prox	0.19285	3	1
1693	257	AS10dist	0.19285	3	1	AS10prox	0.3857	1	1
1694	256	AS10dist	3.4713	1	1	AS10prox	3.857	1	1
1701	249	AS10dist	0.19285	3	1	AS10prox	0.19285	3	1
1702	248	AS10dist	0			AS10prox	0.19285	3	1
1707	243	AS10dist	0			AS10prox	0.19285	3	1
1712	238	AS10dist	0.19285	3	1	AS10prox	0.19285	3	1
1713	237	AS10dist	0.19285	3	1	AS10prox	0.19285	3	1
1714	236	AS10dist	0			AS10prox	0.19285	3	1
1722	228	AS10dist	0			AS10prox	0.19285	3	1
1724	226	AS10dist	0.3857	1	1	AS10prox	0.57855	1	1
1733	217	AS10dist	0.19285	3	1	AS10prox	0		
1738	212	AS10dist	0			AS10prox	0.19285	3	1
1739	211	AS10dist	0			AS10prox	0.19285	3	1
1743	207	AS10dist	0			AS10prox	0.19285	3	1
1746	204	AS10dist	0			AS10prox	0.3857	1	1
1748	202	AS10dist	0.19285	3	1	AS10prox	0.57855	1	1

1751	199	AS10dist	0.3857	1	1	AS10prox	0.19285	3	1
1753	197	AS10dist	0			AS10prox	0.19285	3	1
1754	196	AS10dist	0.3857	1	1	AS10prox	0.19285	1	1
1757	193	AS10dist	0.19285	3	1	AS10prox	0.19285	3	1
1766	184	AS10dist	0.19285	3	1	AS10prox	0		
1771	179	AS10dist	0.57855	2	1	AS10prox	0.57855	2	1
1773	177	AS10dist	0			AS10prox	0.19285	3	1
1784	166	AS10dist	0.3857	3	1	AS10prox	0.3857	3	1
1786	164	AS10dist	0			AS10prox	0.19285	3	1
1787	163	AS10dist	0.19285	3	1	AS10prox	0.19285	3	1
1794	156	AS10dist	0			AS10prox	0.3857	1	1
1797	153	AS10dist	0.57855	1	1	AS10prox	0.19285	1	1
1798	152	AS10dist	0			AS10prox	1.1571	2	1
1799	151	AS10dist	0			AS10prox	0.19285	3	1
1803	147	AS10dist	0.19285	3	1	AS10prox	0		
1808	142	AS10dist	0.19285	3	1	AS10prox	0.19285	3	1
1813	137	AS10dist	0.19285	3	1	AS10prox	0.19285	3	1
1819	131	AS10dist	0.19285	3	1	AS10prox	0.19285	3	1
1820	130	AS10dist	0.3857	3	1	AS10prox	0.7714	3	1
1828	122	AS10dist	0.19285	3	1	AS10prox	0.19285	3	1
1830	120	AS10dist	0			AS10prox	0.19285	3	1
1831	119	AS10dist	0.57855	3	1	AS10prox	0.57855	3	1
1833	117	AS10dist	0			AS10prox	0.19285	3	1
1834	116	AS10dist	2.12135	1	1	AS10prox	3.857	1	1
1835	115	AS10dist	0			AS10prox	0.19285	3	1
1842	108	AS10dist	0			AS10prox	0.19285	3	1
1847	103	AS10dist	0.19285	3	1	AS10prox	0		
1849	101	AS10dist	0			AS10prox	0.19285	3	1
1851	99	AS10dist	0.19285	3	1	AS10prox	0.19285	3	1
1852	98	AS10dist	1.9285	3	1	AS10prox	2.3142	1	1
1853	97	AS10dist	0.19285	3	1	AS10prox	0.19285	3	1
1861	89	AS10dist	0			AS10prox	0.19285	3	1
1867	83	AS10dist	0.19285	3	1	AS10prox	1.5428	1	1
1871	79	AS10dist	0			AS10prox	0.19285	3	1
1872	78	AS10dist	0			AS10prox	1.5428	1	1
1875	75	AS10dist	4.2427	1	1	AS10prox	6.1712	1	1
1882	68	AS10dist	0.19285	3	1	AS10prox	0		
1885	65	AS10dist	0.19285	2	1	AS10prox	1.1571	2	1
1886	64	AS10dist	0			AS10prox	0.19285	3	1
1895	55	AS10dist	0.19285	3	1	AS10prox	0		
1896	54	AS10dist	0.7714	3	1	AS10prox	0.7714	3	1
1901	49	AS10dist	2.3142	2	1	AS10prox	4.2427	2	1
1912	38	AS10dist	0			AS10prox	0.19285	3	1
1917	33	AS10dist	0.7714	3	1	AS10prox	0.57855	3	1
1918	32	AS10dist	0			AS10prox	0.19285	3	1
1922	28	AS10dist	0.19285	3	1	AS10prox	0		
1926	24	AS10dist	1.1571	1	1	AS10prox	1.9285	1	1
1930	20	AS10dist	0			AS10prox	0.3857	3	1
1932	18	AS10dist	0			AS10prox	0.3857	1	1
1934	16	AS10dist	0.19285	3	1	AS10prox	0.3857	3	1
1935	15	AS10dist	1.5428	3	1	AS10prox	2.6999	1	1
1940	10	AS10dist	0.19285	3	1	AS10prox	0.19285	3	1
1942	8	AS10dist	0			AS10prox	1.5428	1	1
1944	6	AS10dist	0.19285	3	1	AS10prox	0.3857	3	1
1951	-1	AS10dist	0.3857	3	1	AS10prox	0.57855	3	1
1955	-5	AS10dist	2.6999	3	1	AS10prox	85	3	1
1962	-12	AS10dist	0.19285	3	1	AS10prox	0.57855	3	1
1966	-16	AS10dist	0.19285	3	1	AS10prox	0		
1970	-20	AS10dist	0.19285	1	1	AS10prox	0.3857	1	1
1982	-32	AS10dist	0.3857	1	1	AS10prox	0.57855	1	1
1992	-42	AS10dist	3.4713	1	1	AS10prox	3.4713	1	1
1993	-43	AS10dist	0.19285	3	1	AS10prox	0.19285	3	1

1997	-47	AS10dist	0.19285	3	1	AS10prox	0.19285	3	1
2008	-58	AS10dist	0.19285	3	1	AS10prox	0.19285	3	1
2015	-65	AS10dist	3.857	1	1	AS10prox	6.1712	1	1
2024	-74	AS10dist	0			AS10prox	0.19285	3	1
2028	-78	AS10dist	0.57855	1	1	AS10prox	0.57855	1	1
2032	-82	AS10dist	2.3142	1	1	AS10prox	2.6999	1	1
2033	-83	AS10dist	2.3142	1	1	AS10prox	1.9285	2	1
2041	-91	AS10dist	2.3142	1	1	AS10prox	2.6999	1	1
2045	-95	AS10dist	0.19285	1	1	AS10prox	0		
2053	-103	AS10dist	0			AS10prox	0.57855	3	1
2054	-104	AS10dist	0.3857	2	1	AS10prox	0.57855	1	1
2059	-109	AS10dist	0.19285	3	1	AS10prox	0		
2069	-119	AS10dist	1.9285	3	1	AS10prox	2.3142	3	1
2078	-128	AS10dist	0.7714	3	1	AS10prox	1.5428	3	1
2081	-131	AS10dist	0			AS10prox	0.57855	3	1
2085	-135	AS10dist	0.3857	3	1	AS10prox	0.57855	3	1
2094	-144	AS10dist	0			AS10prox	0.3857	1	1
2095	-145	AS10dist	0.19285	3	1	AS10prox	0		
2101	-151	AS10dist	0			AS10prox	0.19285	3	1
2104	-154	AS10dist	1.1571	1	1	AS10prox	1.5428	1	1
2109	-159	AS10dist	0.19285	3	1	AS10prox	0		
2118	-168	AS10dist	0			AS10prox	0.3857	3	1
2122	-172	AS10dist	0.57855	3	1	AS10prox	2.12135	3	1
2131	-181	AS10dist	0			AS10prox	0.19285	3	1
2137	-187	AS10dist	0.19285	3	1	AS10prox	0.3857	3	1
2140	-190	AS10dist	0.57855	3	1	AS10prox	0.96425	3	1
2155	-205	AS10dist	0.19285	3	1	AS10prox	0.19285	3	1
2157	-207	AS10dist	0.19285	3	1	AS10prox	1.5428	1	1
2159	-209	AS10dist	0			AS10prox	0.3857	3	1
2167	-217	AS10dist	0			AS10prox	0.19285	3	1
2170	-220	AS10dist	0			AS10prox	0.7714	3	1
2179	-229	AS10dist	0.96425	3	1	AS10prox	1.5428	3	1
2185	-235	AS10dist	0.57855	3	1	AS10prox	0.7714	3	1
2205	-255	AS10dist	0			AS10prox	0.3857	3	1
2208	-258	AS10dist	0.3857	3	1	AS10prox	0.57855	3	1
2220	-270	AS10dist	2.6999	2	1	AS10prox	2.3142	2	1
2228	-278	AS10dist	0.3857	3	1	AS10prox	0.3857	3	1
2233	-283	AS10dist	0.3857	3	1	AS10prox	0.57855	3	1
2254	-304	AS10dist	0.19285	3	1	AS10prox	0		
2262	-312	AS10dist	0			AS10prox	0.3857	1	1
2272	-322	AS10dist	0			AS10prox	0.3857	3	1
2277	-327	AS10dist	0.19285	3	1	AS10prox	0		
2291	-341	AS10dist	0.3857	3	1	AS10prox	0.7714	3	1
2301	-351	AS10dist	0			AS10prox	0.19285	3	1
2305	-355	AS10dist	0			AS10prox	0.3857	3	1
2307	-357	AS10dist	0			AS10prox	0.3857	3	1
2316	-366	AS10dist	0.3857	3	1	AS10prox	0.19285	3	1
2330	-380	AS10dist	0.19285	1	1	AS10prox	0		
2336	-386	AS10dist	0.19285	3	1	AS10prox	0.3857	1	1
2341	-391	AS10dist	0			AS10prox	0.3857	1	1
2345	-395	AS10dist	0.19285	3	1	AS10prox	0		
2347	-397	AS10dist	0.57855	1	1	AS10prox	1.1571	1	1
2351	-401	AS10dist	0.96425	1	1	AS10prox	0.7714	3	1
2352	-402	AS10dist	3.0856	1	1	AS10prox	3.857	1	1
2355	-405	AS10dist	5.7855	1	1	AS10prox	6.36405	1	1
2356	-406	AS10dist	0.3857	3	1	AS10prox	0.19285	3	1
2360	-410	AS10dist	0.3857	3	1	AS10prox	0.57855	3	1
2362	-412	AS10dist	0.19285	3	1	AS10prox	0.57855	3	1
2365	-415	AS10dist	0.19285	2	1	AS10prox	0.19285	2	1
2369	-419	AS10dist	0.19285	3	1	AS10prox	0.3857	3	1
2376	-426	AS10dist	0			AS10prox	0.7714	3	1
2383	-433	AS10dist	3.0856	1	1	AS10prox	0.3857	3	1

2385	-435	AS10dist	0			AS10prox	0.3857	2	1
2386	-436	AS10dist	0.19285	3	1	AS10prox	0.3857	3	1
2387	-437	AS10dist	3.0856	1	1	AS10prox	4.2427	1	1
2400	-450	AS10dist	0.19285	3	1	AS10prox	0		
2402	-452	AS10dist	0.19285	3	1	AS10prox	0.19285	3	1
2412	-462	AS10dist	0			AS10prox	0.19285	3	1
2422	-472	AS10dist	0.19285	3	1	AS10prox	0.3857	3	1
2433	-483	AS10dist	0			AS10prox	0.7714	3	1
2437	-487	AS10dist	0			AS10prox	0.19285	3	1
2444	-494	AS10dist	0.3857	3	1	AS10prox	0.57855	1	1
2452	-502	AS10dist	0.19285	3	1	AS10prox	0.3857	3	1
2459	-509	AS10dist	0.19285	3	1	AS10prox	0.3857	3	1
2465	-515	AS10dist	0.19285	3	1	AS10prox	0.19285	3	1
2476	-526	AS10dist	0			AS10prox	0.3857	3	1
2483	-533	AS10dist	0.19285	3	1	AS10prox	0		
2488	-538	AS10dist	0.19285	3	1	AS10prox	0		
2495	-545	AS10dist	0			AS10prox	0.19285	3	1
2498	-548	AS10dist	2.3142	3	1	AS10prox	3.0856	3	1
2500	-550	AS10dist	0.19285	3	1	AS10prox	0.3857	3	1
2504	-554	AS10dist	4.2427	1	1	AS10prox	5.0141	1	1
2506	-556	AS10dist	0.96425	3	1	AS10prox	1.5428	3	1
2507	-557	AS10dist	0			AS10prox	0.19285	3	1
2511	-561	AS10dist	0			AS10prox	0.19285	3	1
2516	-566	AS10dist	0.19285	3	1	AS10prox	0.3857	3	1
2518	-568	AS10dist	0			AS10prox	0.19285	3	1
2521	-571	AS10dist	0.19285	3	1	AS10prox	0.3857	3	1
2523	-573	AS10dist	0.57855	1	1	AS10prox	0.7714	1	1
2525	-575	AS10dist	0			AS10prox	0.19285	3	1
2529	-579	AS10dist	0.19285	3	1	AS10prox	0.19285	3	1
2530	-580	AS10dist	0.19285	3	1	AS10prox	0.19285	3	1
2531	-581	AS10dist	0.3857	3	1	AS10prox	0.3857	3	1
2534	-584	AS10dist	0.19285	3	1	AS10prox	0		
2537	-587	AS10dist	1.5428	1	1	AS10prox	3.4713	1	1
2539	-589	AS10dist	1.1571	2	1	AS10prox	1.9285	2	1
2540	-590	AS10dist	0.19285	3	1	AS10prox	0.19285	3	1
2541	-591	AS10dist	0			AS10prox	0.3857	3	1
2543	-593	AS10dist	1.9285	2	1	AS10prox	1.9285	2	1
2544	-594	AS10dist	1.5428	2	1	AS10prox	1.5428	2	1
2548	-598	AS10dist	0			AS10prox	0.3857	3	1
2553	-603	AS10dist	1.1571	2	1	AS10prox	1.34995	2	1
2554	-604	AS10dist	0.19285	3	1	AS10prox	0.3857	3	1
2557	-607	AS10dist	0			AS10prox	0.19285	3	1
2563	-613	AS10dist	3.4713	1	1	AS10prox	4.6284	1	1
2564	-614	AS10dist	0.19285	3	1	AS10prox	0.3857	3	1
2569	-619	AS10dist	0.3857	3	1	AS10prox	0.19285	3	1
2576	-626	AS10dist	0			AS10prox	0.3857	3	1
2589	-639	AS10dist	0.19285	3	1	AS10prox	0.3857	3	1
2592	-642	AS10dist	0.19285	3	1	AS10prox	0		
2597	-647	AS10dist	0.19285	3	1	AS10prox	0.19285	3	1
2603	-653	AS10dist	0.19285	3	1	AS10prox	0.3857	3	1
2608	-658	AS10dist	0.19285	3	1	AS10prox	0.19285	3	1
2611	-661	AS10dist	0.19285	3	1	AS10prox	0.19285	3	1
2626	-676	AS10dist	0.19285	3	1	AS10prox	0.3857	3	1
2629	-679	AS10dist	0.19285	3	1	AS10prox	0.19285	3	1
2632	-682	AS10dist	0			AS10prox	0.3857	1	1
2633	-683	AS10dist	0			AS10prox	0.19285	1	1
2640	-690	AS10dist	0.3857	3	1	AS10prox	0.57855	1	1
2645	-695	AS10dist	2.6999	3	1	AS10prox	5.3998	3	1
2654	-704	AS10dist	0.19285	1	1	AS10prox	0.19285	3	1
2657	-707	AS10dist	0.19285	3	1	AS10prox	0		
2664	-714	AS10dist	0			AS10prox	0.3857	1	1
2667	-717	AS10dist	0			AS10prox	0.19285	1	1

2672	-722	AS10dist	0.19285	3	1	AS10prox	0.19285	3	1
2678	-728	AS10dist	0.57855	1	1	AS10prox	3.857	1	1
2679	-729	AS10dist	0			AS10prox	0.3857	3	1
2680	-730	AS10dist	0.57855	1	1	AS10prox	1.1571	1	1
2684	-734	AS10dist	0			AS10prox	0.3857	3	1
2690	-740	AS10dist	0			AS10prox	0.19285	3	1
2691	-741	AS10dist	0.19285	3	1	AS10prox	0.3857	3	1
2693	-743	AS10dist	0			AS10prox	0.19285	3	1
2696	-746	AS10dist	0.3857	3	1	AS10prox	0.3857	3	1
2698	-748	AS10dist	0.19285	3	1	AS10prox	0.3857	3	1
2699	-749	AS10dist	0			AS10prox	0.19285	3	1
2705	-755	AS10dist	0.57855	3	1	AS10prox	0.7714	3	1
2707	-757	AS10dist	0			AS10prox	0.19285	3	1
2709	-759	AS10dist	0			AS10prox	0.19285	3	1
2710	-760	AS10dist	0			AS10prox	0.19285	3	1
2717	-767	AS10dist	0.3857	3	1	AS10prox	1.5428	3	1
2719	-769	AS10dist	0.19285	3	1	AS10prox	0		
2721	-771	AS10dist	0.19285	3	1	AS10prox	0		
2723	-773	AS10dist	0.19285	3	1	AS10prox	0.19285	3	1
2726	-776	AS10dist	0.19285	3	1	AS10prox	0		
2729	-779	AS10dist	0.19285	3	1	AS10prox	0.19285	3	1
2730	-780	AS10dist	0.19285	3	1	AS10prox	0.19285	3	1
2731	-781	AS10dist	0.19285	3	1	AS10prox	0.19285	3	1
2732	-782	AS10dist	0.96425	1	1	AS10prox	0.3857	3	1
2733	-783	AS10dist	0.7714	3	1	AS10prox	2.6999	3	1
2734	-784	AS10dist	0			AS10prox	0.19285	3	1
2739	-789	AS10dist	0			AS10prox	0.3857	3	1
2740	-790	AS10dist	0.57855	1	1	AS10prox	2.12135	1	1
2742	-792	AS10dist	0			AS10prox	2.3142	1	1
2745	-795	AS10dist	0			AS10prox	0.19285	3	1
2746	-796	AS10dist	0.3857	1	1	AS10prox	0.7714	3	1
2747	-797	AS10dist	0.3857	1	1	AS10prox	0.7714	1	1
2750	-800	AS10dist	0.19285	3	1	AS10prox	0		
2752	-802	AS10dist	0.19285	3	1	AS10prox	0.19285	3	1
2753	-803	AS10dist	0.3857	3	1	AS10prox	0.57855	3	1
2754	-804	AS10dist	0			AS10prox	0.3857	3	1
2759	-809	AS10dist	0			AS10prox	0.19285	3	1
2761	-811	AS10dist	0			AS10prox	0.3857	1	1
2765	-815	AS10dist	0.19285	1	1	AS10prox	0.19285	3	1
2766	-816	AS10dist	0.3857	3	1	AS10prox	0.3857	1	1
2768	-818	AS10dist	1.1571	1	1	AS10prox	2.3142	1	1
2769	-819	AS10dist	0.19285	3	1	AS10prox	0.3857	3	1
2770	-820	AS10dist	1.73565	3	1	AS10prox	1.9285	1	1
2772	-822	AS10dist	0			AS10prox	0.3857	3	1
2773	-823	AS10dist	0.3857	3	1	AS10prox	0.3857	3	1
2777	-827	AS10dist	25.4562	3	1	AS10prox	135	3	1
2779	-829	AS10dist	0.19285	3	1	AS10prox	0.19285	3	1
2784	-834	AS10dist	0.19285	3	1	AS10prox	0.19285	3	1
2787	-837	AS10dist	0			AS10prox	0.19285	3	1
2795	-845	AS10dist	0			AS10prox	0.3857	3	1
2797	-847	AS10dist	0.3857	2	1	AS10prox	0.57855	2	1
2798	-848	AS10dist	0.3857	3	1	AS10prox	1.34995	1	1
2800	-850	AS10dist	0			AS10prox	0.19285	3	1
2802	-852	AS10dist	0			AS10prox	0.19285	3	1
2803	-853	AS10dist	0			AS10prox	0.19285	3	1
2814	-864	AS10dist	0			AS10prox	0.19285	3	1
2815	-865	AS10dist	0.19285	3	1	AS10prox	0.3857	1	1
2816	-866	AS10dist	0.19285	3	1	AS10prox	0.19285	1	1
2818	-868	AS10dist	0.3857	1	1	AS10prox	0.3857	1	1
2822	-872	AS10dist	0			AS10prox	0.3857	1	1
2826	-876	AS10dist	0			AS10prox	0.3857	1	1
2830	-880	AS10dist	0			AS10prox	0.57855	1	1

2831	-881	AS10dist	0			AS10prox	0.7714	1	1
2832	-882	AS10dist	0			AS10prox	0.19285	1	1
2833	-883	AS10dist	0			AS10prox	0.3857	1	1
2837	-887	AS10dist	0			AS10prox	1.1571	1	1
2840	-890	AS10dist	0			AS10prox	1.5428	1	1
2848	-898	AS10dist	0			AS10prox	0.19285	3	1
2853	-903	AS10dist	0			AS10prox	0.19285	3	1
2856	-906	AS10dist	0			AS10prox	0.3857	1	1
2859	-909	AS10dist	0			AS10prox	0.19285	3	1
2862	-912	AS10dist	0			AS10prox	0.19285	1	1
2865	-915	AS10dist	0			AS10prox	0.19285	3	1
2869	-919	AS10dist	0			AS10prox	0.3857	1	1
2877	-927	AS10dist	0			AS10prox	0.19285	3	1
2879	-929	AS10dist	0			AS10prox	0.19285	3	1
2881	-931	AS10dist	0			AS10prox	0.3857	1	1
2882	-932	AS10dist	0			AS10prox	0.57855	1	1
2883	-933	AS10dist	0			AS10prox	0.19285	3	1
2884	-934	AS10dist	0			AS10prox	0.3857	1	1
2886	-936	AS10dist	0			AS10prox	0.19285	1	1
2888	-938	AS10dist	0			AS10prox	0.57855	1	1
2890	-940	AS10dist	0			AS10prox	0.57855	3	1
2901	-951	AS10dist	0			AS10prox	0.19285	3	1
2903	-953	AS10dist	0			AS10prox	0.19285	3	1
2905	-955	AS10dist	0			AS10prox	0.19285	3	1
2907	-957	AS10dist	0			AS10prox	0.3857	3	1
2916	-966	AS10dist	0			AS10prox	0.19285	3	1
2917	-967	AS10dist	0			AS10prox	0.19285	1	1
2918	-968	AS10dist	0			AS10prox	1.34995	1	1
2919	-969	AS10dist	0			AS10prox	0.19285	3	1
2920	-970	AS10dist	0			AS10prox	0.19285	3	1
2927	-977	AS10dist	0			AS10prox	0.3857	1	1
2928	-978	AS10dist	0			AS10prox	0.3857	1	1
2934	-984	AS10dist	0			AS10prox	0.19285	3	1
2936	-986	AS10dist	0			AS10prox	0.19285	3	1
2942	-992	AS10dist	0			AS10prox	0.19285	3	1
2945	-995	AS10dist	0			AS10prox	0.19285	3	1
2946	-996	AS10dist	0			AS10prox	0.3857	1	1
2947	-997	AS10dist	0			AS10prox	0.7714	1	1
2948	-998	AS10dist	0			AS10prox	0.19285	3	1
2951	-1001	AS10dist	0			AS10prox	0.3857	1	1
2953	-1003	AS10dist	1.73565	1	1	AS10prox	3.0856	1	1
2954	-1004	AS10dist	0			AS10prox	0.3857	1	1
2956	-1006	AS10dist	0			AS10prox	0.19285	3	1
2960	-1010	AS10dist	0			AS10prox	0.19285	3	1
2962	-1012	AS10dist	5.3998	2	1	AS10prox	6.9426	3	1
2965	-1015	AS10dist	0			AS10prox	0.3857	1	1
2970	-1020	AS10dist	0			AS10prox	0.19285	1	1
2975	-1025	AS10dist	0			AS10prox	0.19285	3	1
2979	-1029	AS10dist	0			AS10prox	0.19285	3	1
2982	-1032	AS10dist	0			AS10prox	2.3142	3	1
2983	-1033	AS10dist	0			AS10prox	1.9285	1	1
2989	-1039	AS10dist	0			AS10prox	0.19285	3	1
2990	-1040	AS10dist	0			AS10prox	0.3857	3	1
2993	-1043	AS10dist	0			AS10prox	0.19285	3	1
2994	-1044	AS10dist	0			AS10prox	1.34995	1	1
2995	-1045	AS10dist	0			AS10prox	0.57855	1	1
2996	-1046	AS10dist	3.0856	2	1	AS10prox	3.857	1	1
2999	-1049	AS10dist	0			AS10prox	0.19285	3	1
3004	-1054	AS10dist	0			AS10prox	0.3857	3	1
3008	-1058	AS10dist	0			AS10prox	0.19285	3	1
3011	-1061	AS10dist	0			AS10prox	0.19285	3	1
3015	-1065	AS10dist	0			AS10prox	0.19285	3	1

3018	-1068	AS10dist	0			AS10prox	0.19285	1	1
3022	-1072	AS10dist	0			AS10prox	0.19285	3	1
3023	-1073	AS10dist	0.3857	2	1	AS10prox	1.9285	1	1
3024	-1074	AS10dist	0			AS10prox	0.19285	3	1
3031	-1081	AS10dist	0			AS10prox	0.19285	3	1
3032	-1082	AS10dist	0			AS10prox	0.3857	1	1
3035	-1085	AS10dist	0			AS10prox	0.19285	3	1
3037	-1087	AS10dist	0			AS10prox	0.19285	3	1
3038	-1088	AS10dist	0			AS10prox	0.19285	3	1
3041	-1091	AS10dist	0			AS10prox	0.3857	1	1
3042	-1092	AS10dist	0			AS10prox	1.1571	1	1
3044	-1094	AS10dist	0			AS10prox	0.3857	1	1
3047	-1097	AS10dist	0			AS10prox	0.19285	3	1
3048	-1098	AS10dist	0			AS10prox	0.19285	3	1
3049	-1099	AS10dist	0			AS10prox	0.19285	3	1
3050	-1100	AS10dist	0			AS10prox	0.3857	1	1
3056	-1106	AS10dist	0			AS10prox	0.19285	3	1
3057	-1107	AS10dist	0			AS10prox	0.3857	3	1
3059	-1109	AS10dist	0			AS10prox	0.3857	3	1
3061	-1111	AS10dist	0			AS10prox	0.19285	1	1
3069	-1119	AS10dist	0			AS10prox	0.19285	3	1
3070	-1120	AS10dist	0			AS10prox	0.3857	1	1
3083	-1133	AS10dist	0.3857	2	1	AS10prox	0.19285	3	1
3089	-1139	AS10dist	3.4713	2	1	AS10prox	5.7855	1	1
3098	-1148	AS10dist	0			AS10prox	0.19285	3	1
3101	-1151	AS10dist	0			AS10prox	0.19285	3	1
3115	-1165	AS10dist	2.3142	2	1	AS10prox	2.3142	2	1
3119	-1169	AS10dist	0			AS10prox	0.19285	3	1
3134	-1184	AS10dist	0			AS10prox	0.19285	3	1
3135	-1185	AS10dist	0			AS10prox	0.19285	3	1
3137	-1187	AS10dist	0			AS10prox	0.3857	3	1
3138	-1188	AS10dist	0			AS10prox	0.3857	3	1
3142	-1192	AS10dist	0			AS10prox	0.19285	3	1
3144	-1194	AS10dist	0			AS10prox	0.19285	3	1
3149	-1199	AS10dist	0			AS10prox	0.19285	3	1
3150	-1200	AS10dist	0			AS10prox	0.19285	3	1
3156	-1206	AS10dist	0			AS10prox	0.19285	3	1
3161	-1211	AS10dist	0			AS10prox	0.19285	3	1
3163	-1213	AS10dist	0			AS10prox	0.19285	3	1
3164	-1214	AS10dist	0			AS10prox	0.19285	3	1
3169	-1219	AS10dist	0			AS10prox	0.19285	3	1
3173	-1223	AS10dist	0			AS10prox	0.19285	3	1
3174	-1224	AS10dist	0			AS10prox	0.3857	3	1
3176	-1226	AS10dist	0			AS10prox	0.19285	3	1
3177	-1227	AS10dist	0			AS10prox	0.19285	3	1
3179	-1229	AS10dist	0			AS10prox	0.19285	3	1
3192	-1242	AS10dist	0			AS10prox	0.19285	3	1
3193	-1243	AS10dist	0			AS10prox	0.19285	3	1
3198	-1248	AS10dist	0			AS10prox	0.19285	1	1
3206	-1256	AS10dist	0			AS10prox	0.19285	3	1
3213	-1263	AS10dist	0			AS10prox	0.19285	3	1
3214	-1264	AS10dist	1.1571	2	1	AS10prox	2.3142	2	1
3216	-1266	AS10dist	0			AS10prox	0.19285	3	1
3236	-1286	AS10dist	0			AS10prox	0.19285	3	1
3244	-1294	AS10dist	0			AS10prox	0.3857	1	1
3245	-1295	AS10dist	0			AS10prox	0.57855	3	1
3253	-1303	AS10dist	0.3857	2	1	AS10prox	0.3857	3	1
3255	-1305	AS10dist	0			AS10prox	0.19285	3	1
3257	-1307	AS10dist	0			AS10prox	0.19285	3	1
3260	-1310	AS10dist	0			AS10prox	0.19285	3	1
3263	-1313	AS10dist	0			AS10prox	0.19285	3	1
3267	-1317	AS10dist	0			AS10prox	0.19285	3	1

3272	-1322	AS10dist	0			AS10prox	0.19285	3	1
3275	-1325	AS10dist	0			AS10prox	0.19285	3	1
3278	-1328	AS10dist	0			AS10prox	0.19285	3	1
3280	-1330	AS10dist	0			AS10prox	0.19285	3	1
3281	-1331	AS10dist	0			AS10prox	0.19285	3	1
3292	-1342	AS10dist	0			AS10prox	0.19285	3	1
3295	-1345	AS10dist	0			AS10prox	0.19285	3	1
3300	-1350	AS10dist	0			AS10prox	0.19285	3	1
3303	-1353	AS10dist	0			AS10prox	0.3857	3	1
3311	-1361	AS10dist	0			AS10prox	0.19285	1	1
3313	-1363	AS10dist	0			AS10prox	0.19285	1	1
3321	-1371	AS10dist	0			AS10prox	0.19285	3	1
3322	-1372	AS10dist	0			AS10prox	0.19285	3	1
3323	-1373	AS10dist	0			AS10prox	0.19285	3	1
3326	-1376	AS10dist	0			AS10prox	0.19285	1	1
3327	-1377	AS10dist	0			AS10prox	0.57855	1	1
3330	-1380	AS10dist	0			AS10prox	0.19285	1	1
3333	-1383	AS10dist	0			AS10prox	0.19285	3	1
3337	-1387	AS10dist	0			AS10prox	0.3857	3	1
3338	-1388	AS10dist	0			AS10prox	0.19285	1	1
3344	-1394	AS10dist	0			AS10prox	0.19285	3	1
3347	-1397	AS10dist	0			AS10prox	0.19285	3	1
3348	-1398	AS10dist	0			AS10prox	0.19285	3	1
3350	-1400	AS10dist	0			AS10prox	0.19285	3	1
3353	-1403	AS10dist	0			AS10prox	0.19285	3	1
3356	-1406	AS10dist	0			AS10prox	0.19285	3	1
3357	-1407	AS10dist	0			AS10prox	0.19285	3	1
3358	-1408	AS10dist	0			AS10prox	0.19285	3	1
3359	-1409	AS10dist	0			AS10prox	0.19285	3	1
3360	-1410	AS10dist	0			AS10prox	0.3857	3	1
3362	-1412	AS10dist	0			AS10prox	0.19285	3	1
3363	-1413	AS10dist	0			AS10prox	0.19285	3	1
3365	-1415	AS10dist	0			AS10prox	0.19285	1	1
3367	-1417	AS10dist	0			AS10prox	0.19285	3	1
3368	-1418	AS10dist	0			AS10prox	0.19285	3	1
3373	-1423	AS10dist	0			AS10prox	0.19285	3	1
3374	-1424	AS10dist	0			AS10prox	0.19285	3	1
3378	-1428	AS10dist	0			AS10prox	0.3857	1	1
3379	-1429	AS10dist	0			AS10prox	0.19285	3	1
3380	-1430	AS10dist	0			AS10prox	0.19285	1	1
3381	-1431	AS10dist	0			AS10prox	0.3857	3	1
3385	-1435	AS10dist	0			AS10prox	0.3857	1	1
3389	-1439	AS10dist	0			AS10prox	0.19285	3	1
3390	-1440	AS10dist	0			AS10prox	0.19285	3	1
3391	-1441	AS10dist	0			AS10prox	0.19285	3	1
3392	-1442	AS10dist	0			AS10prox	0.19285	3	1
3394	-1444	AS10dist	0			AS10prox	0.3857	3	1
3396	-1446	AS10dist	5.3998	3	1	AS10prox	39	3	1
3397	-1447	AS10dist	0			AS10prox	0.3857	3	1
3402	-1452	AS10dist	0			AS10prox	0.19285	3	1
3403	-1453	AS10dist	0			AS10prox	0.3857	1	1
3406	-1456	AS10dist	0			AS10prox	0.19285	3	1
3407	-1457	AS10dist	1.1571	2	1	AS10prox	4.43555	2	1
3412	-1462	AS10dist	0			AS10prox	0.19285	3	1
3413	-1463	AS10dist	0			AS10prox	0.19285	3	1
3415	-1465	AS10dist	0			AS10prox	0.19285	3	1
3416	-1466	AS10dist	0			AS10prox	0.19285	1	1
3417	-1467	AS10dist	0			AS10prox	0.19285	1	1
3419	-1469	AS10dist	0			AS10prox	0.19285	3	1
3421	-1471	AS10dist	0			AS10prox	0.19285	3	1
3424	-1474	AS10dist	0			AS10prox	0.3857	1	1
3427	-1477	AS10dist	0			AS10prox	0.19285	3	1

3430	-1480	AS10dist	0			AS10prox	0.19285	3	1
3432	-1482	AS10dist	0			AS10prox	0.19285	3	1
3434	-1484	AS10dist	0			AS10prox	0.19285	3	1
3435	-1485	AS10dist	0			AS10prox	0.19285	3	1
3443	-1493	AS10dist	0			AS10prox	0.19285	1	1
3446	-1496	AS10dist	0			AS10prox	0.3857	1	1
3448	-1498	AS10dist	0			AS10prox	0.19285	3	1
3449	-1499	AS10dist	0			AS10prox	0.19285	3	1
3451	-1501	AS10dist	0			AS10prox	0.19285	3	1
3454	-1504	AS10dist	0			AS10prox	0.19285	3	1
3455	-1505	AS10dist	0			AS10prox	0.19285	3	1
3458	-1508	AS10dist	0			AS10prox	0.19285	3	1
3460	-1510	AS10dist	0			AS10prox	0.19285	3	1
3464	-1514	AS10dist	0			AS10prox	0.19285	3	1
3465	-1515	AS10dist	0			AS10prox	0.19285	3	1
3466	-1516	AS10dist	0			AS10prox	0.19285	3	1
3467	-1517	AS10dist	0			AS10prox	0.19285	3	1
3473	-1523	AS10dist	0			AS10prox	0.19285	3	1
3475	-1525	AS10dist	0			AS10prox	0.19285	3	1
3490	-1540	AS10dist	0			AS10prox	0.19285	3	1
3494	-1544	AS10dist	0			AS10prox	0.3857	3	1
3495	-1545	AS10dist	0			AS10prox	0.19285	3	1
3496	-1546	AS10dist	0			AS10prox	0.19285	3	1
3497	-1547	AS10dist	0			AS10prox	0.19285	3	1
3499	-1549	AS10dist	0			AS10prox	0.19285	3	1
3502	-1552	AS10dist	0			AS10prox	0.19285	3	1
3504	-1554	AS10dist	0			AS10prox	0.19285	3	1
3506	-1556	AS10dist	0			AS10prox	0.19285	3	1
3511	-1561	AS10dist	0			AS10prox	0.3857	3	1
3516	-1566	AS10dist	0			AS10prox	0.3857	3	1
3522	-1572	AS10dist	0			AS10prox	0.19285	3	1
3524	-1574	AS10dist	0			AS10prox	0.7714	2	1
3534	-1584	AS10dist	0			AS10prox	0.19285	3	1
3538	-1588	AS10dist	0			AS10prox	0.19285	3	1
3539	-1589	AS10dist	0			AS10prox	0.96425	1	1
3541	-1591	AS10dist	0			AS10prox	0.19285	3	1
3542	-1592	AS10dist	0			AS10prox	0.19285	3	1
3544	-1594	AS10dist	0			AS10prox	0.19285	3	1
3548	-1598	AS10dist	0			AS10prox	0.19285	3	1
3549	-1599	AS10dist	0			AS10prox	0.19285	3	1
3551	-1601	AS10dist	0			AS10prox	0.19285	3	1
3552	-1602	AS10dist	0			AS10prox	0.7714	3	1
3555	-1605	AS10dist	0			AS10prox	0.19285	3	1
3557	-1607	AS10dist	0			AS10prox	0.96425	1	1
3558	-1608	AS10dist	0			AS10prox	0.19285	3	1
3560	-1610	AS10dist	0			AS10prox	0.19285	3	1
3561	-1611	AS10dist	0			AS10prox	1.1571	3	1
3562	-1612	AS10dist	0			AS10prox	0.19285	3	1
3563	-1613	AS10dist	0			AS10prox	0.19285	3	1
3564	-1614	AS10dist	0			AS10prox	0.19285	3	1
3570	-1620	AS10dist	0			AS10prox	0.19285	3	1
3571	-1621	AS10dist	0			AS10prox	0.19285	3	1
3575	-1625	AS10dist	1.1571	2	1	AS10prox	0.7714	2	1
3577	-1627	AS10dist	0			AS10prox	0.57855	3	1
3578	-1628	AS10dist	0			AS10prox	0.19285	3	1
3579	-1629	AS10dist	0			AS10prox	0.19285	3	1
3587	-1637	AS10dist	0.3857	2	1	AS10prox	0.19285	3	1
3589	-1639	AS10dist	0			AS10prox	0.3857	3	1
3592	-1642	AS10dist	0			AS10prox	0.19285	3	1
3594	-1644	AS10dist	0			AS10prox	0.19285	3	1
3595	-1645	AS10dist	0			AS10prox	0.3857	3	1
3598	-1648	AS10dist	0			AS10prox	0.19285	3	1

3601	-1651	AS10dist	0			AS10prox	0.19285	3	1
3602	-1652	AS10dist	0			AS10prox	0.3857	3	1
3609	-1659	AS10dist	0			AS10prox	0.19285	3	1
3610	-1660	AS10dist	0			AS10prox	0.19285	3	1
3615	-1665	AS10dist	0			AS10prox	0.19285	3	1
3622	-1672	AS10dist	0			AS10prox	0.19285	3	1
3624	-1674	AS10dist	0.7714	2	1	AS10prox	0.3857	1	1
3625	-1675	AS10dist	0			AS10prox	0.19285	3	1
3633	-1683	AS10dist	0			AS10prox	0.19285	3	1
3635	-1685	AS10dist	0			AS10prox	0.19285	3	1
3639	-1689	AS10dist	0			AS10prox	0.19285	3	1
3645	-1695	AS10dist	0			AS10prox	0.19285	3	1
3646	-1696	AS10dist	0			AS10prox	0.19285	3	1
3650	-1700	AS10dist	0			AS10prox	0.19285	3	1
3652	-1702	AS10dist	0			AS10prox	0.19285	3	1
3666	-1716	AS10dist	0			AS10prox	0.19285	3	1
3668	-1718	AS10dist	0			AS10prox	0.19285	3	1
3677	-1727	AS10dist	0			AS10prox	0.19285	3	1
3679	-1729	AS10dist	0			AS10prox	0.19285	3	1
3681	-1731	AS10dist	0			AS10prox	0.57855	1	1
3682	-1732	AS10dist	0			AS10prox	0.19285	3	1
3687	-1737	AS10dist	0			AS10prox	0.19285	3	1
3697	-1747	AS10dist	0			AS10prox	0.19285	3	1
3699	-1749	AS10dist	0			AS10prox	0.19285	1	1
3706	-1756	AS10dist	0			AS10prox	0.19285	3	1
3708	-1758	AS10dist	0			AS10prox	0.19285	3	1
3711	-1761	AS10dist	0			AS10prox	0.19285	3	1
3717	-1767	AS10dist	0			AS10prox	0.19285	2	1
3718	-1768	AS10dist	0			AS10prox	0.19285	3	1
3721	-1771	AS10dist	0			AS10prox	0.19285	3	1
3725	-1775	AS10dist	0			AS10prox	0.19285	3	1
3728	-1778	AS10dist	0			AS10prox	0.19285	3	1
3735	-1785	AS10dist	0			AS10prox	0.3857	3	1
3736	-1786	AS10dist	0			AS10prox	0.19285	1	1
3741	-1791	AS10dist	0			AS10prox	0.19285	1	1
3745	-1795	AS10dist	0			AS10prox	0.19285	3	1
3746	-1796	AS10dist	0			AS10prox	0.19285	3	1
3750	-1800	AS10dist	0			AS10prox	0.19285	1	1
3755	-1805	AS10dist	0			AS10prox	0.19285	3	1
3759	-1809	AS10dist	0			AS10prox	0.19285	3	1
3764	-1814	AS10dist	0			AS10prox	0.19285	2	1
3766	-1816	AS10dist	0			AS10prox	0.19285	3	1
3770	-1820	AS10dist	0			AS10prox	0.3857	3	1
3779	-1829	AS10dist	0			AS10prox	0.19285	3	1
3788	-1838	AS10dist	0			AS10prox	0.19285	3	1
3794	-1844	AS10dist	0			AS10prox	0.19285	3	1
3796	-1846	AS10dist	0			AS10prox	0.19285	3	1
3802	-1852	AS10dist	0			AS10prox	0.19285	3	1
3809	-1859	AS10dist	0			AS10prox	0.19285	3	1
3813	-1863	AS10dist	0			AS10prox	0.3857	3	1
3818	-1868	AS10dist	0			AS10prox	0.19285	3	1
3823	-1873	AS10dist	0			AS10prox	0.19285	3	1
3830	-1880	AS10dist	0			AS10prox	0.19285	1	1
3841	-1891	AS10dist	0			AS10prox	0.19285	3	1
3848	-1898	AS10dist	1.5428	2	1	AS10prox	1.34995	2	1
3853	-1903	AS10dist	0			AS10prox	0.57855	3	1
3856	-1906	AS10dist	0			AS10prox	0.19285	3	1
3859	-1909	AS10dist	3.0856	2	1	AS10prox	3.4713	2	1
3864	-1914	AS10dist	0			AS10prox	0.96425	1	1
3866	-1916	AS10dist	0			AS10prox	0.57855	3	1
3870	-1920	AS10dist	0			AS10prox	0.19285	3	1
3874	-1924	AS10dist	0			AS10prox	0.3857	3	1

3875	-1925	AS10dist	0			AS10prox	0.19285	3	1
3882	-1932	AS10dist	0			AS10prox	0.19285	3	1
3885	-1935	AS10dist	0			AS10prox	0.19285	3	1
3892	-1942	AS10dist	0			AS10prox	0.19285	3	1
3894	-1944	AS10dist	0			AS10prox	0.19285	3	1
3903	-1953	AS10dist	0			AS10prox	0.19285	3	1
3906	-1956	AS10dist	0			AS10prox	0.3857	1	1
3913	-1963	AS10dist	0.3857	2	1	AS10prox	0.19285	3	1
3921	-1971	AS10dist	0			AS10prox	0.19285	3	1
3922	-1972	AS10dist	0			AS10prox	0.3857	3	1
3926	-1976	AS10dist	0			AS10prox	0.19285	3	1
3934	-1984	AS10dist	0			AS10prox	0.19285	1	1
3939	-1989	AS10dist	0			AS10prox	0.19285	3	1
3943	-1993	AS10dist	0			AS10prox	0.19285	3	1
3944	-1994	AS10dist	0			AS10prox	0.3857	1	1
3947	-1997	AS10dist	0			AS10prox	0.19285	3	1
3949	-1999	AS10dist	0			AS10prox	0.19285	1	1
3952	-2002	AS10dist	0			AS10prox	0.19285	3	1
3956	-2006	AS10dist	0			AS10prox	0.19285	3	1
3958	-2008	AS10dist	0			AS10prox	0.19285	3	1
3960	-2010	AS10dist	0			AS10prox	0.19285	3	1
3961	-2011	AS10dist	0			AS10prox	0.3857	1	1
3962	-2012	AS10dist	2.6999	2	1	AS10prox	4.2427	2	1
3964	-2014	AS10dist	0			AS10prox	0.19285	3	1
3966	-2016	AS10dist	0			AS10prox	0.19285	3	1
3967	-2017	AS10dist	0			AS10prox	0.19285	3	1
3976	-2026	AS10dist	0			AS10prox	0.19285	3	1
3984	-2034	AS10dist	0			AS10prox	0.19285	3	1
3988	-2038	AS10dist	0			AS10prox	0.19285	3	1
3993	-2043	AS10dist	0			AS10prox	0.19285	3	1
3998	-2048	AS10dist	0			AS10prox	0.19285	3	1
3999	-2049	AS10dist	0			AS10prox	0.19285	3	1
4004	-2054	AS10dist	0			AS10prox	0.19285	3	1
4008	-2058	AS10dist	0			AS10prox	0.7714	3	1
4009	-2059	AS10dist	0			AS10prox	0.7714	3	1
4016	-2066	AS10dist	1.1571	2	1	AS10prox	1.5428	2	1
4017	-2067	AS10dist	0			AS10prox	0.19285	3	1
4019	-2069	AS10dist	0			AS10prox	0.19285	3	1
4035	-2085	AS10dist	0			AS10prox	0.19285	3	1
4038	-2088	AS10dist	0			AS10prox	0.19285	3	1
4041	-2091	AS10dist	0			AS10prox	0.19285	3	1
4044	-2094	AS10dist	0			AS10prox	0.3857	3	1
4049	-2099	AS10dist	0			AS10prox	0.19285	3	1
4055	-2105	AS10dist	0			AS10prox	0.3857	1	1
4056	-2106	AS10dist	0			AS10prox	0.19285	3	1
4057	-2107	AS10dist	0			AS10prox	0.3857	3	1
4058	-2108	AS10dist	0			AS10prox	0.3857	3	1
4059	-2109	AS10dist	0			AS10prox	0.3857	3	1
4060	-2110	AS10dist	0			AS10prox	0.7714	2	1
4063	-2113	AS10dist	0			AS10prox	0.19285	3	1
4064	-2114	AS10dist	0			AS10prox	0.19285	3	1
4065	-2115	AS10dist	0			AS10prox	0.3857	3	1
4067	-2117	AS10dist	0			AS10prox	0.19285	3	1
4077	-2127	AS10dist	0			AS10prox	0.19285	3	1
4082	-2132	AS10dist	0			AS10prox	0.19285	3	1
4084	-2134	AS10dist	1.5428	2	1	AS10prox	1.73565	1	1
4086	-2136	AS10dist	0			AS10prox	0.19285	3	1
4089	-2139	AS10dist	0			AS10prox	0.19285	3	1
4097	-2147	AS10dist	0			AS10prox	0.19285	3	1
4100	-2150	AS10dist	0			AS10prox	0.19285	3	1
4105	-2155	AS10dist	0			AS10prox	0.19285	3	1
4108	-2158	AS10dist	0			AS10prox	1.34995	1	1

4109	-2159	AS10dist	0			AS10prox	0.57855	3	1
4110	-2160	AS10dist	0			AS10prox	1.9285	1	1
4112	-2162	AS10dist	0			AS10prox	0.19285	3	1
4113	-2163	AS10dist	7.714	2	1	AS10prox	8.0997	2	1
4116	-2166	AS10dist	0			AS10prox	0.19285	3	1
4123	-2173	AS10dist	0			AS10prox	0.19285	3	1
4124	-2174	AS10dist	0			AS10prox	0.3857	3	1
4125	-2175	AS10dist	0			AS10prox	0.19285	3	1
4127	-2177	AS10dist	0			AS10prox	0.19285	3	1
4129	-2179	AS10dist	0			AS10prox	0.19285	3	1
4136	-2186	AS10dist	0			AS10prox	0.19285	3	1
4144	-2194	AS10dist	0			AS10prox	0.19285	3	1
4151	-2201	AS10dist	0			AS10prox	0.19285	3	1
4155	-2205	AS10dist	0			AS10prox	0.19285	3	1
4156	-2206	AS10dist	0			AS10prox	0.19285	3	1
4160	-2210	AS10dist	0			AS10prox	0.19285	3	1
4162	-2212	AS10dist	0			AS10prox	0.19285	3	1
4165	-2215	AS10dist	0			AS10prox	0.19285	3	1
4170	-2220	AS10dist	0			AS10prox	2.3142	1	1
4179	-2229	AS10dist	0			AS10prox	0.3857	3	1
4180	-2230	AS10dist	0			AS10prox	0.3857	3	1
4182	-2232	AS10dist	0			AS10prox	0.3857	1	1
4183	-2233	AS10dist	0			AS10prox	0.19285	3	1
4189	-2239	AS10dist	0			AS10prox	0.19285	3	1
4194	-2244	AS10dist	0			AS10prox	0.19285	3	1
4197	-2247	AS10dist	0			AS10prox	0.19285	3	1
4208	-2258	AS10dist	0			AS10prox	0.19285	3	1
4213	-2263	AS10dist	0			AS10prox	0.19285	3	1
4222	-2272	AS10dist	0			AS10prox	0.19285	3	1
4223	-2273	AS10dist	0			AS10prox	0.19285	3	1
4231	-2281	AS10dist	0			AS10prox	0.19285	3	1
4239	-2289	AS10dist	0			AS10prox	0.19285	3	1
4240	-2290	AS10dist	0			AS10prox	0.57855	1	1
4241	-2291	AS10dist	0			AS10prox	0.19285	3	1
4247	-2297	AS10dist	0			AS10prox	0.19285	3	1
4249	-2299	AS10dist	0			AS10prox	0.19285	3	1
4257	-2307	AS10dist	0			AS10prox	0.19285	3	1
4261	-2311	AS10dist	0			AS10prox	0.19285	3	1
4266	-2316	AS10dist	0			AS10prox	0.19285	3	1
4268	-2318	AS10dist	0			AS10prox	0.19285	3	1
4269	-2319	AS10dist	0			AS10prox	0.19285	3	1
4271	-2321	AS10dist	0			AS10prox	0.57855	1	1
4274	-2324	AS10dist	0			AS10prox	0.19285	1	1
4278	-2328	AS10dist	0			AS10prox	0.19285	3	1
4280	-2330	AS10dist	0			AS10prox	0.19285	3	1
4284	-2334	AS10dist	0			AS10prox	0.19285	3	1
4286	-2336	AS10dist	0			AS10prox	0.19285	3	1
4296	-2346	AS10dist	0			AS10prox	0.19285	3	1
4299	-2349	AS10dist	0			AS10prox	0.19285	3	1
4303	-2353	AS10dist	0			AS10prox	0.19285	3	1
4307	-2357	AS10dist	0			AS10prox	0.19285	3	1
4308	-2358	AS10dist	0			AS10prox	0.19285	3	1
4309	-2359	AS10dist	0			AS10prox	0.57855	3	1
4311	-2361	AS10dist	0			AS10prox	1.1571	3	1
4312	-2362	AS10dist	0			AS10prox	0.19285	3	1
4313	-2363	AS10dist	0			AS10prox	0.19285	3	1
4315	-2365	AS10dist	0			AS10prox	0.19285	3	1
4318	-2368	AS10dist	0			AS10prox	0.19285	3	1
4320	-2370	AS10dist	0			AS10prox	1.5428	1	1
4323	-2373	AS10dist	0			AS10prox	0.19285	3	1
4326	-2376	AS10dist	0			AS10prox	0.19285	3	1
4328	-2378	AS10dist	0			AS10prox	0.3857	1	1

4330	-2380	AS10dist	0			AS10prox	0.19285	1	1
4336	-2386	AS10dist	0			AS10prox	0.19285	3	1
4346	-2396	AS10dist	0			AS10prox	0.19285	3	1
4350	-2400	AS10dist	0			AS10prox	0.19285	1	1
4353	-2403	AS10dist	0			AS10prox	0.19285	3	1
4357	-2407	AS10dist	0			AS10prox	0.19285	3	1
4358	-2408	AS10dist	0			AS10prox	0.3857	3	1
4371	-2421	AS10dist	0			AS10prox	0.19285	3	1
4375	-2425	AS10dist	0			AS10prox	0.19285	3	1
4376	-2426	AS10dist	0			AS10prox	0.19285	3	1
4377	-2427	AS10dist	0			AS10prox	0.19285	1	1
4379	-2429	AS10dist	0			AS10prox	0.19285	3	1
4384	-2434	AS10dist	0			AS10prox	0.19285	3	1
4385	-2435	AS10dist	0			AS10prox	0.19285	3	1
4386	-2436	AS10dist	0			AS10prox	0.19285	3	1
4388	-2438	AS10dist	0			AS10prox	0.19285	3	1
4389	-2439	AS10dist	0			AS10prox	0.19285	3	1
4391	-2441	AS10dist	0			AS10prox	0.19285	3	1
4392	-2442	AS10dist	0			AS10prox	0.19285	3	1
4393	-2443	AS10dist	0			AS10prox	0.57855	1	1
4394	-2444	AS10dist	0			AS10prox	1.5428	1	1
4397	-2447	AS10dist	0			AS10prox	0.19285	3	1
4399	-2449	AS10dist	0			AS10prox	0.19285	3	1
4403	-2453	AS10dist	0			AS10prox	1.9285	3	1
4408	-2458	AS10dist	0			AS10prox	0.19285	3	1
4409	-2459	AS10dist	0			AS10prox	0.19285	1	1
4411	-2461	AS10dist	1.5428	2	1	AS10prox	3.4713	2	1
4412	-2462	AS10dist	0			AS10prox	0.57855	3	1
4423	-2473	AS10dist	0			AS10prox	0.3857	3	1
4432	-2482	AS10dist	0			AS10prox	0.19285	3	1
4439	-2489	AS10dist	0			AS10prox	0.19285	3	1
4444	-2494	AS10dist	0			AS10prox	0.19285	1	1
4465	-2515	AS10dist	0			AS10prox	0.19285	3	1
4485	-2535	AS10dist	0			AS10prox	0.19285	3	1
4491	-2541	AS10dist	0			AS10prox	0.3857	3	1
4492	-2542	AS10dist	0			AS10prox	0.3857	3	1
4493	-2543	AS10dist	0			AS10prox	0.19285	3	1
4496	-2546	AS10dist	0			AS10prox	1.9285	3	1
4501	-2551	AS10dist	0.3857	2	1	AS10prox	2.6999	1	1
4506	-2556	AS10dist	0.7714	2	1	AS10prox	1.9285	2	1
4509	-2559	AS10dist	0			AS10prox	0.19285	2	1
4511	-2561	AS10dist	0			AS10prox	0.3857	3	1
4515	-2565	AS10dist	0			AS10prox	0.19285	3	1
4516	-2566	AS10dist	0			AS10prox	0.19285	3	1
4517	-2567	AS10dist	0			AS10prox	0.19285	3	1
4523	-2573	AS10dist	0			AS10prox	0.3857	3	1
4524	-2574	AS10dist	0			AS10prox	0.3857	3	1
4525	-2575	AS10dist	0			AS10prox	0.3857	2	1
4527	-2577	AS10dist	0			AS10prox	0.19285	3	1
4529	-2579	AS10dist	0			AS10prox	0.3857	3	1
4532	-2582	AS10dist	0			AS10prox	0.19285	3	1
4533	-2583	AS10dist	0			AS10prox	0.3857	3	1
4536	-2586	AS10dist	0			AS10prox	0.19285	1	1
4542	-2592	AS10dist	0			AS10prox	0.19285	3	1
4543	-2593	AS10dist	0			AS10prox	0.19285	1	1
4545	-2595	AS10dist	0			AS10prox	0.19285	3	1
4546	-2596	AS10dist	0			AS10prox	0.19285	1	1
4554	-2604	AS10dist	0			AS10prox	0.19285	3	1
4562	-2612	AS10dist	0			AS10prox	0.3857	3	1
4566	-2616	AS10dist	0			AS10prox	0.19285	3	1
4571	-2621	AS10dist	0			AS10prox	0.19285	3	1
4575	-2625	AS10dist	0			AS10prox	0.19285	3	1

4576	-2626	AS10dist	0			AS10prox	0.19285	1	1
4580	-2630	AS10dist	0			AS10prox	0.3857	1	1
4581	-2631	AS10dist	0			AS10prox	0.3857	1	1
4591	-2641	AS10dist	0			AS10prox	0.19285	3	1
4592	-2642	AS10dist	0			AS10prox	0.19285	3	1
4593	-2643	AS10dist	0			AS10prox	0.3857	3	1
4595	-2645	AS10dist	0			AS10prox	0.19285	3	1
4597	-2647	AS10dist	0			AS10prox	0.19285	3	1
4600	-2650	AS10dist	0			AS10prox	0.19285	1	1
4602	-2652	AS10dist	0			AS10prox	0.19285	3	1
4607	-2657	AS10dist	0			AS10prox	0.3857	3	1
4614	-2664	AS10dist	0			AS10prox	0.3857	3	1
4617	-2667	AS10dist	0			AS10prox	0.19285	1	1
4621	-2671	AS10dist	0			AS10prox	0.19285	3	1
4623	-2673	AS10dist	0			AS10prox	0.19285	2	1
4631	-2681	AS10dist	0			AS10prox	0.19285	3	1
4638	-2688	AS10dist	0			AS10prox	0.19285	3	1
4641	-2691	AS10dist	0.57855	2	1	AS10prox	1.1571	2	1
4646	-2696	AS10dist	0			AS10prox	0.19285	3	1
4663	-2713	AS10dist	0			AS10prox	0.19285	1	1
4674	-2724	AS10dist	0			AS10prox	0.19285	2	1
4676	-2726	AS10dist	0			AS10prox	0.19285	2	1
4677	-2727	AS10dist	0			AS10prox	0.19285	3	1
4679	-2729	AS10dist	0			AS10prox	0.19285	3	1
4680	-2730	AS10dist	0			AS10prox	0.19285	3	1
4687	-2737	AS10dist	0			AS10prox	0.19285	3	1
4691	-2741	AS10dist	0			AS10prox	0.19285	1	1
4693	-2743	AS10dist	0			AS10prox	0.19285	1	1
4698	-2748	AS10dist	0			AS10prox	0.19285	3	1
4702	-2752	AS10dist	0			AS10prox	0.57855	3	1
4704	-2754	AS10dist	0			AS10prox	0.19285	1	1
4706	-2756	AS10dist	0			AS10prox	0.19285	3	1
4719	-2769	AS10dist	0			AS10prox	0.19285	1	1
4725	-2775	AS10dist	0			AS10prox	0.19285	3	1
4726	-2776	AS10dist	0			AS10prox	0.19285	1	1
4727	-2777	AS10dist	0			AS10prox	0.19285	1	1
4735	-2785	AS10dist	1.5428	2	1	AS10prox	2.89275	2	1
4740	-2790	AS10dist	0			AS10prox	0.19285	3	1
4742	-2792	AS10dist	0			AS10prox	0.19285	3	1
4747	-2797	AS10dist	0			AS10prox	0.19285	3	1
4763	-2813	AS10dist	0			AS10prox	0.3857	3	1
4775	-2825	AS10dist	0			AS10prox	0.19285	3	1
4777	-2827	AS10dist	0			AS10prox	0.19285	3	1
4782	-2832	AS10dist	0			AS10prox	0.19285	3	1
4783	-2833	AS10dist	0			AS10prox	0.19285	3	1
4799	-2849	AS10dist	0			AS10prox	0.19285	1	1
4802	-2852	AS10dist	1.1571	2	1	AS10prox	1.5428	2	1
4803	-2853	AS10dist	0			AS10prox	0.19285	3	1
4805	-2855	AS10dist	0			AS10prox	0.19285	3	1
4806	-2856	AS10dist	0			AS10prox	0.19285	3	1
4807	-2857	AS10dist	0			AS10prox	0.19285	3	1
4809	-2859	AS10dist	0			AS10prox	0.19285	3	1
4810	-2860	AS10dist	0			AS10prox	1.1571	1	1
4812	-2862	AS10dist	0			AS10prox	0.19285	3	1
4813	-2863	AS10dist	0			AS10prox	0.19285	3	1
4817	-2867	AS10dist	0			AS10prox	0.19285	3	1
4819	-2869	AS10dist	0			AS10prox	0.19285	3	1
4820	-2870	AS10dist	0			AS10prox	0.19285	3	1
4822	-2872	AS10dist	0			AS10prox	0.19285	3	1
4824	-2874	AS10dist	0			AS10prox	0.19285	3	1
4826	-2876	AS10dist	0			AS10prox	0.3857	3	1
4828	-2878	AS10dist	0			AS10prox	0.19285	3	1

4830	-2880	AS10dist	0			AS10prox	0.19285	3	1
4833	-2883	AS10dist	0			AS10prox	0.19285	3	1
4835	-2885	AS10dist	0			AS10prox	0.19285	3	1
4836	-2886	AS10dist	0			AS10prox	0.19285	3	1
4840	-2890	AS10dist	0			AS10prox	0.19285	3	1
4843	-2893	AS10dist	0			AS10prox	0.19285	3	1
4845	-2895	AS10dist	0			AS10prox	0.19285	3	1
4852	-2902	AS10dist	0			AS10prox	0.19285	3	1
4865	-2915	AS10dist	1.5428	2	1	AS10prox	1.34995	3	1
4869	-2919	AS10dist	0			AS10prox	1.5428	1	1
4880	-2930	AS10dist	0.3857	2	1	AS10prox	0.19285	3	1
4885	-2935	AS10dist	0			AS10prox	0.19285	3	1
4891	-2941	AS10dist	0			AS10prox	0.19285	3	1
4893	-2943	AS10dist	0			AS10prox	0.19285	3	1
4895	-2945	AS10dist	0			AS10prox	0.19285	3	1
4898	-2948	AS10dist	0			AS10prox	0.19285	3	1
4901	-2951	AS10dist	0			AS10prox	0.19285	3	1
4910	-2960	AS10dist	0			AS10prox	0.19285	3	1
4920	-2970	AS10dist	0			AS10prox	0.19285	3	1
4924	-2974	AS10dist	0			AS10prox	0.19285	3	1
4938	-2988	AS10dist	0			AS10prox	0.19285	3	1
4944	-2994	AS10dist	0			AS10prox	0.19285	3	1
4947	-2997	AS10dist	0			AS10prox	0.19285	3	1
4950	-3000	AS10dist	0			AS10prox	0.19285	3	1
4951	-3001	AS10dist	0			AS10prox	0.19285	3	1
4952	-3002	AS10dist	0			AS10prox	0.19285	3	1
4954	-3004	AS10dist	0			AS10prox	0.19285	3	1
4955	-3005	AS10dist	0			AS10prox	0.19285	3	1
4966	-3016	AS10dist	0			AS10prox	0.19285	3	1
4968	-3018	AS10dist	0			AS10prox	0.19285	3	1
4969	-3019	AS10dist	0			AS10prox	0.19285	3	1
4971	-3021	AS10dist	0			AS10prox	0.19285	3	1
4972	-3022	AS10dist	0			AS10prox	0.19285	3	1
4975	-3025	AS10dist	0			AS10prox	0.19285	3	1
4977	-3027	AS10dist	0			AS10prox	0.3857	2	1
4981	-3031	AS10dist	0			AS10prox	0.19285	3	1
4982	-3032	AS10dist	0			AS10prox	0.19285	3	1
4987	-3037	AS10dist	0			AS10prox	0.19285	3	1
4988	-3038	AS10dist	0			AS10prox	0.3857	3	1
4996	-3046	AS10dist	0			AS10prox	0.19285	3	1
4997	-3047	AS10dist	1.5428	2	1	AS10prox	2.50705	1	1
4998	-3048	AS10dist	0			AS10prox	0.19285	3	1
5006	-3056	AS10dist	0			AS10prox	0.96425	1	1
5020	-3070	AS10dist	0			AS10prox	0.7714	3	1
5024	-3074	AS10dist	0			AS10prox	0.19285	1	1
5025	-3075	AS10dist	0			AS10prox	0.19285	3	1
5032	-3082	AS10dist	0			AS10prox	0.19285	3	1
5044	-3094	AS10dist	0			AS10prox	0.19285	3	1
5046	-3096	AS10dist	0			AS10prox	0.57855	1	1
5049	-3099	AS10dist	0			AS10prox	0.19285	3	1
5054	-3104	AS10dist	2.3142	2	1	AS10prox	5.3998	2	1
5055	-3105	AS10dist	0			AS10prox	0.19285	1	1
5059	-3109	AS10dist	0			AS10prox	1.5428	2	1
5062	-3112	AS10dist	0			AS10prox	0.19285	3	1
5066	-3116	AS10dist	0			AS10prox	0.19285	3	1
5068	-3118	AS10dist	0			AS10prox	0.19285	3	1
5069	-3119	AS10dist	0			AS10prox	0.19285	3	1
5070	-3120	AS10dist	0			AS10prox	0.19285	3	1
5071	-3121	AS10dist	1.5428	2	1	AS10prox	1.5428	2	1
5081	-3131	AS10dist	1.1571	2	1	AS10prox	0.57855	2	1
5089	-3139	AS10dist	0			AS10prox	0.19285	3	1
5107	-3157	AS10dist	0			AS10prox	0.57855	1	1

5109	-3159	AS10dist	0			AS10prox	0.19285	3	1
5118	-3168	AS10dist	0			AS10prox	0.19285	3	1
5122	-3172	AS10dist	0			AS10prox	0.19285	3	1
5124	-3174	AS10dist	0			AS10prox	0.19285	3	1
5125	-3175	AS10dist	0.96425	2	1	AS10prox	1.1571	2	1
5127	-3177	AS10dist	0			AS10prox	0.19285	3	1
5132	-3182	AS10dist	0			AS10prox	0.19285	3	1
5135	-3185	AS10dist	0			AS10prox	0.3857	3	1
5138	-3188	AS10dist	0			AS10prox	0.19285	3	1
5139	-3189	AS10dist	0			AS10prox	0.19285	3	1
5141	-3191	AS10dist	0			AS10prox	0.19285	3	1
5144	-3194	AS10dist	0			AS10prox	0.19285	3	1
5146	-3196	AS10dist	0			AS10prox	2.12135	2	1
5149	-3199	AS10dist	0			AS10prox	0.19285	3	1
5155	-3205	AS10dist	0			AS10prox	0.3857	3	1
5156	-3206	AS10dist	0			AS10prox	0.19285	3	1
5160	-3210	AS10dist	0			AS10prox	0.3857	2	1
5161	-3211	AS10dist	0			AS10prox	0.19285	3	1
5162	-3212	AS10dist	0			AS10prox	0.19285	3	1
5169	-3219	AS10dist	0			AS10prox	0.3857	3	1
5173	-3223	AS10dist	0			AS10prox	0.19285	3	1
5175	-3225	AS10dist	0			AS10prox	0.3857	3	1
5177	-3227	AS10dist	0			AS10prox	0.19285	1	1
5179	-3229	AS10dist	0			AS10prox	0.19285	3	1
5187	-3237	AS10dist	0			AS10prox	0.19285	3	1
5188	-3238	AS10dist	0			AS10prox	0.19285	3	1
5191	-3241	AS10dist	0			AS10prox	0.19285	3	1
5193	-3243	AS10dist	0			AS10prox	0.19285	3	1
5194	-3244	AS10dist	0			AS10prox	0.19285	3	1
5199	-3249	AS10dist	0			AS10prox	0.19285	3	1
5200	-3250	AS10dist	0			AS10prox	1.5428	3	1
5203	-3253	AS10dist	0			AS10prox	0.57855	2	1
5208	-3258	AS10dist	0			AS10prox	0.3857	3	1
5209	-3259	AS10dist	0			AS10prox	0.3857	3	1
5211	-3261	AS10dist	0			AS10prox	0.19285	3	1
5212	-3262	AS10dist	0			AS10prox	0.19285	3	1
5213	-3263	AS10dist	0			AS10prox	0.3857	3	1
5214	-3264	AS10dist	0			AS10prox	1.34995	2	1
5218	-3268	AS10dist	0			AS10prox	0.19285	3	1
5219	-3269	AS10dist	0			AS10prox	0.19285	3	1
5220	-3270	AS10dist	0			AS10prox	0.19285	3	1
5221	-3271	AS10dist	0			AS10prox	0.19285	3	1
5222	-3272	AS10dist	0			AS10prox	0.19285	3	1
5223	-3273	AS10dist	0			AS10prox	0.7714	3	1
5226	-3276	AS10dist	0			AS10prox	0.19285	3	1
5228	-3278	AS10dist	0			AS10prox	0.7714	3	1
5230	-3280	AS10dist	0			AS10prox	0.19285	3	1
5232	-3282	AS10dist	0			AS10prox	0.19285	3	1
5233	-3283	AS10dist	0			AS10prox	0.19285	3	1
5234	-3284	AS10dist	0			AS10prox	0.19285	3	1
5237	-3287	AS10dist	0			AS10prox	0.3857	3	1
5240	-3290	AS10dist	0			AS10prox	0.19285	3	1
5243	-3293	AS10dist	0			AS10prox	0.19285	3	1
5244	-3294	AS10dist	0			AS10prox	0.19285	3	1
5245	-3295	AS10dist	0			AS10prox	0.19285	3	1
5246	-3296	AS10dist	0			AS10prox	0.19285	3	1
5250	-3300	AS10dist	0			AS10prox	0.19285	3	1
5253	-3303	AS10dist	0			AS10prox	0.3857	3	1
5254	-3304	AS10dist	0			AS10prox	1.5428	2	1
5259	-3309	AS10dist	0			AS10prox	0.3857	1	1
5267	-3317	AS10dist	0			AS10prox	0.19285	3	1
5269	-3319	AS10dist	0			AS10prox	0.3857	3	1

5271	-3321	AS10dist	0			AS10prox	0.57855	3	1
5273	-3323	AS10dist	0.3857	2	1	AS10prox	0.96425	3	1
5274	-3324	AS10dist	0			AS10prox	0.19285	3	1
5275	-3325	AS10dist	0			AS10prox	0.19285	3	1
5277	-3327	AS10dist	0			AS10prox	0.3857	1	1
5278	-3328	AS10dist	0.3857	2	1	AS10prox	1.34995	2	1
5282	-3332	AS10dist	0			AS10prox	0.19285	3	1
5283	-3333	AS10dist	0			AS10prox	0.19285	3	1
5284	-3334	AS10dist	0			AS10prox	0.3857	3	1
5285	-3335	AS10dist	0			AS10prox	0.19285	3	1
5287	-3337	AS10dist	0			AS10prox	0.19285	3	1
5288	-3338	AS10dist	0			AS10prox	0.57855	3	1
5291	-3341	AS10dist	0			AS10prox	0.57855	3	1
5292	-3342	AS10dist	0			AS10prox	0.19285	3	1
5293	-3343	AS10dist	0			AS10prox	0.19285	3	1
5294	-3344	AS10dist	0			AS10prox	0.3857	3	1
5295	-3345	AS10dist	0			AS10prox	0.3857	3	1
5296	-3346	AS10dist	0			AS10prox	0.3857	3	1
5299	-3349	AS10dist	0			AS10prox	0.3857	3	1
5301	-3351	AS10dist	0			AS10prox	0.3857	3	1
5302	-3352	AS10dist	0			AS10prox	0.19285	3	1
5303	-3353	AS10dist	0			AS10prox	0.19285	3	1
5306	-3356	AS10dist	0			AS10prox	0.19285	1	1
5307	-3357	AS10dist	0			AS10prox	0.3857	3	1
5308	-3358	AS10dist	0			AS10prox	0.19285	3	1
5310	-3360	AS10dist	1.5428	2	1	AS10prox	2.6999	2	1
5312	-3362	AS10dist	0			AS10prox	0.19285	3	1
5313	-3363	AS10dist	0			AS10prox	0.19285	3	1
5314	-3364	AS10dist	0			AS10prox	0.19285	3	1
5316	-3366	AS10dist	0			AS10prox	0.19285	3	1
5319	-3369	AS10dist	0			AS10prox	0.3857	3	1
5322	-3372	AS10dist	0			AS10prox	1.5428	3	1
5324	-3374	AS10dist	0			AS10prox	0.19285	3	1
5326	-3376	AS10dist	0			AS10prox	0.19285	3	1
5327	-3377	AS10dist	0			AS10prox	0.19285	3	1
5328	-3378	AS10dist	0			AS10prox	0.3857	3	1
5331	-3381	AS10dist	0			AS10prox	0.19285	3	1
5333	-3383	AS10dist	0			AS10prox	0.19285	3	1
5336	-3386	AS10dist	0			AS10prox	0.19285	3	1
5340	-3390	AS10dist	0			AS10prox	0.19285	3	1
5341	-3391	AS10dist	0			AS10prox	0.3857	3	1
5342	-3392	AS10dist	0			AS10prox	0.19285	3	1
5343	-3393	AS10dist	0			AS10prox	0.19285	3	1
5346	-3396	AS10dist	0			AS10prox	0.19285	3	1
5348	-3398	AS10dist	0.7714	2	1	AS10prox	1.5428	3	1
5349	-3399	AS10dist	0			AS10prox	0.19285	3	1
5352	-3402	AS10dist	0			AS10prox	0.19285	3	1
5354	-3404	AS10dist	0			AS10prox	0.19285	3	1
5359	-3409	AS10dist	0			AS10prox	0.3857	3	1
5360	-3410	AS10dist	0			AS10prox	0.19285	3	1
5361	-3411	AS10dist	0			AS10prox	0.57855	3	1
5364	-3414	AS10dist	0			AS10prox	0.3857	3	1
5366	-3416	AS10dist	0			AS10prox	0.3857	3	1
5367	-3417	AS10dist	0			AS10prox	0.19285	3	1
5370	-3420	AS10dist	0			AS10prox	0.19285	1	1
5375	-3425	AS10dist	0			AS10prox	1.1571	2	1
5376	-3426	AS10dist	0			AS10prox	0.19285	3	1
5385	-3435	AS10dist	0.7714	2	1	AS10prox	1.1571	3	1
5386	-3436	AS10dist	0			AS10prox	0.19285	3	1
5394	-3444	AS10dist	0			AS10prox	0.19285	3	1
5400	-3450	AS10dist	0			AS10prox	0.19285	3	1
5402	-3452	AS10dist	0			AS10prox	0.19285	3	1

5404	-3454	AS10dist	0	AS10prox	0.19285	3	1
5407	-3457	AS10dist	0	AS10prox	1.1571	2	1
5411	-3461	AS10dist	0	AS10prox	0.3857	2	1
5412	-3462	AS10dist	0	AS10prox	0.19285	3	1
5413	-3463	AS10dist	0	AS10prox	0.3857	3	1
5414	-3464	AS10dist	0	AS10prox	0.19285	3	1
5416	-3466	AS10dist	0	AS10prox	0.19285	3	1
5424	-3474	AS10dist	0	AS10prox	0.19285	3	1
5425	-3475	AS10dist	0	AS10prox	0.19285	3	1
5426	-3476	AS10dist	0	AS10prox	1.34995	3	1
5437	-3487	AS10dist	0	AS10prox	0.19285	3	1
5438	-3488	AS10dist	0	AS10prox	0.19285	3	1
5457	-3507	AS10dist	0	AS10prox	0.19285	3	1
5458	-3508	AS10dist	0	AS10prox	0.19285	3	1
5459	-3509	AS10dist	0	AS10prox	0.19285	3	1
5460	-3510	AS10dist	0	AS10prox	0.19285	3	1
5464	-3514	AS10dist	0	AS10prox	0.19285	3	1
5465	-3515	AS10dist	0	AS10prox	0.19285	3	1
5467	-3517	AS10dist	0	AS10prox	0.19285	3	1
5468	-3518	AS10dist	0	AS10prox	0.19285	3	1
5469	-3519	AS10dist	0	AS10prox	0.19285	3	1
5470	-3520	AS10dist	0	AS10prox	0.19285	3	1
5473	-3523	AS10dist	0	AS10prox	0.19285	3	1
5474	-3524	AS10dist	0	AS10prox	0.19285	3	1
5475	-3525	AS10dist	0	AS10prox	0.19285	3	1
5476	-3526	AS10dist	0	AS10prox	0.19285	3	1
5488	-3538	AS10dist	0	AS10prox	0.19285	3	1
5490	-3540	AS10dist	0	AS10prox	0.19285	3	1
5497	-3547	AS10dist	0	AS10prox	0.19285	3	1
5498	-3548	AS10dist	0	AS10prox	0.19285	3	1
5502	-3552	AS10dist	0	AS10prox	0.19285	3	1
5505	-3555	AS10dist	0	AS10prox	0.19285	3	1
5513	-3563	AS10dist	0	AS10prox	0.7714	2	1

Appendix B. AMS ^{14}C dates obtained from terrestrial macrofossils in Lake Ammersee sediment cores. Conventional ^{14}C ages were calibrated to years BP using the CALIB 6.0 program operating with the IntCal09 calibration curve.

Sample name	Dated Material	AMS 14 C age BP	Calibrated age (cal. yr BP 2σ range)
AS10-A1O 76-77	leave	340 ± 30	311-480
AS10-D2O 48.5-49.5	leave	1585 ± 30	1406-1537
AS09-A1 128	leave	1595 ± 30	1409-1542
AS10-D2O 55.5-56.5	leave	1620 ± 30	1412-1592
AS10-D2O 74-75	leave	1770 ± 30	1605-1813
AS10-A2O 22-23	leave	1795 ± 35	1616-1821
AS10-D2U 59.5-60.5	leave	2440 ± 30	2355-2700
AS09-A2 40	leave	2580 ± 35	2505-2764
AS10-A2U 22.5-23.5	leave	2655 ± 30	2740-2844
AS10-D3O 16-17	leave	2800 ± 35	2794-2993
AS09-A2 189	leave	3580 ± 50	3719-4068
AS09-A3/2 92.5	leave	4565 ± 35	5023-5441
AS10-D4O 82.5-83.5	twig	5120 ± 40	5747-5980
AS10-D4O 83.5-84.5	twig	5130 ± 40	5749-5986

List of publications

Czymzik, M., Dulski, P., Plessen, B., von Grafenstein, U., Naumann, R., Brauer, A. (2010). A 450-year record of spring-summer flood layers in annually laminated sediments from Lake Ammersee (southern Germany). *Water Resour. Res.* **46**, W11528.

Czymzik, M., Brauer, A., Dulski, P., Plessen, B., von Grafenstein, U., Naumann, R., Scheffler, R. (2012). Shifts of Mid- to Late Holocene flood magnitude in detrital layers from varved sediments of pre-alpine Lake Ammersee (southern Germany). *Quat. Sci. Rev.* **submitted**.

Czymzik, M., Brauer, A., Lohmann, G,. Rimbu, N., Dulski, P. (2012). Atmospheric control of flood frequency in central Europe throughout the past 5500 years. **in prep**

Curriculum vitae

This page contains personal data. It is thus not part of the online publication

Erklärung

Hiermit erkläre ich gemäß § 9 Abs. 7 der Promotionsordnung der Mathematisch-Naturwissenschaftlichen Fakultät der Universität Potsdam, dass ich die von mir vorgelegte Dissertation mit dem Titel

Mid- to Late Holocene flood reconstruction from two varved sediment profiles of pre-alpine Lake Ammersee (southern Germany)

selbstständig angefertigt, die benutzten Quellen und Hilfsmittel vollständig angegeben und wörtliche und sinngemäße Zitate als solche gekennzeichnet habe, sowie Tabellen, Karten und Abbildungen, die anderen Werken in Wortlaut oder dem Sinn nach entnommen sind, in jedem Einzelfall als Entlehnung kenntlich gemacht habe. Ich erkläre außerdem, dass diese Dissertation noch keiner anderen Fakultät oder Hochschule zur Prüfung vorgelegen hat; dass sie, abgesehen von den unten angegebenen Teilpublikationen, noch nicht veröffentlicht worden ist sowie, dass ich eine solche Veröffentlichung vor Abschluss des Promotionsverfahrens nicht vornehmen werde. Die Bestimmungen der Promotionsordnung sind mir bekannt.

Teilpublikationen

Czymzik, M., Dulski, P., Plessen, B., von Grafenstein, U., Naumann, R., Brauer, A. (2010). A 450 year record of spring-summer flood layers in annually laminated sediments from Lake Ammersee (southern Germany). *Water Resources Research* **46**, W11528.

Czymzik, M., Brauer, A., Dulski, P., Plessen, B., von Grafenstein, U., Naumann, R., Scheffler, R. (2012). Shifts of Mid- to Late Holocene flood magnitude in detrital layers from varved sediments of pre-alpine Lake Ammersee (southern Germany). *Quaternary Science Review* **submitted**.

Czymzik, M., Brauer, A., Lohmann, G,. Rimbu, N., Dulski, P. (2012). Atmospheric control of flood frequency in central Europe throughout the past 5500 years. **in prep**.

Potsdam, den 29. August 2012